University of Plymouth

PEARL **https://pearl.plymouth.ac.uk**

04 University of Plymouth Research Theses 01 Research Theses Main Collection

2018

Storm Impact and Recovery Along the South West Coast of England

Burvingt, Olivier Jean-Patrick

http://hdl.handle.net/10026.1/12830

http://dx.doi.org/10.24382/997
University of Plymouth

All content in PEARL is protected by copyright law. Author manuscripts are made available in accordance with publisher policies. Please cite only the published version using the details provided on the item record or document. In the absence of an open licence (e.g. Creative Commons), permissions for further reuse of content should be sought from the publisher or author.

This copy of the thesis has been supplied on condition that anyone who consults it is understood to recognise that its copyright rests with its author and that no quotation from the thesis and no information derived from it may be published without the author's prior consent.

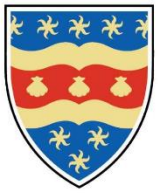

UNIVERSITY OF
PLYMOUTH
School of Biological and
Marine Sciences

STORM IMPACT AND RECOVERY ALONG THE SOUTH WEST COAST OF ENGLAND

by

OLIVIER JEAN PATRICK BURVINGT

A thesis submitted to Plymouth University in partial fulfilment for the degree of

DOCTOR OF PHILOSOPHY

School of Biological and Marine Sciences

July 2018

Abstract

Name: Olivier Burvingt

Title: Storm impact and recovery along the south west coast of England

Extreme storms are responsible for rapid changes to coastlines worldwide. During the 2013/14 winter, the west coast of Europe experienced a sequence of large, storm-induced wave events, representing the most energetic period of waves in the last 60 years. The southwest coast of England underwent significant geomorphological change during that period, but exhibited a range of spatially variable and complex morphological responses, despite being subjected to the same storm sequence.

The 2013/14 storm response along the southwest coast of England was first used as a natural field laboratory to explain the variability in storm response through the introduction and evaluation of a new classification of how sandy and gravel beaches respond to extreme storms. Cluster analysis was conducted using an unique data set of pre- and post-storm airborne Light Detection and Ranging (LiDAR) data from 157 beach sites and the calculation of volumetric beach changes and a novel parameter, the longshore variation index which quantifies the alongshore morphological variability in beach response. The method used can be applied to any sandy and gravel beaches where topographic data with sufficient spatial resolution is available. Four main beach response types were identified that ranged from large and alongshore uniform offshore sediment losses up to 170 m^3 m^{-1} (at exposed, cross-shore dominated sites) to considerable alongshore sediment redistribution but limited net sediment change (at more sheltered sites with oblique waves). The key factors in determining the type of beach response are: exposure to the storm waves, angle of storm wave approach and the degree to which the beach is embayed. These findings provide crucial information for the development of coastal studies at regional scale, especially along coastal areas where abrupt changes in coastline orientation can be observed.

A 10-year time series (2007–2017) of supra- and intertidal beach volume from exposed and cross-shore transport-dominated sites was used to examine the extent to which beach behaviour is coherent over a relatively large region (100-km stretch of coast) and predictably coupled to incident wave forcing. Over the study period, 10 beaches, exposed to similar wave/tide conditions, but having different sediment characteristics, beach lengths and degrees of embaymentisation, showed coherent and synchronous variations in sediment volumes, albeit at different magnitudes. This result is crucial for studying coastal changes in remote coastal areas or

in areas where only few topographic data are available. The sequence of extreme storms of the 2013/14 winter, which represents the most erosive event over at least a decade along most of the Atlantic coast of Europe, is included in the data set, and three years after this winter, beach recovery is still on-going for some of the 10 beaches. Post-storm beach recovery was shown to be mainly controlled by post-storm winter wave conditions, while summer conditions consistently contributed to modest beach recovery. Skilful hindcasts of regional changes in beach volume were obtained using an equilibrium-type shoreline model, demonstrating that beach changes are coherently linked to changes in the offshore wave climate and are sensitive to the antecedent conditions. Furthermore, a good correlation was found between the beach volume changes and the new climate index WEPA (West Europe Pressure Anomaly), which offers new perspectives for the role and the use of climatic variations proxies to forecast coastline evolution.

A process based model, XBeach, was used to model storm response at one macrotidal beach characterized by the largest sediment losses during the 2013/14 sequence of extreme storms. Beach volume changes were modelled over hypothetical scenarios with varying hydrodynamics conditions and beach states to investigate the relative roles of hydrodynamic forcing (i.e., waves and tides), beach antecedent state and beach-dune morphology in beach response to extreme storms. This modelling approach is applicable to any beach system where process based models have been implemented. Beside significant wave height and peak wave period, the beach antecedent state was shown to be the dominant factor in controlling the volumes of sediment erosion and accretion along this cross-shore dominated beach. Modelled volumes of erosion were, on average, up to three times higher along an accreted beach compared to an eroded beach for the same wave conditions. The presence of a dune, being only significantly active during spring tides and storm conditions along this macrotidal beach, was shown to reduce erosion or even cause accretion along the intertidal beach.

This work provides a detailed, quantitative insight of the hydrodynamic and morphological processes involved in storm response and beach recovery on a number of spatial and temporal scales. This improved understanding of the potential impact of extreme events will hopefully aid future research efforts and ensure effective management of sedimentary coastlines.

Author's declaration

At no time during the registration for the degree of Doctor of Philosophy has the author been registered for any other University award without prior agreement of the Doctoral College Quality Sub-Committee.

Work submitted for this research degree at the University of Plymouth has not formed part of any other degree either at the University of Plymouth or at another establishment.

The PhD supervisory team consisted of Prof. Gerd Masselink (Director of Studies), Prof. Paul Russell and Dr. Tim Scott from the School of Biological and Marine Sciences, Plymouth University.

This research was funded by NERC grants NE/M004996/1 (Urgency Grant) and NE/N015525/1 (Strategic Highlights Topic grant).

Relevant scientific conferences and symposiums were regularly attended throughout the duration of this thesis, at which work was often presented and several papers were prepared for publication

Word count of main body of thesis: 34,655

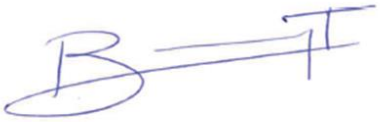

Signed.....

Date……20/07/18…….

PhD outputs

Refereed Journal publications:

Burvingt, O., Masselink, G., Russell, P., Scott, T., 2017. Classification of beach response to extreme storms. Geomorphology 295, 722–737. doi.org/10.1016/j.geomorph.2017.07.022

Burvingt, O., Masselink, G., Scott, T., Davidson, M., Russell, P., 2018. Climate forcing of regionally-coherent extreme storm impact and recovery on embayed beaches. Marine Geology 401, 112–128. doi.org/10.1016/j.margeo.2018.04.004

Refereed Conference Proceedings:

Burvingt, O., Masselink, G., Russell, P. and Scott, T., 2016. Beach response to consecutive extreme storms using LiDAR along the south west coast of England. Journal of Coastal Research 75, 1052–1056. 10.2112/SI75-211.1

Burvingt, O., Masselink, G., Russell, P. and Scott, T., 2017. Beach evolution and recovery from a sequence of extreme storms. Coastal Dynamics ’17, 167.

Conference attendances:

Young Coastal Scientists and Engineers Conference (YCSEC), Manchester (UK), 2015. *Oral presentation*.

International Coastal Symposium (ICS), Sydney (Australia), 2016. *Oral presentation.*

Coastal Dynamics, Helsingor (Denmark), 2017. *Poster presentation.*

Ocean Science Meeting (AGU), Portland (USA), 2018. *Oral presentation.*

Grants Awarded:

Plymouth Marine Institute Education Fund: Grant-in-aid 2018. £400 awarded to attend the Ocean Science Meeting (AGU), Portland (USA), 2018.

Contents

List of figures

offshore wave height, the red circle its subsequent landfall, and the horizontal red line represents 500N latitude. The inset in each of the storm wave plots represents the south west coast of England with the arrows representing the inshore wave height (thickness and length of arrow) and direction modelled by the Met Office 8-km grid WWIII model for 20–30m water depth along the north coast, off the tip of Cornwall and along the south coast. Source: Masselink et al., 2015.

Fig. 1.9. Generalised geological map of southwest England and the adjacent English channel. Source: Ian West, 2010.

Fig. 1.10. Map of Britain with: (a) M2 tidal amplitude (adapted from Proudman and Doodson, 1924); (b) 10% exceedence significant wave height, $H_{s10\%}$, (Draper, 1991); and (c) 1-in-50 year storm surge level (Flather, 1987). Source: Scott, 2009.

Fig. 2.1. Pictorial overview of storm impacts during the 2013/14 winter along the coast of south west England (numbers related to sites indicated in Figure 2.2). (a) The gravel barrier at Westward Ho! #19 experienced overwash (photo: Richard Murgatroyd). (b1 before; b2 after) Large quantities of sand were removed from Whipsiderry beach #39, exposing the underlying rocky shore platform (photo: Mike Searle). (c) The seawall below Fistral Blu bar in Newquay #41 collapsed and causing damage to property (photo: Richard Murgatroyd). (d) The Watering Hole in Perranporth #46 required human interventions to protect the restaurant (photo from Mail Online, SWNS). (e) The coastal town of Looe #100 was flooded a number of times (photo: Nic Randall). (f) The coastal dunes at Thurlestone #119 experienced more than 5 m of erosion (photo: National Trust Southwest). (g) At the end of the winter, the beach in front of the seawall at Beesands #123 had completely disappeared. (h1 before; h2 after) The road that runs along the gravel barrier of Slapton Sands #124 became covered with gravel due to overwash (photo from BBC News, Press Association). (i) The most costly damage occurred to the London-Penzance railway line at Dawlish #139 (photo from BBC News, Press Association).

Fig. 2.2. Map of south west England and location of the 157 beaches for which LiDAR data are available. Pictures of (anti-clockwise): Porlock #10, Bossiney #26, Hayle #51, Pentewan #90 and Slapton Sands #124, illustrating the diversity of beach systems along the south west coastline of England. Black numbers indicates the different tidal ranges along the coast.

Fig. 2.3. Illustration of the process of extracting useful data from the LiDAR titles: (a) raw LiDAR data; (b) aerial picture of the same area; (c) digitized shapefiles drawn around the two beaches (Fistral #42 and Crantock #43); (d) digitized shapefiles overlapped with LiDAR data; and (e) the image of subtracted new rasters of LiDAR data surveyed in April 2012 (pre-storm) and April 2014 (post-storm) at both sites.

Fig. 2.4. Illustration of the process of calculating longshore variation index (*LVI*): (a) example of DoD obtained when post- and pre-storm LiDAR rasters are subtracted at Carlyon beach #94 (surveyed in May 2014 and March 2012, respectively); (b) rotated DoD overlapped with a grid in which every row of data represents a 1 m cross-shore transect and every column a 1 m longshore one (not to scale for graphic purpose); (c) alongshore variation in the net cross-shore volumetric change dQ_{cross} with the alongshore-averaged change Q_{mean} plotted as a horizontal red line and values of the variables used in Equation 2.5.

Fig. 2.5. (a) Along-coast variability in modelled average winter 2013/14 wave power $|P|$ and (b) percentage of wave power increase relative to 2012/13 winter at 46 'deep-water' grid points along the southwest coast of England.

Fig. 2.6. Along-coast variation in (a) net volumetric change per unit m beach dQ_{net} and (b) longshore variation index *LVI*. Every bar represents a study site and the sites are geographically ordered in an anti-clockwise direction from north to south. The black vertical dashed line marks the separation between the north and the south coast. Geographical distribution of (c) dQ_{net} and (d) *LVI* along the south west coast of England. The colours of the bars and the symbols represent: blue = $dQ_{net} > 0$; red = $dQ_{net} < 0$; clear blue *LVI* < 0.7; purple = *LVI* > 0.7).

Fig. 2.7. Dendrogram clustered using weighted pair group average (UPGMA) method showing the hierarchical clustering of the 157 beaches (Cluster 1 = Yellow; Cluster 2 = Green; Cluster 3 = Red; Cluster 4 = Blue).

Fig. 2.8. Box plots showing the distribution of (a) net volumetric change per unit m width dQ_{net} and (b) longshore variation index *LVI* among the four clusters defined by the cluster analysis. Each box plot displays the values of the 25% quantile (bottom line); the median (middle line); the 75% quantile (top line). The maximum whisker length is specified as 1.0 times the interquartile range, and data points beyond the whiskers are displayed using red crosses.

Fig. 2.9. Examples of DODs obtained from LiDAR data at (a) Croyde beach #17 (Cluster 2 example) surveyed in May 2012 and June 2014; (b) Watergate Bay #39 (Cluster 1 example) surveyed in April 2012 and April 2014; (c) Broadsands #130 (Cluster 3 example) surveyed in April 2012 and April 2014; Praa Sands #62 (Cluster 4 example) surveyed in October 2010 and May 2014. Erosion is coloured in red whereas accretion is coloured in blue.

Fig. 2.10. Scatter plot of dQ_{upper} and dQ_{lower} with the symbol colour representing the cluster type (Cluster 1 = Yellow; Cluster 2 = Green; Cluster 3 = Red; Cluster 4 = Blue; Outliers = Black with PRR = Perran Sands #46 and BLK = Blackpool Sands #125). The diagrams in the corners of the plot are schematic profile responses typical for each of the quadrants, with solid and dashed line representing the profile before and after the 2013/14 winter storms, respectively.

Fig. 2.11. Top panel: box plots showing the distribution of (a) incident wave angle, (b) cross-shore wave power, (c) normalized beach length among the four clusters defined by the cluster analysis. Each box plot displays the values of the 25% quantile (bottom line); the median (middle line); the 75% quantile (top line). The maximum whisker length is specified as 1.0 times the interquartile range, and data points beyond the whiskers are displayed using red crosses. Bottom panel: scatter plots of net volumetric change dQ_{net} and longshore variation index *LVI* with the symbol colour representing the cluster type (Cluster 1 = Yellow; Cluster 2 = Green; Cluster 3 = Red; Cluster 4 = Blue). The symbols are scaled according the different variables (a) incident wave angle; (b) cross-shore wave power; (c) normalized beach length.

Fig. 2.12. Geographical distribution of the 157 beaches in the LiDAR dataset and their cluster type (Cluster 1 = Yellow; Cluster 2 = Green; Cluster 3 = Red; Cluster 4 = Blue; Outliers = Black). The four beach examples presented earlier (Fig. 2.9.) and the two bays presented later (Fig. 2.13) are also located.

Fig. 2.13. DoDs obtained from LiDAR data along (a) St. Ives Bay beach surveyed in April 2012 and April 2014, and (b) Start Bay surveyed in April 2012 and April 2014, illustrating spatial change in beach response and sediment connectivity between adjacent beaches at a local scale. Their location along the south west coast of England is presented in Fig. 2.12. Erosion is coloured in red whereas accretion is coloured in blue.

Fig. 4.10. Conceptual model of a macrotidal and cross-shore dominated beach response to 24 hours of extreme storm wave conditions as a function of the beach antecedent state, the tidal stage and dune activity.

List of tables

Table 4.2. Ranges of the significant wave height, H_s, peak wave period T_p, total water level *TWL*, used to force XBeach model and the selected initial beach profile chosen to run the model in the four scenarios (ST-AP: spring tides and accreted profile; NT-AP: neap tides and accreted profile; ST-EP: spring tides and eroded profile; NT-EP: neap tides and eroded profile).

Acknowledgments

Firstly I would like to give my thanks to Prof. Gerd Masselink, Prof. Paul Russell and Dr. Scott who provided me a great level of support throughout this PhD. I am grateful for the experiences and skills I have gained over the last few years, and I am hoping to get more collaborations with you in the near future. I would also like to thank Dr. Davidson for his valuable support and guidance with the ShoreFor model.

I would also like to thank Dr. O'Hare and Dr. Kroon, the viva was a great experience and I enjoyed talking with you about my thesis for a couple of hours.

Thanks to the whole Plymouth Coastal Observatory team who has been collecting a huge amount of data that was priceless for my research.

A massive thank to all whom have kindly accompanied me on fieldwork, Kris, Mark, Nieves, Oli (memorable experience at Perran Sands), Pedro, Sam, and all other friendly people I met at Uni, Aaron, Adam, Andrea, Carlos (please keep the Kurdish's restaurant tradition alive), Claire, Daniel, Davide, Diego (aka Antoñito), Ed(s), Ellie, Erin, Erwin, Gregorio, Guio, Jak, Jill, Jonas, Kieran, Kit, Marcus, Mark, Matt, Natalia, Peter, Phillipe, Pilou, Riccardo, Rob, Robert, Sam, Thomas, Tim, Will…

Paul and Benji, I tried to escape from you guys but you also managed to fly across the English Channel. Good luck for the end of your PhDs, I am sure you will do great.

On a personal note, I deeply thank my parents, my grandparents and my girlfriend who support me through the whole of this experience, and who believed me when I told them a coastal science degree was not a cover-up so that I could go surfing more often.

There were many rainy Sunday afternoons but it was all worth it, and I highly recommend visiting the stunning landscapes of Devon and Cornwall.

Chapter 1 – Introduction

1.1 Context

Coastal areas are dynamic systems that are constantly evolving in response to variable hydrodynamic and meteorological processes (Wright and Thom, 1977). Coastline changes can be monitored over time scales and spatial scales spanning seconds to decades, and centimetres to kilometres, respectively. At the interface between the land and the ocean, coastal areas have been of particular interest over last decades in a context of global warming and sea-level rise (Stocker et al., 2013). Along with the reshaping of our coastlines, sea-level rise also represents a social and economic issue given that coastal zones are globally more densely populated than the hinterland and exhibit higher rates of population growth and urbanisation that are expected to continue into the future . A potential increase in storminess at some areas of the globe also represents a major concern for coastal areas since storm events often cause rapid and extreme increase of sea level (Voudouskas et al., 2017). Additionally, extreme storm events also deeply and rapidly reshape the coastline (Short, 1999). A better knowledge and understanding of past and present records of coastline change due to extreme storms are necessary to be able to predict the future coastline evolution, offering the best opportunity for coastal communities to adapt accordingly.

1.2 Storminess in North Atlantic

1.2.1 Tropical and extra-tropical storms

Generally speaking, events called ‘storms’, ‘cyclones’ or ‘typhoons’ are extreme atmospheric and oceanic disturbances. These disturbances are either categorized as tropical or extra-tropical, depending on the considered latitude, for which different processes are involved. An extra-tropical storm is a disturbance that primarily gets its energy from the horizontal temperature contrasts that exist in the atmosphere. They are low pressure systems with associated cold fronts, warm fronts, and occluded fronts. Tropical cyclones, in contrast, typically have little to no temperature difference across the storm at the surface, and their winds are derived from the release of energy due to cloud/rain formation from the warm moist air of the tropics (Merrill, 1993).

Studying storm activity involves looking at the number of storms over a defined period of time and their respective intensity. The definition of intensity usually implies arbitrary thresholds for deciding the issue of severity. A scale was first devised in 1805 by the Irish hydrographer Francis Beaufort (Huller, 2004). This scale, originally ranging from 0 to 12, is an empirical measure that relates wind speed to observed conditions at sea or on land (Fig. 1.1). Later in 1971, another scale was developed by civil engineer Herbert Saffir and meteorologist Robert Simpson. This scale is specifically used for all tropical cyclones, including hurricanes (US term), typhoons (Asian term) and cyclones (Australian term). These 5 categories are

also distinguished by the intensities of their sustained winds where Category 1 is equivalent to Beaufort 12.

These tropical and extra-tropical storms cause water level rise and coastal flood defined as a storm surge, storm flood or storm tide. The pressure effects of a tropical cyclone will cause the water level in the open ocean to rise in regions of low atmospheric pressure and fall in regions of high atmospheric pressure. The rising water level will counteract the low atmospheric pressure such that the total pressure at some plane beneath the water surface remains constant. This effect is estimated at a 10 mm increase in sea level for every millibar (hPa) drop in atmospheric pressure (Harris, 1963). Extra-tropical storms generally cause smaller storm surge because of less intense low pressure systems and relatively milder wind conditions.

Storm events are also associated with the formation of large and high waves that represent another threat for coastal areas and play a key role in coastline morphological change. Both wave height and period, expressed in meter and second respectively, vary as a function of the storm characteristics: (1) the wind strength, *i.e.* the stronger the wind the larger the waves it can create; (2) the duration of the storm, *i.e.* the longer a storm blows the larger the waves it can create; and (3) the fetch, *i.e.* the larger the area over which the wind is blowing the bigger waves it can create. Wave direction, often expressed as an angle in degrees with regards to N-S or W-E axis, varies as a function of the storm track.

BEAUFORT SCALE					
Beaufort Number	Name	Knots	MPH	Effects Observed Far From Land	Effects Observed On Land
0	Calm	Under 1	Under 1	Sea like mirror.	Calm; smoke rises vertically.
1	Light Air	1-3	1-3	Ripples with appearances of scales; no foam crests.	Direction of wind shown by smoke drift, but not by wind vanes.
2	Light Breeze	4-6	4-7	Small wavelets; crests of glassy appearance, not breaking.	Wind felt on face; leaves rustle; ordinary vane moved by wind.
3	Gentle Breeze	7-10	8-12	Large wavelets; crests begin to break; scattered whitecaps.	Leaves and small twigs in constant motion; wind extends light flag.
4	Moderate Breeze	11-16	13-18	Small waves, becoming longer; numerous whitecaps.	Raises dust and loose paper, small branches are moved.
5	Fresh Breeze	17-21	19-24	Moderate waves, taking longer form; many whitecaps; some spray.	Small trees in leaf begin to sway; crested wavelets form on inland waters.
6	Strong Breeze	22-27	25-31	Larger waves forming; whitecaps everywhere; more spray.	Large branches in motion; whistling heard in telegraph wires; umbrellas used with difficulty.
7	Near Gale	28-33	32-38	Sea heaps up; white foam from breaking waves begins to be blown in streaks.	Whole trees in motion; inconvenience felt in walking against the wind.
8	Gale	34-40	39-46	Moderately high waves of greater length; edges of crests begin to break into spindrift; foam is blown in well-marked streaks.	Breaks twigs off trees; generally impedes progress.
9	Strong Gale	41-47	47-54	High waves; sea begins to roll; dense streaks of foam; spray may reduce visibility.	Slight structural damage occurs (chimney pots and slate removed).
10	Storm	48-55	55-63	Very high waves with overhanging crests; sea takes white appearance as foam is blown in very dense streaks; rolling is heavy and visibility reduced.	Seldom experienced inland; trees uprooted; considerable structural damage occurs.
11	Violent Storm	56-63	64-72	Exceptionally high waves; sea covered with white foam patches; visibility still more reduced.	Very rarely experienced; accompanied by widespread damage.
12	Hurricane	64 and over	73 and over	Air filled with foam; sea completely white with driving spray; visibility reduced.	

Figure 1.1: Example of the empirical Beaufort scale relating wind speed to observed conditions at sea or on land, that first proposed by the Irish hydrographer Francis Beaufort. Source: solentribcharter.co.uk

1.2.2 Monitoring of storminess

Storm activity can be monitored by using measured wave conditions at deep or shallow waters. These wave conditions, such as wave height, period, and direction are often measured by wave buoys deployed in the coastal and offshore waters. For example, the commonly used Waverider buoys are surface following buoys anchored to the sea bed by means of an elastic mooring. An accelerometer mounted within the buoy registers the rate at which the buoy is rising or falling as it follows the pattern of waves. By

integrating against time, the acceleration signal can be converted to vertical displacement, which is often relayed to a recording station on the shore. A wide network of wave buoys exists over all oceans of the world (Fig. 1.2) and a common means of identifying coastal storm events for a particular coastal location is through statistical analysis of the significant wave height, H_s, time series (Ciavola and Coco, 2017). The identification of coastal storms from H_s time series is usually undertaken through the application of the so-called peaks-over-threshold (POT) method (Lemm et al., 1999; Houser and Greenwood, 2005; Almeida et al., 2012; Plomaritis et al., 2015). Other technologies, such as Land-based LiDAR technology (Blenkinsopp et al., 2012; Almeida et al., 2014; Martins et al., 2017) and High Frequency Radar (Wyatt , 1995; Lopez et al., 2015) can also be used for studying breaking waves in the surf zone and wave spectra, respectively, while constant improvement are achieved in wave spectra evaluation using satellite altimetry (Ardhuin et al., 2018).

Along with wave conditions, the large increase in water level along the coast caused by storm events can be used as a proxy for storm activity. The total water level (*TWL*) represents the sum of both astronomical tides and non-tidal residuals, also known as tidal anomalies. Storm surge, considered as a non-tidal residual, can be measured directly at coastal tidal stations as the difference between the forecast tide and the measured rise of water level (Boon, 2007). Old tide-measuring stations use mechanical floats and recorders, while modern monitoring stations use advanced acoustics and electronics to measure water levels. Water level measurements, also

recorded over a wide network of coastal stations spread around the globe, are used to build water levels time series. Historical water level time series represent a valuable source of information for the understanding of spatial and temporal variability of extreme sea level and storm surge events along coastal areas (Haigh et al., 2016). The approach taken to identifying coastal storm events from water-level time-series is similar to that taken for wave time-series (POT method). Thresholds can be defined using the total water level (Aagaard et al., 2007) or based on the non-tidal residuals where tidal variability is removed (Zhang et al., 2000).

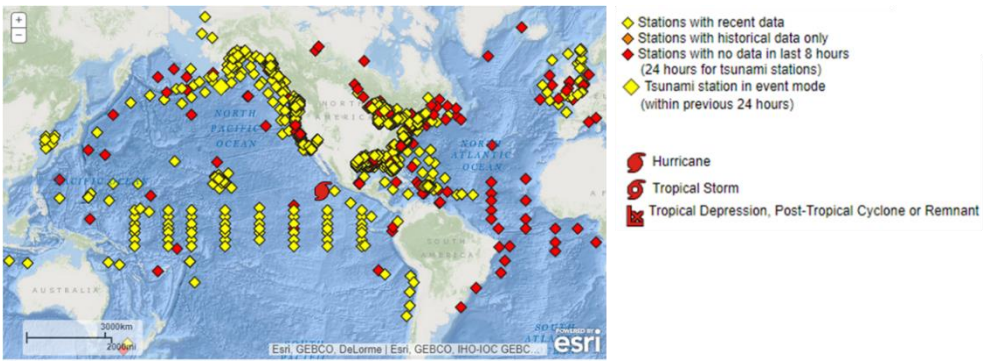

Figure 1.2: Map of a non-exhaustive network of wave buoys/stations spread over the Atlantic and Pacific oceans. Source: noaa.gov

1.2.3 Spatial and temporal variability in storminess

The north Atlantic ocean is characterised by relatively strong and spatially variable storminess with extra-tropical storms generating and circulating at high latitudes (e.g., Labrador sea, Norwegian sea, Fig. 1.3a), and tropical storms developing around low to medium latitudes (e.g., Caribbean sea, east of coast of the USA, Fig. 1.3b). Although most of these storms are dissipated offshore, some of them are of particular interest when their track crosses populated coastal areas and cause dramatic loss of human life and damage,

as, for example, the extreme tropical storm Katrina along the SE coast of the USA in 2005 or the extreme extra-tropical storm Xynthia along the NW coast of France in 2010. The west coast of Europe, and more specifically the south west coast of England, is only exposed to extra-tropical storms (Lozano et al., 2004) and the rest of this review therefore focusses on these high latitude atmospheric perturbations and its consequences.

Records of extra-tropical storms and the resulting storm waves show strong seasonal variation with a higher activity during winter months spanning from October to March (Dolan and Davis, 1992; Santos et al., 2017; Dodet et al., 2010). Wave hindcasts also show that the northeast area of the North Atlantic Ocean has experienced significant multidecadal variations in the last century, and that the winter-mean wave height, variability, and periodicity all increased significantly over the last seven decades (Wang and Swail, 2002; Castelle et al., 2018). Meeker and Mayewski (2002) even showed that these variations could occur over several centuries. Using Greenland ice core chemistry data, they identified a major reorganisation in atmospheric circulation that took place at the beginning of the Little Ice Age and resulted in a sustained increase in the frequency and severity of North Atlantic winter storms. However, Trouet et al. (2012) mentioned the difficulty of determining if the enhanced storminess recorded in proxies over the last centuries is a product of more intense rather than more frequent storms.

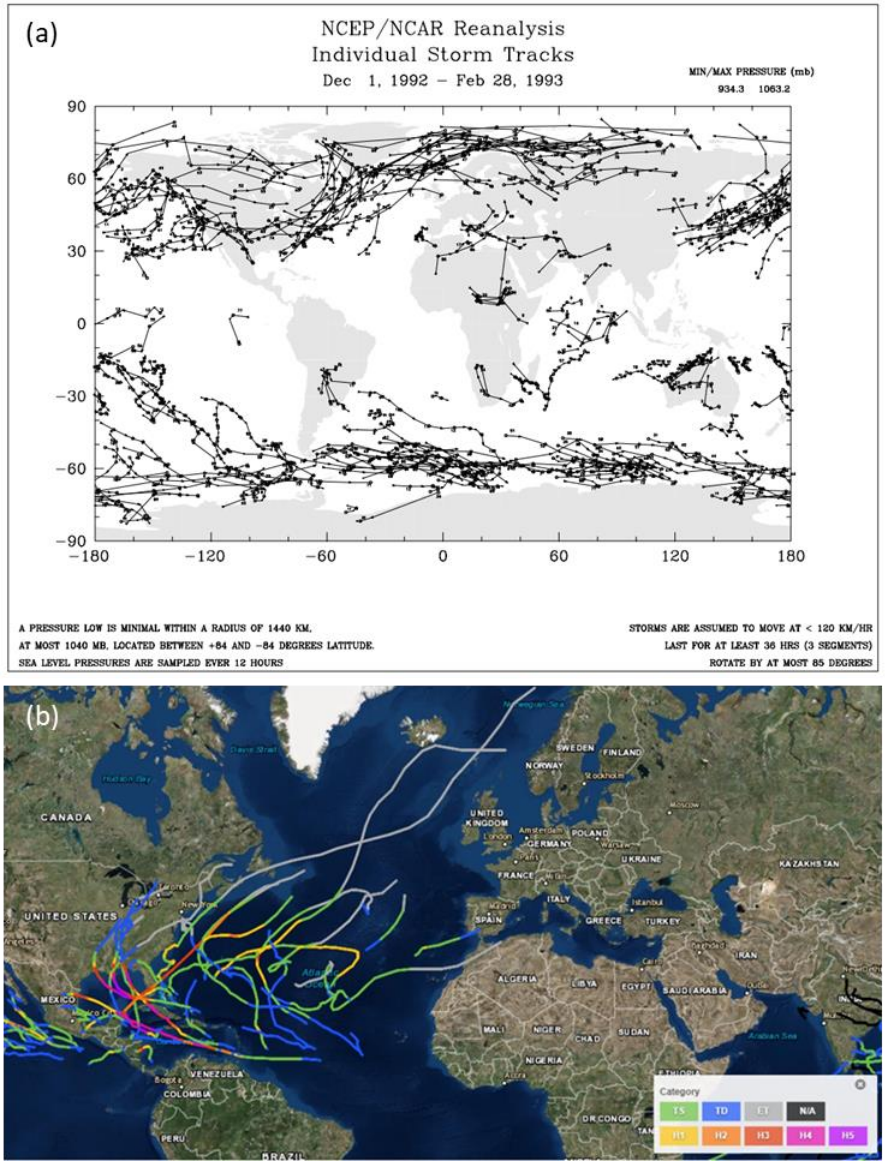

Figure 1.3: Map of (a) individual extra-tropical storm tracks of the 1992/1993 winter including the 'Braer Storm' of 1993, one of the lowest-ever recorded central pressures (914 mb) in the North Atlantic (McCallum and Grahame, 1993; Burt, 1993); and (b) individual tropical storm tracks of the year 2005 including the category 5 hurricane Katrina coloured in purple. Source: nasa.gov and noaa.gov respectively.

1.2.4 Influence of large scale atmospheric patterns on storminess

Historically, the North Atlantic Oscillation (NAO) is the primary mode of climate variability across the North Atlantic region. It is associated with an oscillation in atmospheric mass between the Arctic and subtropical North Atlantic, and its amplitude is largest during the boreal winter when the

atmosphere is dynamically the most active (Hurrell, 2001). The NAO index is expressed as the difference in normalized sea-level pressures across the mid-latitude Atlantic (Hurrell, 1995; Jones et al., 1997), between stations with suitably long records in the south (Lisbon; Ponta Delgada in The Azores; Gibraltar) and the north (southwest Iceland). Positive phases in the index, describing a north-eastward orientation in the NAO, correspond to wetter and stormier weather in northwest Europe, dominated by strong mid-latitude westerlies; negative phases, describing an east to west alignment of the NAO, are associated with drier and calmer weather in northwest Europe, and storms tracking into Mediterranean Europe (Hurrell, 1995; Serreze et al., 1997; Dodet et al., 2010; Bromirski and Cayan, 2015; Fig. 1.4). Using instrumental wind records from 53 stations in northwest Europe, Burningham and French (2012) demonstrated that the NAO is highly correlated with wind direction frequency, with positive phases in the NAO winter index associated with increased frequency of winds from the southwest. However, the same authors also showed that evidence for connections between the NAO and wind speed or storminess measures is far less convincing, particularly in terms of the frequency of extreme wind speed events.

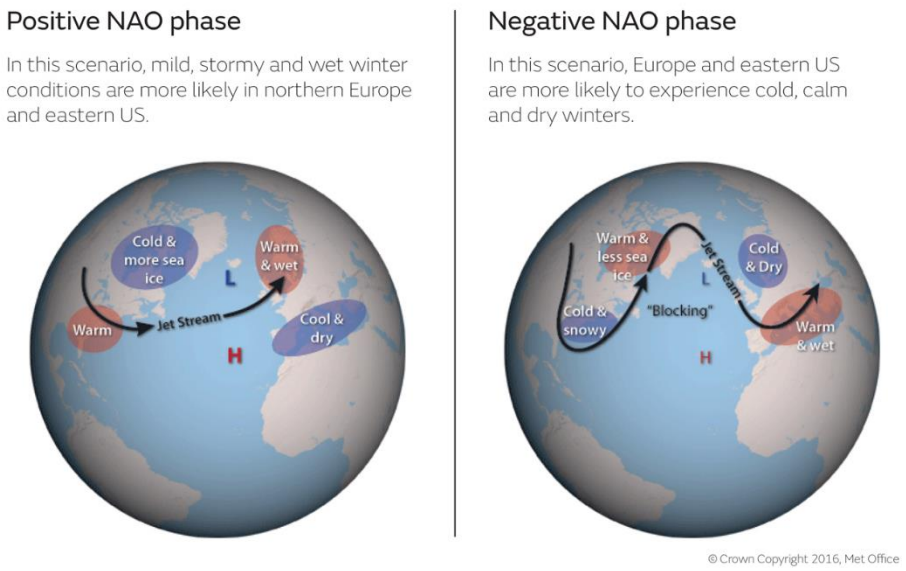

Figure 1.4: Diagrams of the jet stream trajectory and the resulting weather along the northeast coast of the USA and Europe during the positive and negative phases of the North Atlantic Oscillation (NAO). Source: metoffice.gov

More recently, a new index called the West Europe Pressure Anomaly (WEPA) and proposed by Castelle et al. (2017b), was shown to outscore other leading atmospheric modes in explaining winter-averaged significant wave height along European coastal areas south to 52° latitude (i.e. from UK to Spain), and was the only climate index that captured the 2013/2014 winter, characterized by extreme wave activity (Fig. 1.5). The WEPA index is based on the normalized sea level pressure (*SLP*) difference measured between the stations Valentia (Ireland) and Santa Cruz de Tenerife (Canary Islands, Spain). The positive phase of WEPA reflects intensified latitudinal SLP gradient in the NE Atlantic that drives increased W-SW winds around 45° associated with severe storms, many eventually passing over UK, which funnel high-energy waves toward western Europe.

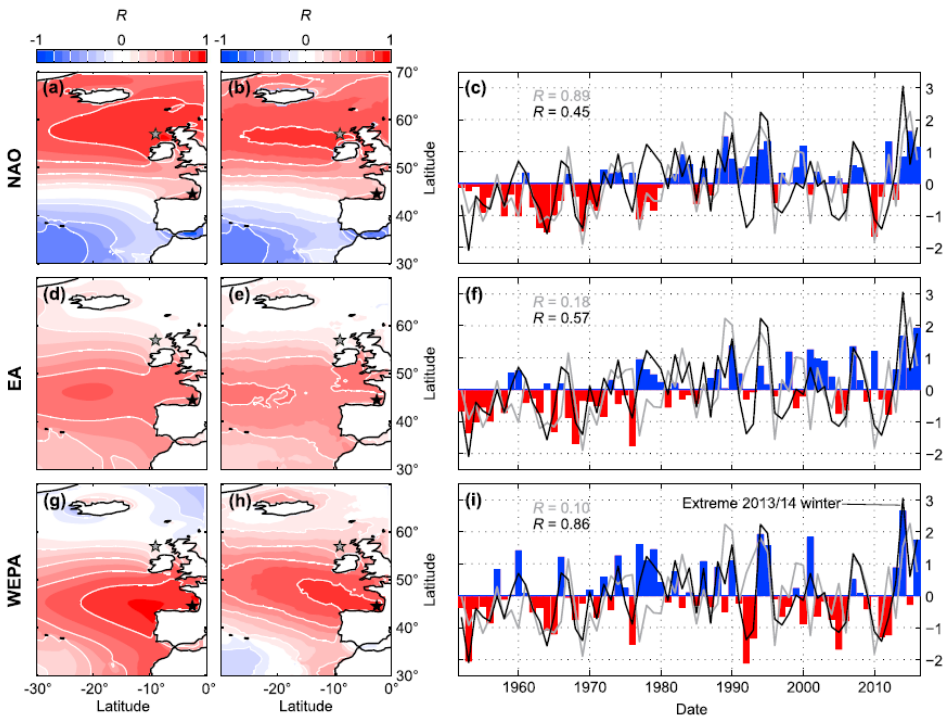

Figure 1.5: (a, b, d, e, g, and h) The spatial correlation of the winter (DJFM)-averaged H_s and $H_{s95\%}$, respectively, against the winter-averaged NAO (Figures 1.5a and 1.5b) and EA indices (Figures 1.5d and 1.5e), and against our new WEPA index (Figures 1.5g and 1.5h) computed as the normalized *SLP* difference measured between station Valentia (Ireland) and station Santa Cruz de Tenerife (Canary Islands, Spain). (c, f, and i) Time series of the corresponding indices with superimposed normalized winter-averaged H_s simulated at the buoys SC (Scotland, black) and BI (Biscay, grey) with corresponding correlation coefficient. Source: Castelle et al., 2017.

1.2.5 Future predictions of storminess

Future scenarios up to the year 2100 indicate mostly an increase in winter storm intensity over the North Atlantic and western Europe (Feser et al., 2014). However, future trends in total storm numbers are quite heterogeneous and depend on the model generation used (Lozano et al., 2004; Feser et al., 2014). These future predictions are naturally linked with climate change scenarios, and satellite observations indicate that changes in mid-latitude storm-track location and intensity may be acting as a positive feedback to global warming (Stephenson, 2006). Furthermore, the melt of

the Arctic sea ice due to global warming may have an impact on the strength of the storms with less sea ice leading to stronger storms and strengthening of the storm track north of the British Isles (Bader et al., 2011).

1.3 Storminess and coastal response along the Atlantic coast of Europe

1.3.1 Monitoring of coastal response

Coastal changes due to storms along the Atlantic coastline of Europe over the last decades or even centuries were documented and analysed using historical records (Garnier et al., 2018), historical maps (Pye and Blott, 2008) or aerial photography images (Castelle et al., 2018). These data are however relatively sparse and qualitative, or only provide a 2D view on coastal changes when quantitative. The first beach transects were obtained using a simple, rapid and low-cost technique proposed by Emery (1961), that only requires a measuring tape for measuring cross-shore distance and two graded rods for measuring vertical elevation changes. New survey technologies such as RTK-GPS (Real-Time Kinematic Global Positioning System) and coastal imaging (ARGUS) have facilitated analysis of spatial variability by allowing three-dimensional survey data to be collected both rapidly, at high spatial density and accuracy (approximately ± 3 cm). The conventional RTK-GPS surveys and image-derived shorelines were shown to have a comparable level of vertical accuracy to the conventional surveys (Harley et al., 2011). LiDAR (Light Detection And Ranging) technology is also now commonly used for coastal monitoring, but is suggested to be mainly used for large event-based changes (Sallenger et al., 2001) because of its

larger vertical error (approximately ± 15 cm). More recently, coastal monitoring using UAV (unmanned aerial vehicle) was developed (Brock et al., 2002; Turner et al., 2016) with vertical accuracy of ± 5 cm (Goncalves and Henriques, 2015). Satellite images were also recently and successfully used to study shoreline (García-Rubio et al., 2014; Luijendijk et al., 2018) or bathymetric (Capo et al., 2014) changes along coastal areas.

1.3.2 Temporal and spatial variability of coastline response to storms

Historical results in countries like the United Kingdom, France, Portugal and Italy showed that storm impacts were reported back in the 17th century (Garnier et al., 2018, Table 1.1). Monitoring of frontal dune erosion and accretion on the Sefton coast in northwest England over the past 50 years has revealed relatively high dune erosion rates at Formby Point 1958–1968 were associated with a relatively large number of storm tides (Pye and Blott, 2008). Furthermore, a relatively steady overall erosion trend was observed along the south west coast of France over the last 64 years with the dune restoration and management strategy being hypothesized to have limited the coastal erosion over the last decades (Castelle et al., 2018). Unfortunately, high-resolution (monthly) records of beach change exceeding 5 years along the Atlantic coast of Europe are extremely rare (Masselink et al., 2016). Ongoing multi-annual surveys over the north Cornish coast (UK, Masselink et al., 2015), the south Devon coast (UK, Ruiz de Alegria-Arzaburu and Masselink, 2010), the north coast of Brittany (France, Suanez et al., 2012), the south coast of Brittany (France, Dehouck

et al., 2009) and the Aquitaine coast (France, Castelle et al., 2015) showed that all beaches showed temporal and spatial variability in shoreline/sediment volume changes correlated with storm and waves records. Many factors account for this variability in coastal response to storms, including both the nature of the storm forcing and the characteristics of the coast (Cooper et al., 2004). Coastal areas respond differently when exposed to an individual or a cluster of storm (Lee et al., 1998; Karunarathna et al., 2014; Senechal et al., 2015; Splinter et al., 2014b), and the chronological order of storms within a cluster in terms of intensity can also play a key role (Coco et al., 2014; Senechal et al., 2015). The tidal stage during the peak of the storm can also affect the coastal impact of the storm (Anthony, 2013; Masselink et al., 2015), while the coastline orientation relative to storm tracks will affect the wave incident angle and therefore influences beach and/or dune response through its control on longshore sediment transport (Costas et al., 2005; Anthony, 2013; Castelle et al., 2015). In addition to the sensitivity of coastal response to the forcing factors, variability in beach response is also affected by the beach characteristics that act as controlling factors. Nearshore and offshore sandbank morphology were shown to create alongshore variability in beach response (Haerens et al., 2012), while a low-tide terrace beach was shown to be more responsive to storm waves than a dissipative beach (Qi et al., 2010). Prodger et al. (2016) also demonstrated that changes in grain size and sorting were related to periods of high steepness storm waves, while Loureiro et al. (2012) highlighted extreme beach erosion enhanced by the formation and persistence of megarips during storm conditions.

Given that temporal variability in coastal response is primarily driven by varying wave forcing and storminess, the correlations between storm activity and large scale climate indexes (NAO, WEPA) were also observed between the records of coastal changes and the same indexes. The beach state and nearshore bar configuration of Perranporth beach along the north coast of Cornwall (UK, Masselink et al., 2015), the oscillations of the Cap-Ferret spit-end (France, Nahon et al. 2015), the erosion and accretion phases at Vougot beach in North Brittany (France, Suanez et al., 2015), and the beach rotation at Start Bay along the south coast of Devon (UK, Wiggins et al., 2018), were all shown to be correlated with the winter NAO index. The increase in the shoreline erosion rate over the last decade along the Aquitanian coast (France, Robinet et al., 2016), on the other hand, was shown to be correlated to the WEPA index.

Table 1.1: Number of historical storm events with major damages in the analysed case study sites between 1600 and 2000. These are compared also with similar events that occurred between
2000 and 2016. Source: Garnier et al., 2018.

Century	17th	18th	19th	20th	2000–2016	Total
North Norfolk	2	4	2	3	1	12
Ria Formosa			4	4	3	11
Liguria	2		2	6	10	20
Porto Garibaldi	1	2	4	3	1	11
La Faute-sur-Mer		2	2	4	1	9
Total	5	8	14	20	16	63

1.3.4 Modelling coastal response to storms

Modelling coastal response to storms implies numerical analysis of the sediment transport and hydrodynamic processes involved. One of the earliest approaches to modelling shoreline retreat was the development of

the Bruun Rule, formulated under the assumption that all sediment remains within the active profile (Bruun, 1954), but this approach was strongly discussed with regards to its application (Cooper and Pilkey, 2004b). Morphological models simulating wave-related, current and sediment transport processes (Johnson et al., 1994; Johnson and Zyserman, 2002; Niemann et al., 2006), or more complex coastal hydrodynamics models (Horikawa, 1988; Sánchez-Arcilla and Lemos, 1990) were developed to simulate coastal processes. More recently, a robust and physics-based public-domain model that combined coastal hydro- and morpho-dynamic, XBeach, has been developed with which the various stages in hurricane impacts on barrier coasts can be modelled seamlessly (Roelvink et al., 2009). Since then, this model has been extensively calibrated and validated for many field or laboratory experiments along energetic coastal systems (McCall et al., 2010; Bolle et al., 2010; Splinter and Palmsten, 2012; Voudouskas et al., 2012b; Karunarathna et al., 2014; Dissanayake et al., 2014). XBeach models both inshore wave and tide hydrodynamics and the resulting sediment transport along a beach profile by solving shallow water equations, and offers the possibility to study beach response to extreme storms over hourly/daily time-scale.

The prediction of beach change, especially shoreline change, along sandy coastlines over time-scales spanning several years to decades have also been developed in recent years. Although some of the existing models generally include a considerable level of empiricism, and may be termed top-down or data-driven models (Avdeev et al., 2009; Cowell et al., 2003; Horrillo-

Caraballo and Reeve, 2010; Karunarathna et al., 2009; Różyński, 2003), other generalized models in shoreline prediction due to predominantly cross-shore sediment transport processes have been proposed (Yates et al., 2009; Davidson et al., 2010; Splinter et al., 2014a). These models, described as equilibrium models, concluded that a practical approach to hindcasting and potentially forecasting (Davidson et al., 2017) of multi-year shoreline variability may be developed from a combined consideration of the evolving disequilibrium state of a beach through time, and the rapidly-varying forcing caused by prevailing wave conditions. These core ideas build upon earlier disequilibrium concepts introduced by several authors; notable examples include the work of Wright et al. (1985), Plant et al. (1999) and Miller and Dean (2004), where the evolution of beach-state, sand bars and shorelines were examined, respectively.

1.4 The 2013/14 winter storms and coastal response along the Atlantic coast of Europe

1.4.1 Climatology of the 2013/14 winter

The extreme weather events recorded along the Atlantic coast of Europe during the 2013/14 winter were linked to a persistent pattern of perturbations to the jet stream over the Pacific Ocean and North America, and, although no individual storm can be regarded as exceptional, the clustering and persistence of the storms was highly unusual (Slingo et al., 2014). In the troposphere, the North Pacific jet was deflected a long way north, with a secondary branch extending southwards into the tropical

Pacific accentuating the separation of the Pacific and Atlantic jet streams (Fig. 1.6). The deflection of the jet to the north led to colder air being carried south over Canada and the northern US to enter the North Atlantic jet and establish a stronger than normal temperature gradient that strengthened the jet, to as much as 30% stronger than normal, and provided the conditions for active cyclogenesis (Slingo et al., 2014).

Above the troposphere, westerly winter winds in the polar night jet stream were very strong during the 2013/14 winter, with the polar night jet exceeding twice its normal strength at times. A strengthening of the polar night jet often precedes periods of a strong Atlantic jet stream below and a positive North Atlantic Oscillation pattern, as was seen during the whole December 2013 to January 2014 period (Slingo et al., 2014). Although internal fluctuations in the strength of the polar night jet cannot be excluded, the Quasi-Biennial Oscillation has also been an external factor in the current winter, again in the tropics, that has helped to precondition the system for a strong polar night jet. In the tropical stratosphere the winds circulate around the globe from west to east in some years and from east to west in others. This cycling of the tropical winds occurs roughly every two years - hence its name, the Quasi-Biennial Oscillation (QBO). Historical records show that when the QBO winds are westerly, this increases the chance of the positive phase of the North Atlantic Oscillation and a strong jet stream. The QBO was in an unusually strong westerly phase throughout the 2013/14 winter (Slingo et al., 2014).

In conclusion, the evidence suggests that the Pacific Ocean has been a major driver of the 2013/14 winter's severe weather, whilst the strong polar vortex

and its influence on the North Atlantic and Arctic Oscillation, potentially influenced by the unusually strong westerly phase of the QBO, was also an important contributor to the very strong North Atlantic jet stream. As yet, there is no definitive answer on the possible contribution of climate change to the recent storminess (Slingo et al., 2014).

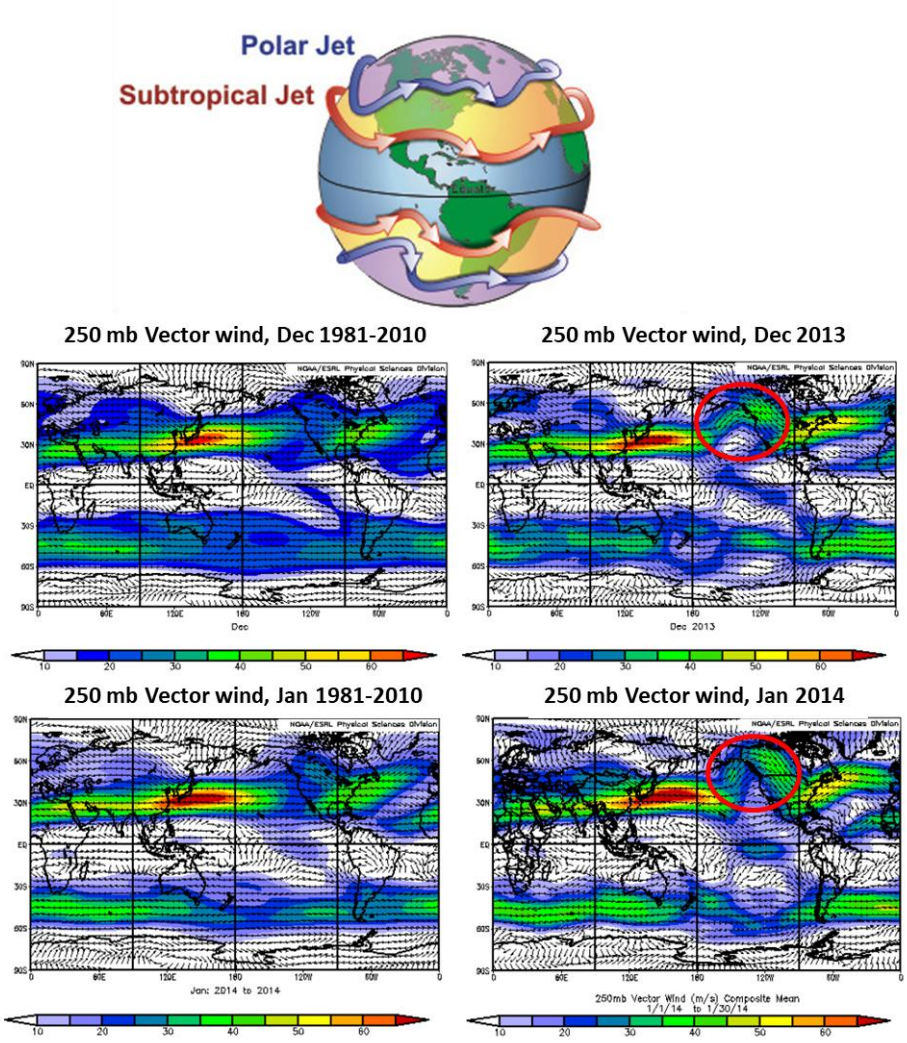

Figure 1.6: Climatological distribution of the winds in the upper troposphere at 250mb during December and January (left panels) and the actual distribution during December 2013 and January 2014 (right panels). Vectors show the direction of the winds and the colours indicate the strength of the winds (m/s). The deflection of the North Pacific jet during the 2013/14 winter is highlighted by a red circle. Source: metoffice.gov

1.4.2 The 2013/14 winter sequence of extreme storms

The 2013/14 winter was the most energetic winter along most of the Atlantic coast of Europe since at least 1948 (Masselink et al., 2016). Based on hindcast data derived from a regional implementation of the spectral wave model Wave Watch III along the continental shelf edge (1000m isobaths) from 1948 to 2015, the 2013/2014 winter ranks highest in terms of the winter-averaged significant wave height, with the exception of south Portugal and north Ireland (Fig. 1.7). The largest winter-averaged wave conditions (H_s=5–6m) were experienced off the coast of Brittany, southwest England, and south Ireland (Masselink et al., 2016). Shorter time series of observational wave data collected by wave buoys also demonstrated that the 2013/2014 winter represents the most energetic and that the number of storms and the total storm duration during that winter was generally at least 100% larger than the second most energetic winter (Masselink et al., 2016).

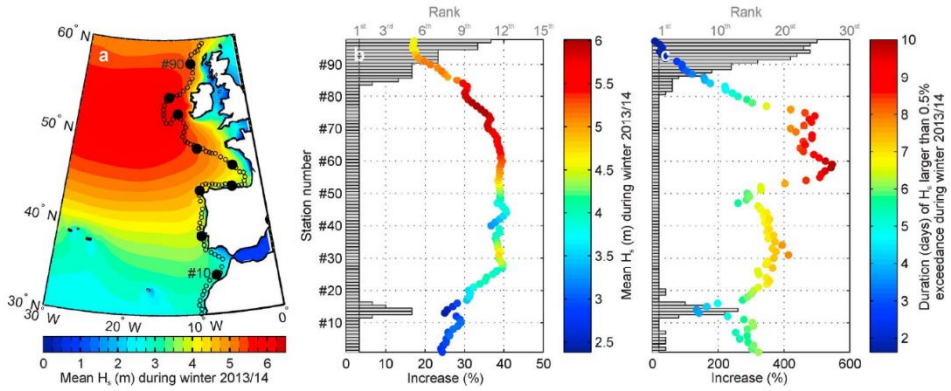

Figure 1.7: Spatial and temporal analysis of 67 years of Wave Watch III modeled wave data. (a) Location map of Atlantic coast of Europe with modeled average significant winter wave height H_s during 2013/2014 winter (DJFM) and location of model grid points along the continental slope (1000m contour line). Grid points run from North Africa (#1) to north Scotland (#97). (b) Winter-averaged significant wave height and (c) cumulative number of days with significant wave height exceeding the 0.5% exceedence level; the horizontal bars and symbols represent, respectively, the ranking and the percentage increase relative to the long-term average of the 2013/2014 winter. The colour of the symbols represents the value of the parameter plotted (refer to legend on the right of the panels). Source: Masselink et al., 2016.

For the two energetic storm events of 06/01/2014 and 01/02/2014, the centre of the storm wave field tended to be north of 50° latitude (Fig. 1.8), and these storms produced large and almost normal-incident waves along the north coast of Cornwall (Masselink et al., 2015), the north coast of Brittany (Blaise et al., 2015) and the southwest coast of France (Castelle et al., 2015). On the other hand, the two storms on 05/02/2014 and 14/02/2014 had the centre of the storm wave field south of 50° latitude (Fig. 1.6), and these storms created large waves along the south coast of Cornwall and Devon (Masselink et al., 2015), and the south coast of Britany (Blaise et al., 2015). Furthermore, both clusters of storms at the start of January and February in 2014 coincided with relatively large spring tides, enhancing large wave-driven set-up and runup along the coast (Masselink et al., 2015). On

the other hand, positive residuals related to storm surge play a minor role along the south west coast of England and rarely exceed 1m.

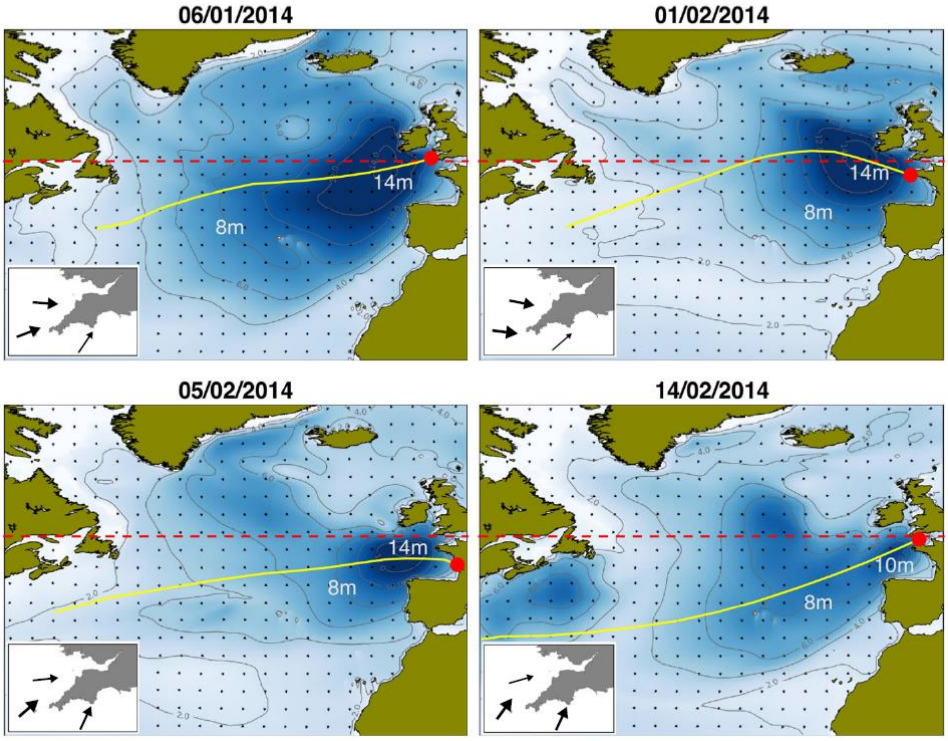

Figure 1.8: Significant wave height H_s prediction according to MetOffice wave model (WWIII) for the three storms having most impact that occurred during the 2013/2014 winter (06/01/2014, 05/02/2014 and 14/02/2014), and the storm with the largest offshore significant wave height (01/02/2014). The wave maps represent the time during which the storm waves peaked at the Sevenstones Lightship. The yellow line represents the track of the peak westerly-directed offshore wave height, the red circle its subsequent landfall, and the horizontal red line represents 500N latitude. The inset in each of the storm wave plots represents the south west coast of England with the arrows representing the inshore wave height (thickness and length of arrow) and direction modelled by the Met Office 8-km grid WWIII model for 20–30m water depth along the north coast, off the tip of Cornwall and along the south coast. Source: Masselink et al., 2015.

1.4.3 Coastal response to the 2013/14 winter sequence of extreme storms

High-resolution records of beach change along the Atlantic coast of Europe showed that storm impacts during the 2013/2014 winter were very

extensive (Masselink et al., 2016). The beach monitoring data reveal that Perranporth (Cornwall, UK), Slapton (Devon, UK), Vougot (North Brittany, France), Porsmilin (South Brittany, France) and Truc vert (Aquitaine, France) beaches after the 2013/14 winter were in their most depleted state since measurements began. Some of the beaches experienced a lowering of the beach profile relative to the mean profile of several meters, due to either dune erosion (Vougot, Truc Vert) or barrier retreat (Slapton Sands). Perranporth experienced a uniform lowering of approximately 0.5m across the entire intertidal profile (Masselink et al., 2016). The most exposed sites (Perranporth and Truc Vert) lost in excess of 200 $m^3 m^{-1}$ from the intertidal beach and dune system, and such storm response was observed to be typical of most exposed beaches along the coast of south west England and France during the 2013/2014 winter (Castelle et al., 2015; Masselink et al., 2015). The sediment loss was transported offshore, contributing to the subtidal bar systems (Castelle et al., 2015; Scott et al., 2016). Contrasting responses occurred at the more sheltered sites: Porsmilin lost 50 $m^3 m^{-1}$, but subaerial beach volume at Vougot was not much impacted. At Vougot, the coastal dune retreated by more than 5m (Blaise et al., 2015), but the sediment appears to have been retained within the intertidal zone. At Slapton Sands, the middle of the beach experienced a sediment loss of 100 $m^3 m^{-1}$, whereas accretion of a similar amount occurred at the north part of the beach. The beach response at this location is the result of an alongshore redistribution of sediment (Masselink et al., 2015), due to the south-to south westerly waves impacting on a southeast facing shoreline.

Furthermore, coastal cliff erosion from storm waves was observed along the south coast of Cornwall at Porthleven (UK) during the 2013/14 winter (Earlie et al., 2015). Cliff-top ground motions showed vertical ground displacements in excess of 50 – 100 µm, which is an order of magnitude larger than observations made previously. Cliff face volume loss was 2 orders of magnitude larger than the long-term erosion rate (0.1 m yr^{-1}).

1.5 Study area

1.5.1 Geology of the south west coast of England

Over 150 diverse beaches are spread along the south west coast of England and this diversity in coastal geomorphology was mainly attributed to the variety of rocks in England by Steers (1960). The large-scale solid geology, characterised by a decrease in age from west to east, forms the template of the overall coastal topography and the outline of the coast. The geology exerts its control on coastal morphology mainly through the resistance of the rocks to denudation and this explains the high-relief, mainly rocky coasts of west England, in contrast with the low-relief, mainly unconsolidated coasts of east England (Clayton and Shamoon, 1998). On a smaller scale, coastal landforms such as headlands, bays and inlets reflect contrasts in rock strength, and it is the local contrasts that lead to the detail and diversity of our coasts (May and Hansom, 2003). Devonian and Carboniferous slates, shales, sandstones and limestone were intensely deformed, and then intruded by highly resistant granite bodies (Clayton and Shamoon, 1998; Fig. 1.9). In addition to the solid geology, the drift geology is also important,

mainly a legacy of the most recent and penultimate glaciations, the Devensian and Wolstonian, respectively. During deglaciation, large quantities of glacial and paraglacial sediments, comprising the full spectrum of sediment sizes from mud to boulders, were left by the retreating glaciers. The coarser material, most of which was deposited on what is now the continental shelf has been transported onshore during the post-glacial transgression and has been incorporated in dunes, beaches, barriers and estuaries (Anon, 2002). This sediment source is now mostly depleted and offshore sediment supply to the coast by natural processes is very limited. However, most of the material that was deposited on what is now land is still present and represents an important sediment source to the nearshore system through cliff erosion (Bray and Hooke, 1997). The finer fractions of these eroded glacially-derived sediments (mud and silt) are being deposited on salt marshes and tidal flats in estuarine environments (Dyer and Moffat, 1998), while the coarser fractions (sand and gravel) enter the littoral system and are distributed along the coast (Scott, 2009).

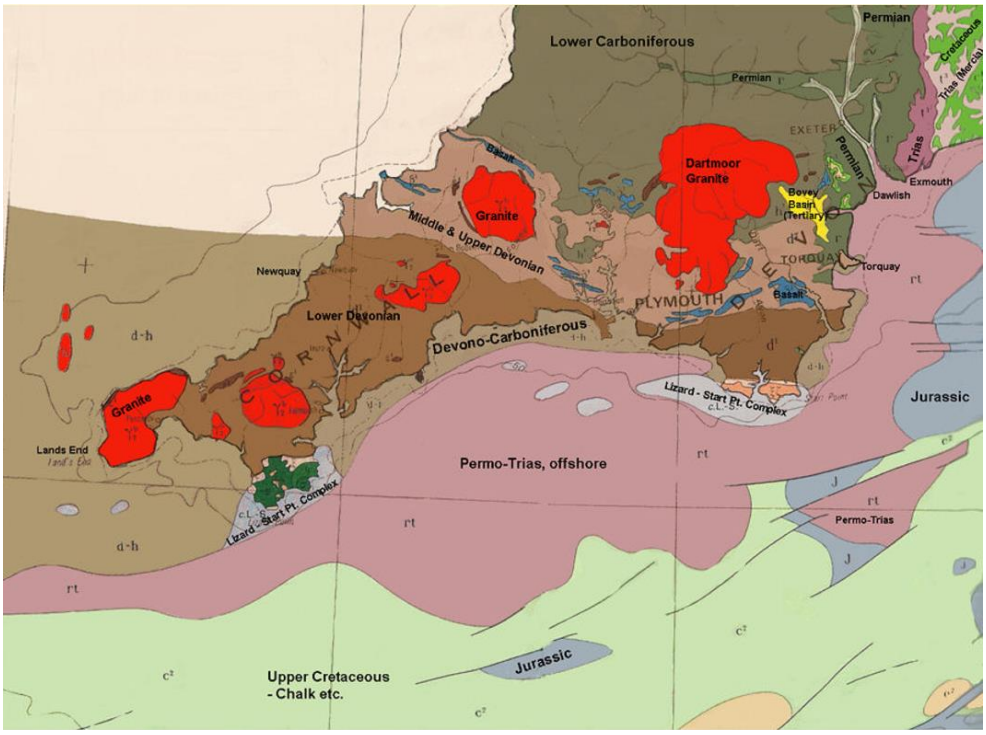

Figure 1.9: Generalised geological map of southwest England and the adjacent English channel. Source: Ian West, 2010.

1.5.2 Hydrodynamics along the south west coast of England

1.5.2.1 Sea level

Long-term coastal evolution is largely driven by changes in sea level (Zhang et al., 2002). At the end of the glacial maximum, around 18,000 years ago, sea level started to rise rapidly from around 120 m below present sea level, attaining its present level around 4,000 years ago (Fairbanks, 1989). The effect of this sea-level rise on the coastline of England must be considered in combination with the changes in the land level associated with glacio-isostatic effects, in particular isostatic rebound of the formerly glaciated areas in the north, and collapse of the forebulge of areas near the ice margin in the south. The post-glacial sea-level rise ceased about 4,000 years ago,

but over the last 130 years sea level has begun rising again by 0.2 m, equalling to a rate of rise of 1.5 mm yr^{-1} (Church and White, 2006) while the current rate of sea-level rise, based on a decade of satellite altimeter data, is 3.4 mm yr^{-1} (Nerem et al., 2018).

1.5.2.2 Tidal regime and wave climate

The tidal regime and wave climate exhibit a large spatial variability and play an important role in explaining the diversity in coastal landforms along the south west coast of England (Scott, 2009). The tidal range varies along the coast due to the presence of several amphidromic systems and the interactions between the tidal motion and the coastal topography. The largest tides occur in the Bristol Channel due to the 'funnelling effect' of the coastal topography. For the majority of the coast, the amplitude of the M2 tidal component is larger than 1.5 m and the mean spring tide range exceeds 4 m (Fig. 1.10).

Within England, the most energetic wave conditions are experienced in the southwest, where the 10% exceedance significant wave height ($H_{s,10\%}$) is larger than 3 m (Fig. 1.10) and the wave climate is a mixture of Atlantic swell and locally-generated wind waves (Scott, 2009). The influence of exposure to the Atlantic Ocean in the southwest of England increases the contribution of long-period, swell waves to the wave spectrum. The complexities of coastal orientation and exposure around the coasts of England and Wales lead to a dynamic balance of clearly defined high-/Iow-energy, and wind/swell wave components that is often characterised by a bi-modal wave energy spectrum with multiple directional sources in many regions

(Bradbury et al., 2004). Mean seasonal variation in wave climate is significant in many coastal regions with strong summer-winter wave energy variations (Scott, 2009).

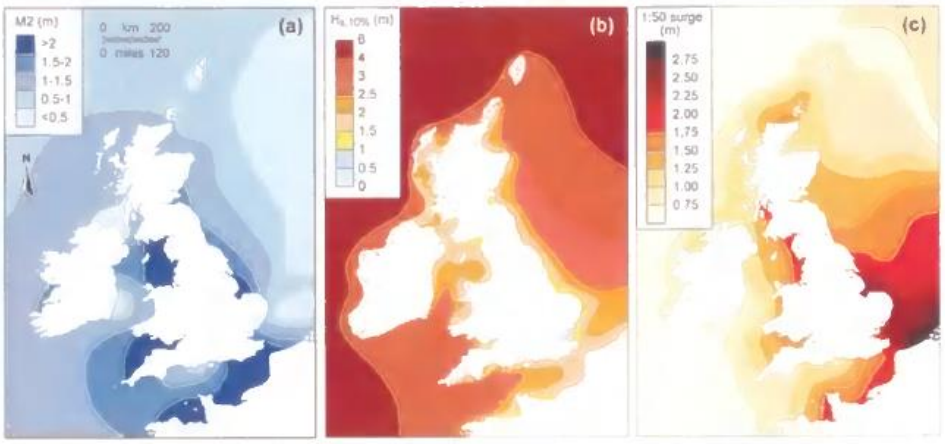

Figure 1.10: Map of Britain with: (a) M2 tidal amplitude (adapted from Proudman and Doodson, 1924); (b) 10% exceedence significant wave height, $H_{s10\%}$, (Draper, 1991); and (c) 1-in-50 year storm surge level (Flather, 1987). Source: Scott, 2009.

1.6 Aims and objectives

The central theme of this PhD research project is to analyse beach response and recovery to a sequence of extreme storms at different spatial and temporal scales, and to investigate the key factors forcing and controlling them. Additionally, the influence of large scale climatic variations in beach response and recovery is examined.

To achieve the above targets and to also improve the understanding and knowledge of beach response and recovery to extreme storms, a range of physical and digital field data have been used on a large number of contrasting beach sites at different temporal scales.

Two specific aims were defined:

1. Investigate the regional storm response to, and recovery from, the 2013/14 winter sequence of extreme storms along the south west coast of England.

2. Determine the key factors that force and control storm response and beach recovery along the south west coast of England using observed and modelled beach volume changes.

1.7. Structure of the thesis

This chapter gives an overview to the literature that relates to temporal and spatial variability in storm activity in the North Atlantic Ocean, along with its controlling mechanisms, and its impact on the Atlantic coast of Europe. The sequence of extreme storms during the 2013/14 winter were specifically detailed since it represents the core of the analyses presented within the following chapters. An overview of the geological and hydrodynamic characteristics of the south west coast of England where all study sites introduced in the following chapters are located is also presented. The various methods used to collect data are referred in each particular chapter.

In Chapter 2 the 2013/14 winter storm response of 157 diverse study sites located all around the south west coast of England using airborne LiDAR data is explored. Modelled offshore wave data and geological boundaries are used to explain the spatial variability in beach response.

In Chapter 3 the subsequent beach recovery to the 2013/14 extreme storms was investigated using multi annual time series of RTK-GPS data at 10 fully exposed beaches, that were shown to have lost some of the largest volumes of sediment in Chapter 2. An equilibrium model is also used to hindcast multi

annual and regionally-coherent beach behaviour, and climate-driven beach changes, are explored.

In Chapter 4, a process-based model is used to study the relative role played by the tidal conditions, the antecedent beach state and the presence of dune, defined as key factors for beach response to extreme storms in Chapter 3. The model was calibrated using RTK-GPS data measures of the 2013/14 storm response at Perranporth beach located along the north coast of Cornwall.

Chapter 5 provides a synthesis and the conclusions of Chapters 2, 3 and 4 and brings together the various themes that have been examined into a conceptual model that extends the forcing and controlling factors of beach response to extreme storms and recovery.

Chapter 2 – Classification of beach response to extreme storms

2.1 Introduction

Within the next decades, coastal areas will have to face human and environmental challenges such as climate change, sea level rise and growing population (Jackson et al., 2013). While climate change and sea-level rise are gradual and global processes, coastlines are also affected by extreme and regional-scale events, such as extreme storms or sequence of storms.

The majority of storms that affect European Atlantic coasts originate in the mid-latitude westerly wind belt and are referred to as extratropical storms (Lozano et al., 2004). Storminess in the Atlantic due to extra-tropical storms is strongly linked to the North Atlantic Oscillation (NAO; Bromirski and Cayan, 2015) and the West Europe Pressure Anomaly (WEPA; Castelle et al., 2017b), which are characterized by considerable inter-annual and inter-decadal variability. This temporal variability in atmospheric forcing is transferred to storminess and, in turn, to variations in the coastal response with short episodes of storm erosion alternated by longer periods of beach recovery (e.g., Scott et al., 2016). Coastal response to extreme storms is also characterized by significant spatial variability. Large-scale variability in storm response can generally be attributed to spatial variations in the hydrodynamic forcing (wave, tides and storm surge), but variability on a regional scale is more likely the result of site-specific conditions, such as beach type and/or local geology (Loureiro et al., 2012).

The extreme storm wave conditions in the Atlantic during the 2013/14 winter are considered the most energetic since at least 1948 (Masselink et al., 2016) and represent a recent example of the impact that large waves can have along the Atlantic coast of Europe. The wave conditions during this winter, specific to south west England, have been analysed by Masselink et al. (2015). They found that from October 2013 to April 2014, 22 storm-induced wave events, defined as events during which the peak significant wave height exceeded the 1% exceedance significant wave height, were recorded at the Seven Stones wave buoy 30 km off the tip of south west England. Wave conditions in these storms were outstanding, characterized by an average peak and mean significant wave height H_s of 8.1 m and 6.1 m, respectively, and peak wave periods of up to 22 s, and with an average storm duration of 29 hours. On average, 17 storm events (peak H_s>4 m) and 5 severe storm events (peak H_s>6m) occur annually (Scott, 2009). Two clusters of storms were associated with relatively large spring tides augmenting the storm surge (0.5-1 m), thus increasing storm wave impact at the coast. Most of the Atlantic coast of Europe, from Ireland to Portugal, was affected by these storms and their morphological impact on beaches has been well documented (Blaise et al., 2015; Castelle et al., 2015; Dissanayake et al., 2015; Masselink et al., 2015; Autret et al., 2016; Pye and Blott, 2016).

Beach response to extreme storms has been studied globally during the last decades and is naturally highly variable. Many factors account for this variability, including both the nature of the storm forcing and the characteristics of the coast (Cooper et al., 2004). Beach response to extreme storms is primarily dependent on the number of storms and their intensity.

Recent studies showed that beach erosion resulting from a cluster of storms can be more extensive than an individual storm (Lee et al., 1998; Karunarathna et al., 2014; Senechal et al., 2015; Splinter et al, 2014b). However, erosion tends to reduce in magnitude and reach an equilibrium during an extended storm phase despite high energy levels being maintained (Aagaard et al., 2012). The chronological order of storms within a cluster in terms of intensity can also play a key role (Coco et al., 2014; Senechal et al., 2015). Storm wave height and peak wave period can be combined to calculate the storm wave power as a key parameter for relating wave forcing to morphological response (Splinter et al., 2014b), and for defining a threshold for storm impact (Almeida et al., 2012). The tidal stage during the peak of the storm can also affect the coastal impact of the storm (Anthony, 2013; Masselink et al., 2015). Shoreline orientation relative to storm tracks will affect the wave incident angle and therefore influences beach and/or dune response through its control on longshore sediment transport (Costas et al., 2005; Anthony, 2013; Castelle et al., 2015). In addition to the sensitivity of coastal response to the forcing factors, variability in beach response is also affected by controlling factors such as beach morphology (Haerens et al., 2012), beach type (Qi et al., 2010) sediment size (Prodger et al., 2016) and geology (Loureiro et al., 2012).

Large-scale coastal change studies are relatively scarce (Barnard et al., 2015; Blaise et al., 2015; Masselink et al., 2016) and although better knowledge about beach response to extreme storms has been developed, many questions remain, such as the complex interplay between offshore wave characteristics, their transformation across the surf zone and pre-existing

bathymetry (Coco et al., 2014). Moreover, studies about storm impact on beach response are often limited by the quantity of data and focus on a relatively small stretch of coastline or a small number of beaches (e.g., Lee et al., 1998; Costas et al., 2005; Qi et al., 2010; Aagaard et al., 2012; Almeida et al., 2012; Anthony, 2013; Coco et al., 2014; Karunarathna et al., 2014; Senechal et al., 2015; Splinter et al, 2014b; Dissanayake et al., 2015; Castelle et al., 2015; Pye and Blott, 2016). The regional variability in the coastal response in south west England was of particular interest in recent studies (Masselink et al., 2015; Scott et al., 2016) where vastly different responses occurred to the same sequence of storms within south west England (Fig. 2.1).

Figure 2.1: Pictorial overview of storm impacts during the 2013/14 winter along the coast of south west England (same site numbering system as in Figure 2.2). (a) The gravel barrier at Westward Ho! #19 experienced overwash (photo: Richard Murgatroyd). (b1 before; b2 after) Large quantities of sand were removed from Whipsiderry beach #39, exposing the underlying rocky shore platform (photo: Mike Searle). (c) The seawall below Fistral Blu bar in Newquay #41 collapsed and causing damage to property (photo: Richard Murgatroyd). (d) The Watering Hole in Perranporth #46 required human interventions to protect the restaurant (photo from Mail Online, SWNS). (e) The coastal town of Looe #100 was flooded a number of times (photo: Nic Randall). (f) The coastal dunes at Thurlestone #119 experienced more than 5 m of erosion (photo: National Trust Southwest). (g) At the end of the winter, the beach in front of the seawall at Beesands #123 had completely disappeared. (h1 before; h2 after) The road that runs along the gravel barrier of Slapton Sands #124 became covered with gravel due to overwash (photo from BBC News, Press Association). (i) The most costly damage occurred to the London-Penzance railway line at Dawlish #139 (photo from BBC News, Press Association).

The south west coast of England has a wide variety of beach types, geological boundaries and hydrodynamic conditions (Scott et al, 2011), and provides an ideal natural laboratory to investigate the factors that control the spatial variability in coastal response of a relatively large region to the same sequence of extreme storms. In their analysis of extreme storm response along the south west coast of England, Masselink et al. (2015) and Scott et al. (2016) mainly used morphological data derived from RTK-GPS cross-shore profiles surveyed at 38 beaches, and broadly distinguished between

dominantly cross-shore and longshore beach responses. This chapter extends this analysis by utilising vastly superior spatial coverage provided by airborne LiDAR surveys collected before and after the 2013/14 winter on 157 beaches spread along the same coastline. The LiDAR data covers the entire intertidal beach area, enabling the response for each beach to be quantified in terms of a number of morphological change parameters, including net and gross volume change, and alongshore and vertical variability in the morphological response. A hierarchical clustering highlighted four key types of beach response, differentiated by the net intertidal beach volumetric change and longshore variability in beach response. Wave forcing proxies and geological variables were used to evaluate their role in causing the observed the regional variability in the coastal response.

2.2 Study area and datasets

2.2.1 Study area

Along the southwest coast of England, Devonian and Carboniferous slates, shales, sandstones and limestone were intensely deformed, and then intruded by highly resistant granite bodies (Clayton and Shamoon, 1998), producing a diverse coastal scenery. The area itself was not glaciated, but periglacial processes resulted in the production of large quantities of superficial sediments, occupying a full spectrum of sediment sizes from mud to boulders. This peninsula, which can be divided in north and south coast (Fig. 2.2), offers a large number of beaches, including long and wide sandy beaches, gravel barriers, small pocket beaches and beaches backed by extensive dunes systems or high rocky cliffs. The high diversity in beach

morphology is due to variable dynamic (waves, tides) and static (shoreline orientation, geology, sediment size and abundance, bar morphology) boundary conditions, and has led to the identification of nine distinct beach types ranging from fully reflective to ultra-dissipative beaches (Scott et al, 2011). Beach type was found to be mainly controlled by the average wave/tide conditions and sediment size characteristics, but geological setting was also found to play a significant role.

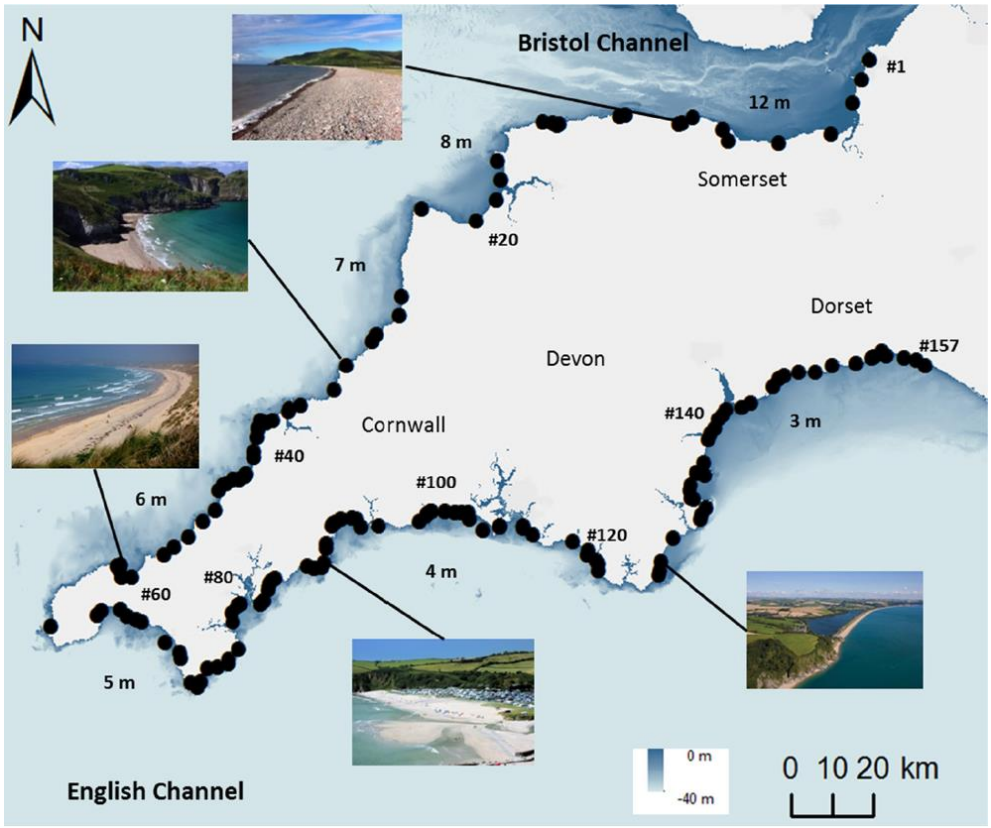

Figure 2.2: Map of south west England and location of the 157 beaches for which LiDAR data are available. Pictures of (anti-clockwise): Porlock #10, Bossiney #26, Hayle #51, Pentewan #90 and Slapton Sands #124, illustrating the diversity of beach systems along the south west coastline of England. Black numbers indicates the different tidal ranges along the coast.

For this study, 157 beaches are considered, numbered sequentially in an anti-clockwise direction, and the study sites are distributed fairly evenly

along the south west coast of England. They are located in the following five regions (Fig. 2.2).

Somerset (#1-16) – The first 16 sites are located along the southern margin of the Bristol Channel in Somerset. Waves are predominantly incident from the west with 10% exceedance significant wave height, $H_{s10\%}$, ranging from 1 to 2 m and the tidal range is the largest in the region (mean spring tide range 8 to 12 m) (BERR, 2008). The coastal geomorphology is characterized by rapidly eroding cliffs (Minehead #7) and the eastward longshore drift has result in a full suite of accretionary landforms: sandy beaches (Weston-super-Mare #2), storm ridges (Porlock #10), salt marsh (Steart #4), and sand dunes (Berrow sand #3) (Kidson et al., 2008).

North Devon (#17-21) – Proceeding along the coastline in an anticlockwise direction, 5 study sites are located in North Devon. The sites facing west are very large sandy beaches backed by imposing dune systems (at Croyde #17 and Saunton #18) while the sites facing north are relatively small beaches constrained between rocky platforms (Bucks Mills #20 and Shipload Bay #21). This stretch of coastline experiences a smaller tidal range (mean spring tide range from 7 to 8 m) and larger wave exposure from the west ($H_{s10\%}$ between 2 and 3 m) than the study sites in Somerset (BERR, 2008).

North Cornwall (#22-56) – The next 35 sites are located along the north coast of Cornwall which is characterized by sandy beaches with high cliffs (Bude #22), rocky headlands (Porthtowan #48) and several large coastal sand dune systems (Gwithian #51, Perran Sands #46). The mean spring tide

range decreases from north (7 m) to south (5 m) with $H_{s10\%}$ ranging from 2 to 4 m (BERR, 2008).

South Cornwall (#57-113) – Cornering the tip of the peninsula, the 57 sites spread along this stretch of coastline are highly variable, but mainly consist of coarser sand beaches interspersed by rocky sections (Penzance #58 and Marazion #59 for example). Beaches are more sheltered from wave energy coming from the west compared to the north coast of Cornwall, but some are fully exposed to SW wave energy (and also potentially from SE wind waves). Wave exposure is highly dependent on the shoreline orientation - which varies greatly along this stretch of coast. The mean spring tide range and 10% exceedance significant wave height generally decreases from west to east (5 to 4 m and 4 to 2 m, respectively) (BERR, 2008).

South Devon (#114-157) –The last 44 study sites are located in South Devon and Dorset. Similar to the south coast of Cornwall, the study sites along the western part of this stretch of coast consist of coarse-sand beaches interspersed by rocky sections (Challaborough #117, Milton Sands #120). Further east, a large number of thin and long beaches composed of a mixture of sand and gravel can be found (Slapton Sands #124, Sidmouth #146, West Bay #157). Shoreline orientation is also very variable and largely determines wave exposure. The mean spring tide range and $H_{s10\%}$ generally decreases from west to east (4 to 3 m, 2 to 1 m, respectively) (BERR, 2008).

2.2.2 LiDAR dataset

Commissioned by the Environment Agency (EA), the coastline of south west England is surveyed every few years by airborne LiDAR (http://www.channelcoast.org/southwest/). Different sections of the coast are surveyed in different years, almost always during the spring months, and the whole coast was surveyed in spring 2014 following the extreme events of the winter 2013/2014. Airborne LiDAR surveys are usually carried out during spring tides to maximise beach coverage. Every beach in south west England with at least 70% LiDAR coverage is used for analysis, resulting in 157 study sites spread out along the south west peninsula with 56 beaches located on the north coast and 101 on the south coast (Fig. 2.2).

Airborne LiDAR data has the advantage of offering a large spatial coverage and can be used to produce digital elevation models (DEMs) with at least 1-m horizontal spatial resolution, but in comparison to in-situ survey methods, the vertical accuracy of LiDAR is lower. Whereas RTK-GPS measurements have c. ± 3 cm vertical accuracy (Harley et al., 2011), the vertical accuracy of LiDAR data is c. ± 15 cm (Sallenger et al., 2001). However, many studies showed that the accuracy of LiDAR surveys does not impede the quantification of large morphological changes due to extreme events and its extensive spatial coverage makes it a valuable tool to study beach morphological change (White et al., 2003; Saye et al., 2005; Sallenger et al., 2001; Sherman et al., 2013; Pye and Blott, 2016).

Since LiDAR campaigns have not been carried out every year at each site, the timing of the 'pre-storm' datasets is an issue. The most recent pre-storm

surveys were carried out in April 2012, while the oldest pre-storm surveys dated from October 2010. First, using data collected over Spring or Autumn as the pre-storm dataset represents an issue for beaches that are exposed to a seasonal wave climate, often characterised by erosion in winter and accretion in summer. The north coast is more exposed to storm waves than the south coast, and topographic changes of beaches located along this stretch of coastline are largely influenced by winter conditions. Because the vast majority of pre-storm surveys at beaches located along the north coast were surveyed around Spring (post-winter), the few beaches with pre-storm surveys carried out in Autumn (pre-winter) were disregarded for this study. However, the most sheltered beaches located on the south coast with pre-storm surveys carried out in Autumn (pre-winter) were considered, since only very small seasonal topographic changes are observed at these sites and are negligible compare to the changes observed during the 2013/14 winter. Second, since this study focuses on the changes that occurred during the winter of 2013/14, for many beaches the pre- and post-storm datasets are more than 2 years apart. This makes attributing the difference in morphology to the 2013/14 storms potentially problematic. However, analysis of monthly survey data from Perranporth (North Cornwall) demonstrates that by far the most significant change in beach volume occurred during the 2013/2014 winter period along the north coast, and that the spring beach volumes during 2010, 2012 and 2013 were very similar (Masselink et al., 2016; Scott et al., 2016). Along the south coast, morphological changes observed at Slapton Sands (South Devon) observed during the 2012/13 winter were significant in comparison to the previous

winters, but relatively small compare to the 2013/14 winter (Scott et al., 2016). In addition, annual surveys collated/conducted by the Plymouth Coastal Observatory also demonstrate the unprecedented nature of beach profile changes at many beaches in Cornwall and Devon in 2013/14 (http://www.coastalmonitoring.org/reports). The changes in beach volume derived from the LiDAR data are therefore considered to represent mainly the changes that occurred during the 2013/14 winter.

Preparing the LiDAR data for analysis comprises a number of processing steps, ultimately leading to the extraction of overlapping pre- and post-storm DEMs corresponding to the active area of the beach. Figure 2.3 shows this process for two adjoining beaches located on the north coast of Cornwall (Fistral #42 and Crantock #43). LiDAR surveys generally extend from Spring Low Water Level to several 100s m landward and the beach area cannot be directly and easily identified (Fig. 2.3a). Therefore, using high resolution aerial pictures (Fig. 2.3b), every beach area was digitized by drawing polygonal shapefiles on ArcMap 10.2.2 software (Fig. 2.3c). The beach areas were digitized accurately and included the active beach/dune area based on tide and surge water levels, but excluded relatively static elements such as coastal cliffs, large rock outcrops and infrastructure. The beach area captured by these shape files did not extend beyond the spatial limitations of the LiDAR data. Then, using the same coordinate system (British National Grid Projected Coordinates System), both beach area shapefiles and LiDAR rasters were overlapped (Fig. 2.3d) and the overlapped data were extracted. The extraction is done twice (pre- and post-storm

rasters, using same beach area shape file) for each of the 157 beaches, and the post- and pre-storm rasters are subtracted to obtain a difference DEM, also referred as DoD (Wheaton et al., 2010) (Fig. 2.3e). These DoDs are then converted into ASCII files, to be next processed with Matlab R2013®. A GoogleEarth dataset for the 157 DoDs is also available online.

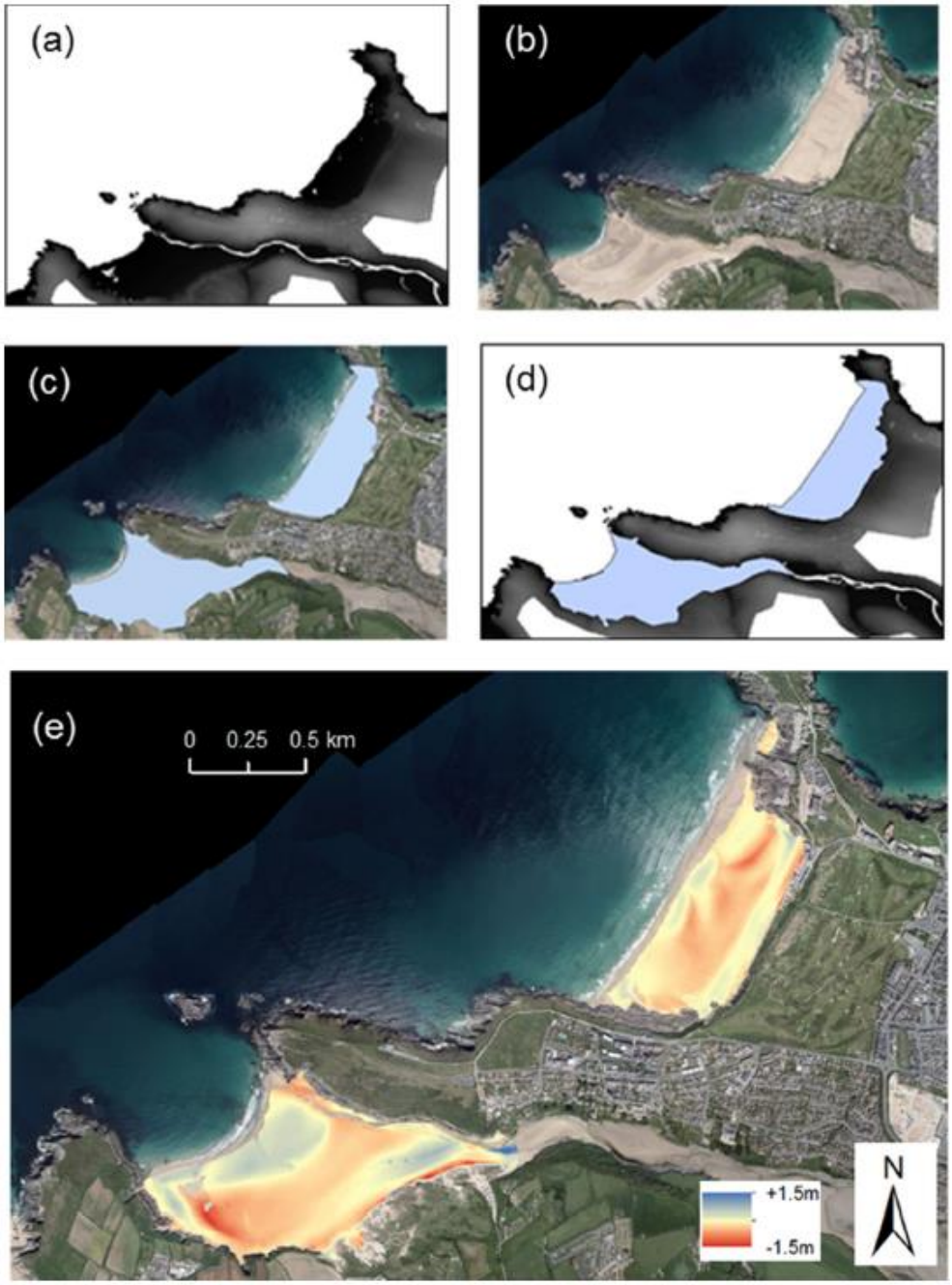

Figure 2.3: Illustration of the process of extracting useful data from the LiDAR titles: (a) raw LiDAR data; (b) aerial picture of the same area; (c) digitized shapefiles drawn around the two beaches (Fistral #42 and Crantock #43); (d) digitized shapefiles overlapped with LiDAR data; and (e) the image of subtracted new rasters of LiDAR data surveyed in April 2012 (pre-storm) and April 2014 (post-storm) at both sites.

2.3 Methods

2.3.1 Beach response variables

The DoDs were used to extract a range of parameters that best quantify the morphological storm response. The most obvious of these are the net volumetric change, the gross volumetric change and the vertical change.

The total volumetric change dQ_{tot} (in m^3) corresponds to the difference in beach volume between the post- and pre-storm DEM and quantifies the total volume of sediment lost or gained over the survey period, attributed to the 2013/14 storm season:

$$dQ_{tot} = \sum_1^N dQ_i \quad (2.1)$$

To compare the total volumetric change between different study sites, dQ_{tot} is normalized by beach alongshore length L_S (in m), yielding the net volumetric change per unit m beach width, dQ_{net} (in $m^3\ m^{-1}$ or m^2):

$$dQ_{net} = {}^1/_{L_S} \sum_1^N dQ_i \quad (2.2)$$

The gross volumetric change per unit meter beach width, dQ_{gross} (in $m^3\ m^{-1}$ or m^2) corresponds to the sum of the absolute value of topographic change between post- and pre-storm DEM normalized by the length of the beach L_S (in m):

$$dQ_{gross} = {}^1/_{L_S} \sum_1^N |dQ_i| \quad (2.3)$$

This variable represents the total volume of sediment that has been mobile along the beach during the 2013/14 winter period. The mean vertical

elevation change *dz* (in m) corresponds to the total volumetric change divided by the surface area of the active beach area *S* (in m^2):

$$dz = {}^{1}/_{S} \sum_{1}^{N} dQ_i \quad (2.4)$$

The net volumetric change per unit meter beach width for different areas of the beach was also calculated. The beach area was divided into three zones based on the tidal levels: (1) a lower beach area was defined as extending between the lowest level surveyed during LiDAR measurements (usually just above mean low water spring level MLWS), and mean sea level (MSL); (2) an upper area was defined between MSL and mean high water springs (MHWS); and (3) a supra-tidal area was defined between MHWS and the top of the active area of the beach/dune system. The volumetric changes corresponding to these three different areas (dQ_{lower}, dQ_{upper} and dQ_{dune}, respectively) were calculated using Eq.2.1 using the appropriate tidal level.

All morphological change parameters defined above disregard the alongshore variability in the beach response and a parameter was formulated to quantify the alongshore morphological variability, which can be considerable (Fig. 2.4a). The DoD rasters are first rotated onto a local coordinate system, such that the cross-shore and alongshore direction of the beach represent the x- and y-coordinate, respectively (Fig. 2.4b). The grid size of this rotated raster remains 1 m and the net volumetric change dQ_{cross} is determined for each cross-shore transect, providing information on the alongshore variation in the cross-shore volumetric change (Fig. 2.4c). Then, the standard deviation Q_{std} is used to quantify the amount of variation of all

the dQ_{cross} values. The longshore variation in the morphological response *LVI* is then defined as:

$$LVI = \frac{1}{\frac{|Q_{mean}|}{Q_{std}} + 1} \quad (2.5)$$

Where $|Q_{mean}|$ is the absolute value of the mean of dQ_{cross} values and is used to normalize Q_{std} values between the different beaches. This index is dimensionless and varies between 0 and 1 with higher values representing greater longshore variability in beach response. At beaches where storm waves caused large sediment transport in the cross-shore direction, dQ_{cross} values will be practically equivalent and show only small variation (Q_{std} close to 0) resulting in *LVI* values close to 0. On the other hand, for beaches where storm waves caused large alongshore sediment redistribution, dQ_{cross} values will be highly variable (Fig 2.4c), characterised by large Q_{std} values resulting in *LVI* values close to 1. Nevertheless, the parameter is not simply representing the ratio between longshore and cross-shore sediment transport, where *LVI* = 1 implied longshore sediment transport dominance, and *LVI* = 0 indicates cross-shore sediment transport is dominant. A non-zero value for *LVI* can also be caused by an along-coast variation in cross-shore sediment transport due to specific beach characteristics such as the presence of: a large rip current (Croyde beach #17), a large rocky platform (Widemouth #23), or an irregular dune system (Perran Sands #46). For this reason, a threshold value of LVI = 0.7 is used in the following analysis to differentiate cross-shore dominated sediment transport from longshore dominated sediment transport.

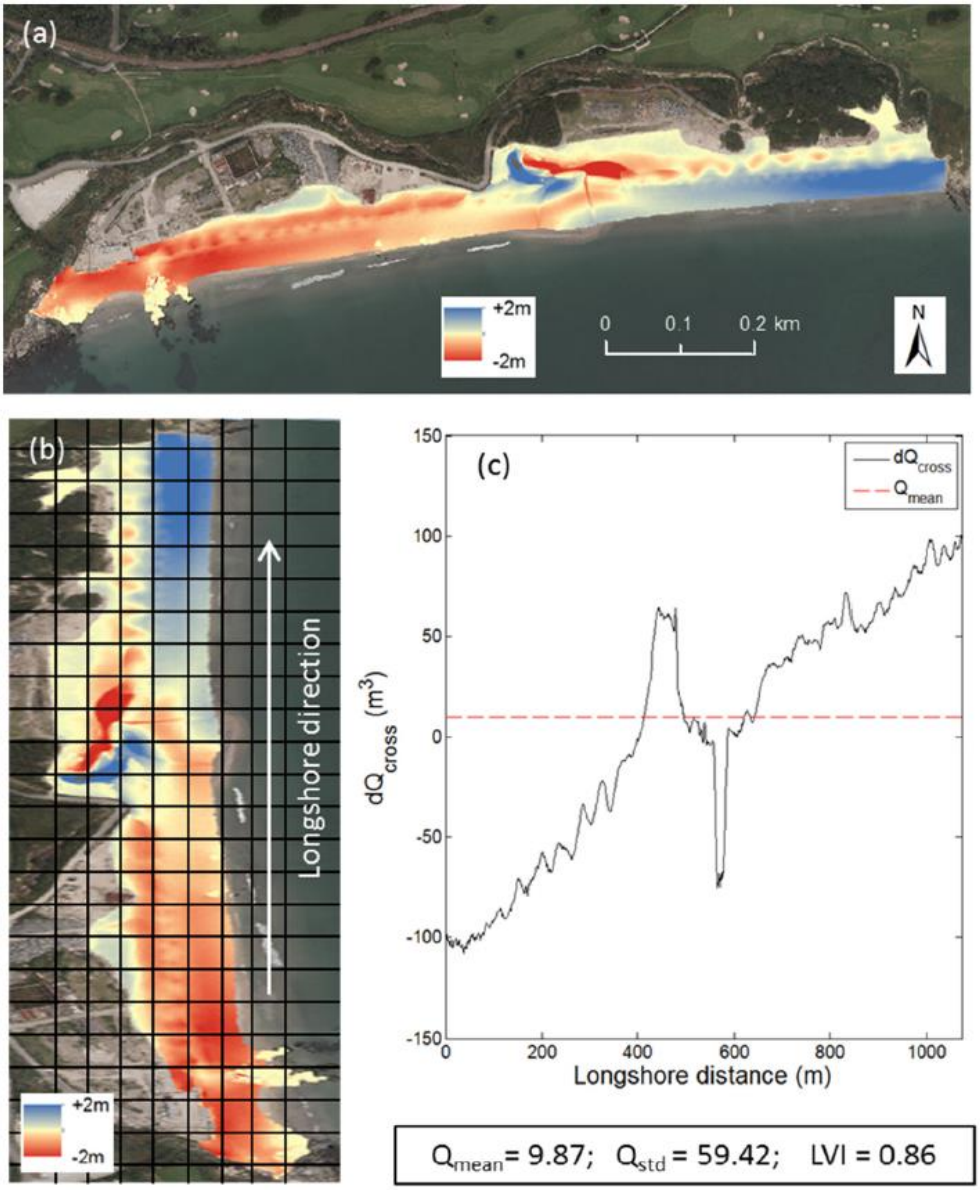

Figure 2.4: Illustration of the process of calculating longshore variation index (*LVI*): (a) example of DoD obtained when post- and pre-storm LiDAR rasters are subtracted at Carlyon beach #94 (surveyed in May 2014 and March 2012, respectively); (b) rotated DoD overlapped with a grid in which every row of data represents a 1 m cross-shore transect and every column a 1 m longshore one (not to scale for graphic purpose); (c) alongshore variation in the net cross-shore volumetric change dQ_{cross} with the alongshore-averaged change Q_{mean} plotted as a horizontal red line and values of the variables used in Equation 2.5.

2.3.2 Geological control

Geological boundaries can play an important role in beach dynamics (Jackson et al., 2005; Scott et al., 2011). To consider the impact of embayment dimensions and geometry on beach response, the dimensionless embayment scaling parameter is generally used (Short , 1999; Castelle and Coco , 2012; Loureiro et al., 2012). This parameter relates the embayment configuration to the incident breaking wave conditions. Here, due to the absence of inshore wave conditions data for every beach, the normalized beach length, *NBL*, was computed as the ratio between the beach alongshore length L_s and the cross-shore length L_c (from MLWS to MHWS):

$$NBL = {}^{L_s}/_{L_c} \tag{2.6}$$

'Short' embayed beaches are characterised by small *NBL* values approaching 1, whereas for 'long' beaches, *NBL* is larger by at least one order of magnitude . This parameter is applicable for the strongly-embayed coast of Cornwall and Devon where the most open beaches do not exceed 6.5 km, and the mean alongshore beach length for all study sites is equal to 1.3 km. This parameter would not be valid and tend to infinite values at coastal areas, where beaches extend over hundreds of kilometres with relatively small cross-shore lengths (e.g. south west coast of France, west coast of Denmark, etc.).

2.3.3 Offshore wave data and forcing

Modelled wave data were obtained from the Met Office's 8-km grid WAVEWATCH III model, one of the most frequently used model for wave simulation that has been validated for extreme events (Moon et al., 2003). 46 grid points located around the south west coast of England were selected for this study (Fig. 2.5). The water depths vary between 15 and 50 m dependent on the cell location, and grid points are considered to be in deep water. For each model grid point, hourly values of significant wave height H_s, wave energy period T_e, and wave direction were extracted for the 3-month period from 1 December 2013 to 28 February 2014, corresponding to 2160 hours of data for each grid point. For comparative purposes, wave data were also obtained from the relatively calm 2012/13 winter.

Offshore wave power P was used to quantify wave forcing and was calculated for every hour using the deep water wave equation (Herbich, 2000):

$$P = \frac{1}{64\pi}\rho g^2 {H_S}^2 T_e \tag{2.7}$$

Where ρ is water density and g is gravity. The offshore wave power P calculated at each grid point was averaged over the 3-month winter period and Figure 2.5a shows the distribution of the 2013/14 winter average wave power value $|P|$ along the south west of England. Generally, the north coast received more wave power than the south coast because it is more exposed to the prevailing waves approaching from the west. Along the north coast, $|P|$ increases from 20 kW m^{-1} to 100 kW.m^{-1} at the tip of the peninsula.

Along the south coast, $|P|$ decreases in an eastward direction from 90 to 10 $kW.m^{-1}$.

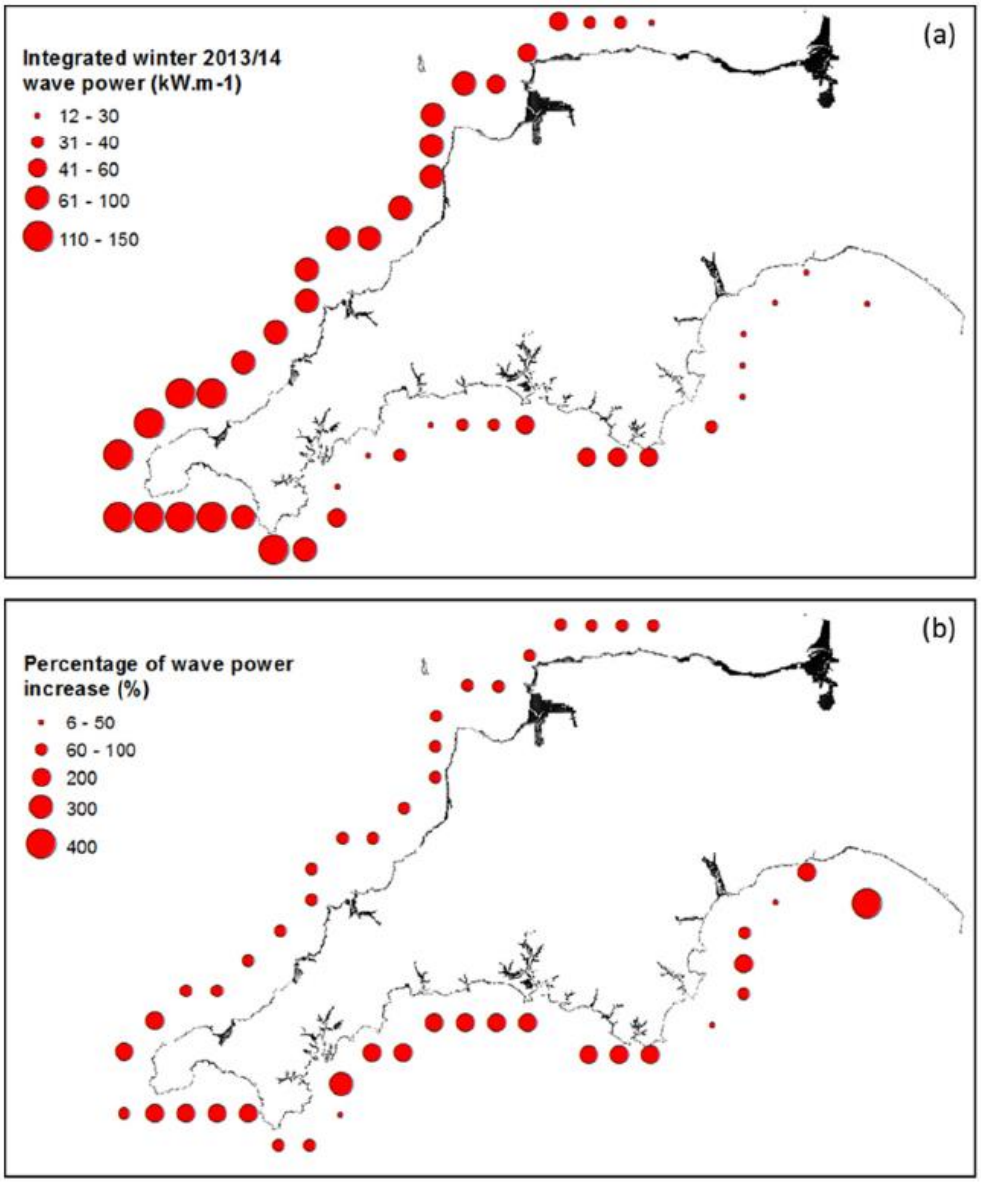

Figure 2.5: (a) Along-coast variability in modelled average winter 2013/14 wave power $|P|$ and (b) percentage of wave power increase relative to 2012/13 winter at 46 'deep-water' grid points along the south west coast of England.

Recent beach response models (e.g. Davidson et al., 2013; Castelle et al., 2014; Splinter et al., 2014a; Scott et al., 2016) have highlighted that wave conditions relative to the long-term antecedent wave conditions, referred to as disequilibrium wave conditions, are more important in driving beach

change than the instantaneous wave conditions. Based on the same wave variables and the same grid points, the percentage change in the average wave power over the 2013/14 winter period compared to that over the previous winter was calculated. The results show that wave power was around 100 % higher along the north coast during the 2013/14 winter while it was much more variable on the south coast with values ranging from no change to a 400% increase (Fig. 2.5b). Thus, whereas the actual wave power during the 2013/14 winter was higher along the north coast, the wave conditions along the south coast were generally more exceptional, i.e., in greater disequilibrium.

The south west coast of England offers a large range of wave exposure due to its specific geomorphology. Although offshore wave conditions are a good indicator of wave forcing at a regional scale, the impact on beaches is strongly dependent on storm wave direction and shoreline orientation (cf. Masselink et al., 2015). The relationship between the deep-water wave angle and shoreline orientation in determining the relative degree of wave exposure/shelter was considered in a semi-quantitative way. Each study site was associated with one of the 46 wave model grid points and in most cases, the study sites were associated to the closest model wave grid point. For areas where abrupt changes of coastline orientation (e.g. #19 - #21 and #51 - #54) or complex offshore bathymetry (e.g., #30 - # 35 and #120 - #124) are observed, the model grid point assumed to be the most appropriate was associated to the corresponding study site. Furthermore, minor differences in wave height, period and direction were observed between neighbouring

model wave grid points that are only distant of few km. The incident wave angle (0° angle correspond to shore-normal waves) between the variable offshore wave direction and the constant shoreline orientation was integrated over the 3-month winter period. Based on this angle, hourly wave power was decomposed into a cross-shore (normal to shoreline) and a longshore (parallel to shoreline) component. The cross-shore and longshore energy fluxes were subsequently integrated over the whole winter period. The objective of the decomposition into cross-shore and longshore wave energy fluxes is to provide an indication of the inshore wave conditions that are affecting the beaches without having to resort to developing a regional-scale wave propagation model (e.g. SWAN). There are issues with the decomposition of the offshore wave flux into cross-shore and longshore components when the wave approach is away from the coast (e.g., westerly waves approaching an east-facing coastline). In that case, the cross-shore energy flux was set to zero. For computing the longshore wave fluxes, absolute values were used for opposing directions.

Time series of the modelled wave conditions around the south west coast of England is also available within the GoogleEarth database from the online article.

2.4 Results

An initial analysis of the correlations between the different morphological response parameters for all the 157 beaches reveals that the net volumetric change is strongly and significantly correlated with all other volumetric variables (Table 2.1). Beaches that have experienced significant erosion

(dQ_{net} << 0) also show a large movement of sediment (dQ_{gross} >> 0) and a considerable lowering over their entire area (dz << 0), and vice versa. These relatively high correlation coefficients also show cross-shore uniformity in terms of response type: when the whole beach erodes (dQ_{net} < 0), both upper and lower beach areas are likely to erode as well (dQ_{upper} and dQ_{lower} <0; R = 0.75 and R = 0.88, respectively). However, the quantities of sediment lost or gained in the upper and lower beach area are weakly correlated (R = 0.34). There is no clear relation between the volumetric changes in the coastal dune area (dQ_{dune}) and the other volumetric changes. The alongshore variability in morphological response parameterised by *LVI* shows relatively modest correlation coefficients with the other variables and this index therefore fulfils its intended purpose by complementing, rather than duplicating, the volumetric change parameters.

Table 2.1: Pearson's correlation coefficients, R, between beach response variables (dQ_{net}: net volumetric change per unit m beach width; dQ_{gross}: gross volumetric change per unit m beach width; dZ: mean vertical elevation change; dQ_{upper}: net volumetric change per unit m beach width over the upper part of the beach; dQ_{lower}: net volumetric change per unit m beach width over the lower part of the beach; dQ_{dune}: net volumetric change per unit m beach width over the dunes; *LVI*: longshore variation index). Correlations exceeding the 99% confidence level are specified using bold text.

	dQ_{net}	dQ_{gross}	dZ	dQ_{upper}	dQ_{lower}	dQ_{dune}	LVI
dQ_{net}		**−0.78**	**+0.79**	**+0.75**	**+0.88**	**+0.38**	**+0.46**
dQ_{gross}			**−0.47**	**−0.56**	**−0.70**	**−0.25**	**−0.31**
dZ				**+0.49**	**+0.74**	**+0.43**	**+0.31**
dQ_{upper}					**+0.34**	**+0.47**	**+0.34**
dQ_{lower}						+0.14	**+0.41**
dQ_{dune}							+0.07
LVI							

The along-coast variation in dQ_{net} and *LVI*, and their geographical distribution along the south west coast are presented in Figure 2.6. The

results show that 104 (66%) beaches lost sediment, while the other 53 (34%) beaches gained sediment during the 2013/14 winter. Large volumes of sediment, of up to 100 - 200 m^3 m^{-1}, were lost at several study sites, but other sites experienced an increase in the sediment volume of up to 30 - 60 m^3 m^{-1} (Fig. 2.6a). On 59 (38%) beaches, the longshore variation index exceeded 0.7 while for the other 98 (62%) beaches, $LVI < 0.7$ (Fig. 2.6b). Visual observation of the LiDAR data reveals that for $LVI > 0.7$, the morphological response is characterised by a very significant longshore variability (cf. Fig. 2.4).

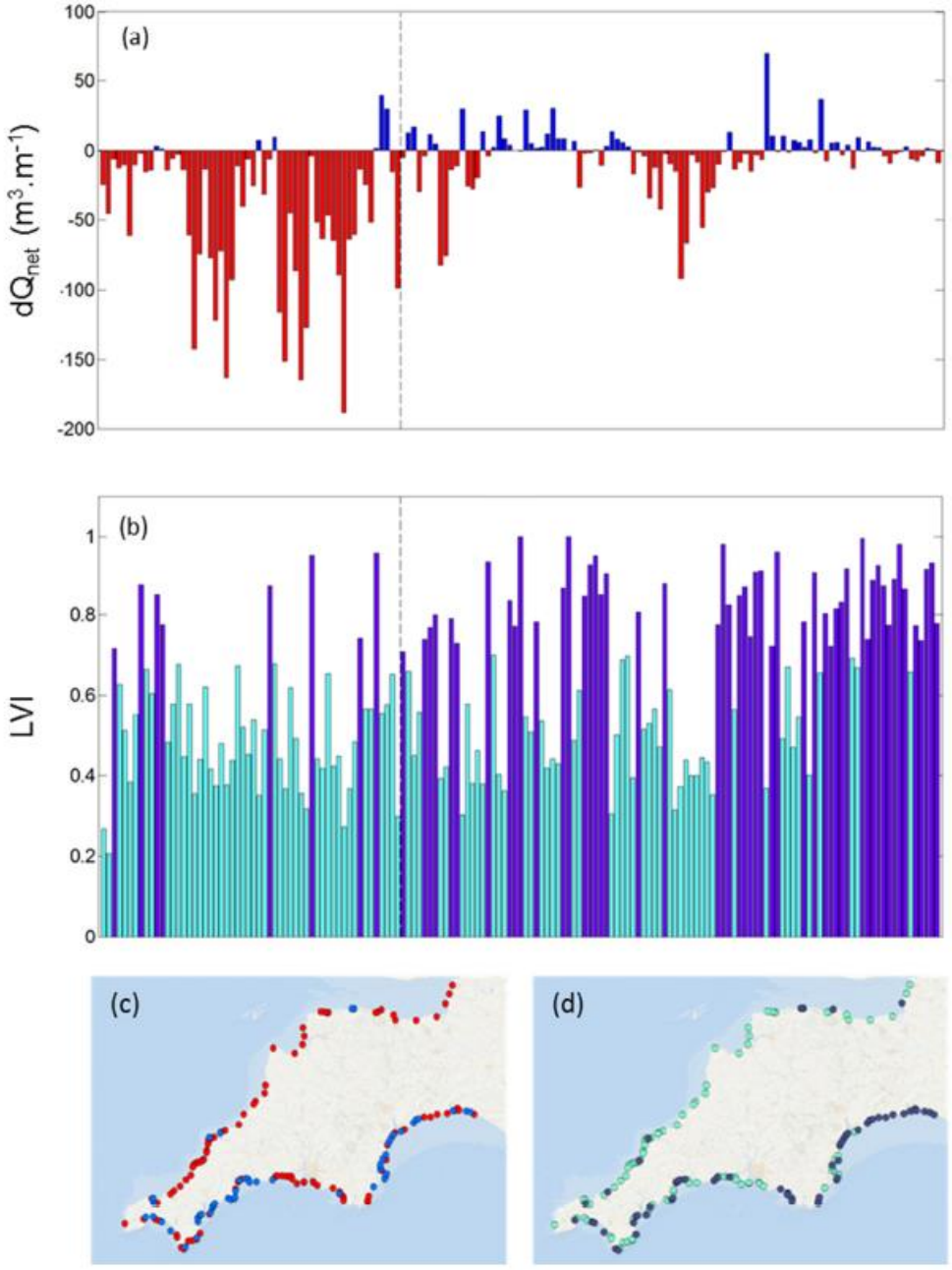

Figure 2.6: Along-coast variation in (a) net volumetric change per unit m beach dQ_{net} and (b) longshore variation index *LVI*. Every bar represents a study site and the sites are geographically ordered in an anti-clockwise direction from north to south. The black vertical dashed line marks the separation between the north and the south coast. Geographical distribution of (c) dQ_{net} and (d) *LVI* along the south west coast of England. The colours of the bars and the symbols represent: blue = $dQ_{net} > 0$; red = $dQ_{net} < 0$; clear blue $LVI < 0.7$; purple = $LVI > 0.7$).

The storm response parameters dQ_{net} and *LVI* also show a distinct geographical demarcation (Fig. 2.6c and 2.6d). Beaches located on the north coast generally experienced more erosion and a relatively along-shore

uniform coastal response. South coast beaches, on the other end, generally eroded less, or even accreted, and displayed considerably greater alongshore variability in the coastal response. Masselink et al. (2015) and Scott et al. (2016) also noted this regional variability in storm response and attributed this to the shoreline orientation in relation to the offshore wave direction. The dominant wave direction during the 2013/14 winter storms was from the west; therefore, the west-facing beaches (including WNW- and WSW-facing), dominantly located on the north coast, were fully exposed to the storm waves, causing extensive and largely alongshore-uniform erosion. On beaches not directly facing the Atlantic storm waves, mainly located on the south coast, the storm waves generally approached from large angles providing opportunity for alongshore redistribution of sediment, resulting in both relatively modest sediment losses and large alongshore variability in the coastal response. However, the relation between wave angle and shoreline orientation only accounts for part of the regional variability in storm response along the south west coast of England. This is further explored in the next section.

2.5 Grouping of the beach responses

2.5.1 Hierarchical clustering of the beach responses

Cluster analysis is a multivariate statistical technique for identifying structure within a dataset, and has been successfully employed for classifying beach types (Hegge et al, 1996; Travers, 2007; Scott et al, 2011). Here, the technique will be used to classify storm response characteristics.

A critical first step in the analysis is to define the variables used for identifying the clusters. Section 2.4 showed the suitability of the net volumetric change dQ_{net} and the longshore variation index *LVI* to quantify storm response. The other volumetric variables were all significantly correlated at a 99% confidence level to the net volumetric change (cf., Table 2.1) and were not included in the cluster analysis to avoid multi-collinearity issues. The second step is the standardisation of the two variables to assign them an equal weight. Dimensionless normal scores (Gower and Ross, 1969) were obtained by subtracting the population mean from the raw scores and then dividing the difference by the population standard deviation. The third step consists of finding a method to assess the similarity between the different study sites across the two variables used in the analysis. Euclidean distance was chosen to measure this similarity, with higher (lower) values representing greater (lesser) dissimilarity. Finally, the hierarchical clustering is made using the weighted pair group average method (UPGMA) which defines similarity between clusters as the shortest distance from any object in one cluster to any object in the other (Gower and Ross, 1969). This hierarchical procedure based on an agglomerative algorithm can be represented by a dendrogram (Fig. 2.7).

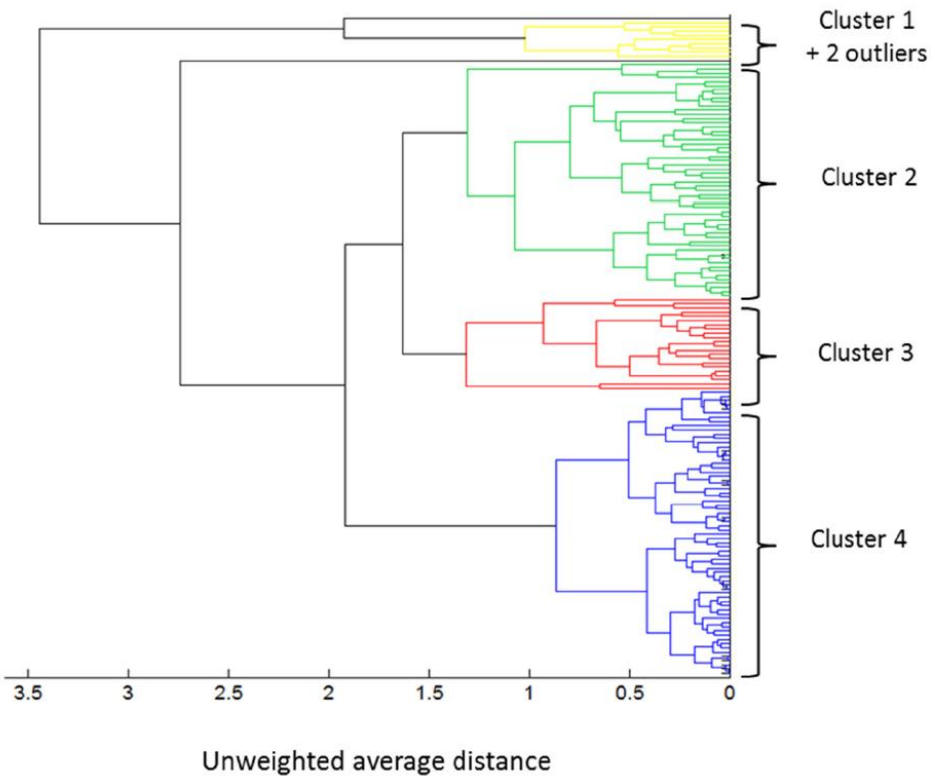

Figure 2.7: Dendrogram clustered using weighted pair group average (UPGMA) method showing the hierarchical clustering of the 157 beaches (Cluster 1 = Yellow; Cluster 2 = Green; Cluster 3 = Red; Cluster 4 = Blue).

Despite the statistical rigour of cluster analysis, there is an element of operator's experience, knowledge and understanding, especially when it comes to finalising the identified clusters and interpreting the results. A cut-off through the dendrogram and its different agglomeration levels were used to decide the final grouping of beaches. Although this cut-off level can seem arbitrary, it was selected based on the knowledge of the different study sites and the observation of the 157 LiDAR DoDs, leading to four different clusters and two outliers (Fig. 2.7). A less selective cut-off (*i.e.* larger value of the unweighted average distance) would reorganise the clusters with beaches in Clusters 2 and 3 being gathered in one cluster. This combination would be coherent on a numerical basis (nearest *LVI* values),

but not necessarily on a morphodynamical one. Most beaches in Clusters 2 correspond to rather dissipative beaches located on the north coast and therefore frequently exposed to storms waves, while most beaches in Cluster 3 correspond to low-tide terrace or reflective beaches that are located on the south coast and only rarely exposed to storm waves.

2.5.2 Characterisation of the clusters

Box plots of the dQ_{net} and *LVI* values for the four clusters (Fig. 2.8) are used in combination with examples of the DoDs (Fig. 2.9) to help interpret the different storm response types:

- Cluster 1 is characterized by the largest sediment losses (cluster-mean dQ_{net} = -108 m^3 m^{-1}) and the smallest average longshore variation index (*LVI* = 0.37). Watergate Bay located on the north coast is a good example of a Cluster 1 response, showing a large alongshore-uniform sediment loss across the entire supra- and inter-tidal beach disregarding rip channels (Fig. 2.9b).
- Cluster 2 is characterized by considerable sediment losses (cluster-mean dQ_{net} = -53 m^3 m^{-1}) and limited alongshore-variability in the morphological response (*LVI* = 0.44). This cluster is similar to the previous cluster, but with less extreme sediment losses. A good example of a Cluster 2 response is Croyde located on the north coast, where the deposition across the lower part of the beach profile partly balances the upper beach erosion (Fig. 2.9a).
- Cluster 3 is characterised by small net changes in the sediment volume (cluster-mean dQ_{net} = -3 m^3 m^{-1}) and some alongshore

variability in the morphological response (*LVI* = 0.51). Broadsands located on the south coast is a good example of a Cluster 3 response, showing limited net morphological changes because deposition (upper and lower beach) and erosion (mid-beach) are more or less balanced (Fig. 2.9c).

- Cluster 4 is very different from the previous three clusters in that the net volumetric change is very small (cluster-mean dQ_{net} = -1 m^3 m^{-1}) across all beaches in this cluster, but the alongshore variability in the morphological response is very large (*LVI* = 0.83). A good example of a Cluster 4 response is Praa Sands located on the south coast, where the erosion in the western part of the beach is almost completely balanced by the accretion at the eastern end of the beach (Fig. 2.9d).

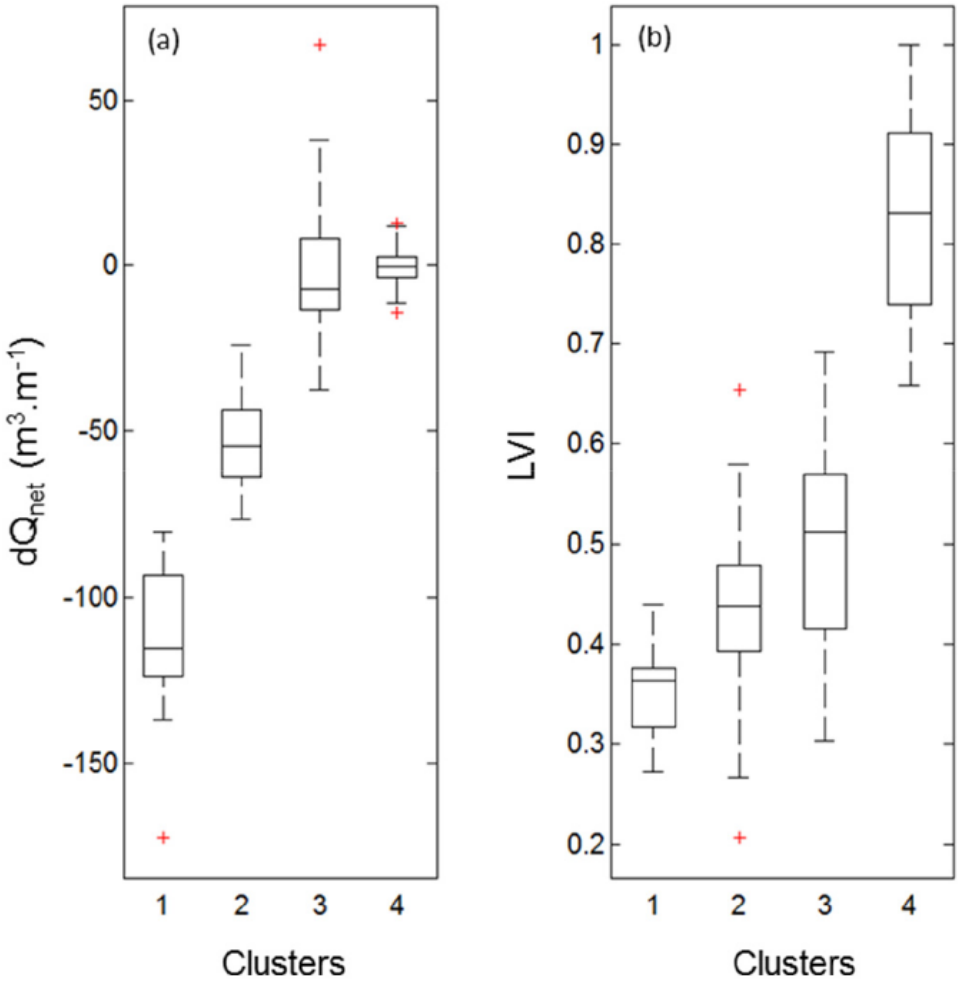

Figure 2.8: Box plots showing the distribution of (a) net volumetric change per unit m width dQ_{net} and (b) longshore variation index *LVI* among the four clusters defined by the cluster analysis. Each box plot displays the values of the 25% quantile (bottom line); the median (middle line); the 75% quantile (top line). The maximum whisker length is specified as 1.0 times the interquartile range, and data points beyond the whiskers are displayed using red crosses.

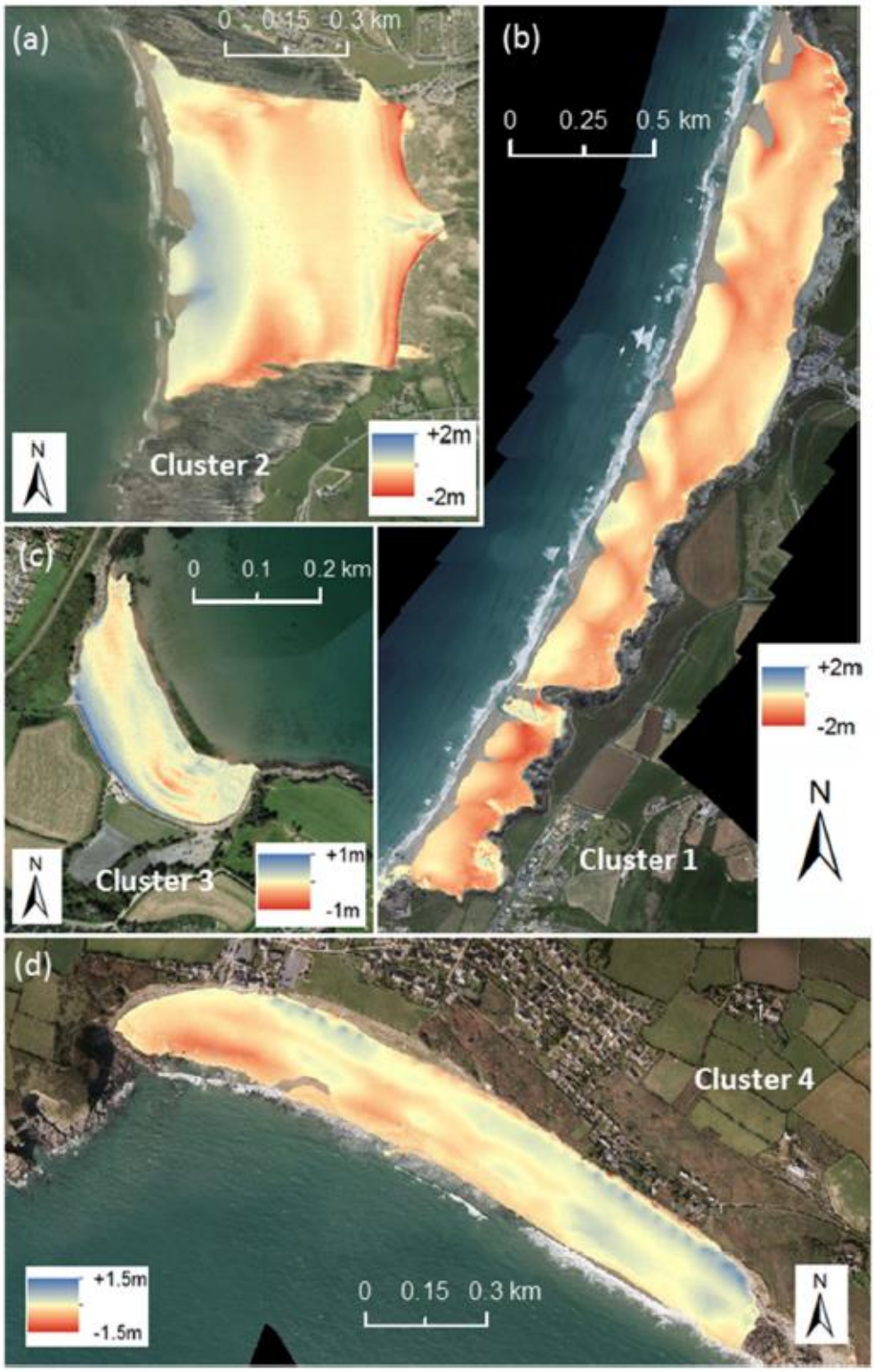

Figure 2.9: Examples of DODs obtained from LiDAR data at (a) Croyde beach #17 (Cluster 2 example) surveyed in May 2012 and June 2014; (b) Watergate Bay #39 (Cluster 1 example) surveyed in April 2012 and April 2014; (c) Broadsands #130 (Cluster 3 example) surveyed in April 2012 and April 2014; Praa Sands #62 (Cluster 4 example) surveyed in October 2010 and May 2014. Erosion is coloured in red whereas accretion is coloured in blue.

Sediment volumetric change was also considered at different levels on the beach (dQ_{upper} and dQ_{lower}). These response parameters were not included in the cluster analysis, because they did not contribute to a better definition of the clusters, but their consideration can shed additional light on the cross-shore sediment exchange for the different clusters. The values for dQ_{upper} and dQ_{lower} for all 157 beaches are plotted in a scatter diagram that comprises four distinct 'quadrants' (Fig. 2.10). The top-left and bottom-right quadrants represent a vertically non-uniform morphological response with a pivot point: the beach is either flattening (upper beach erosion – lower beach accretion) or steepening (upper beach accretion – lower beach erosion). The top-right and bottom-left quadrants represent a vertically uniform response: the beach either advances or retreats. The vast majority of the beaches in Clusters 1 and 2 eroded and are located in the bottom-left quadrant, indicating that both upper and lower beach areas lost sediment. It is suggested that these beaches mainly lost sediment offshore due to cross-shore sediment transport processes. Beaches in Cluster 3 are located tightly around the origin, but are spread across all four quadrants, suggesting that the full range of cross-shore responses are represented, including vertical rotation due to cross-shore sediment exchange. Beaches in Cluster 4 are concentrated even closer around the origin of the diagram because the dominant sediment exchange occurred in an alongshore direction without large net changes in the sediment volume. Furthermore, some beaches in Cluster 4 are spread along a diagonal crossing the top-left and bottom-right quadrants, suggesting some vertical beach rotation superimposed on the alongshore variability captured by the *LVI* parameter.

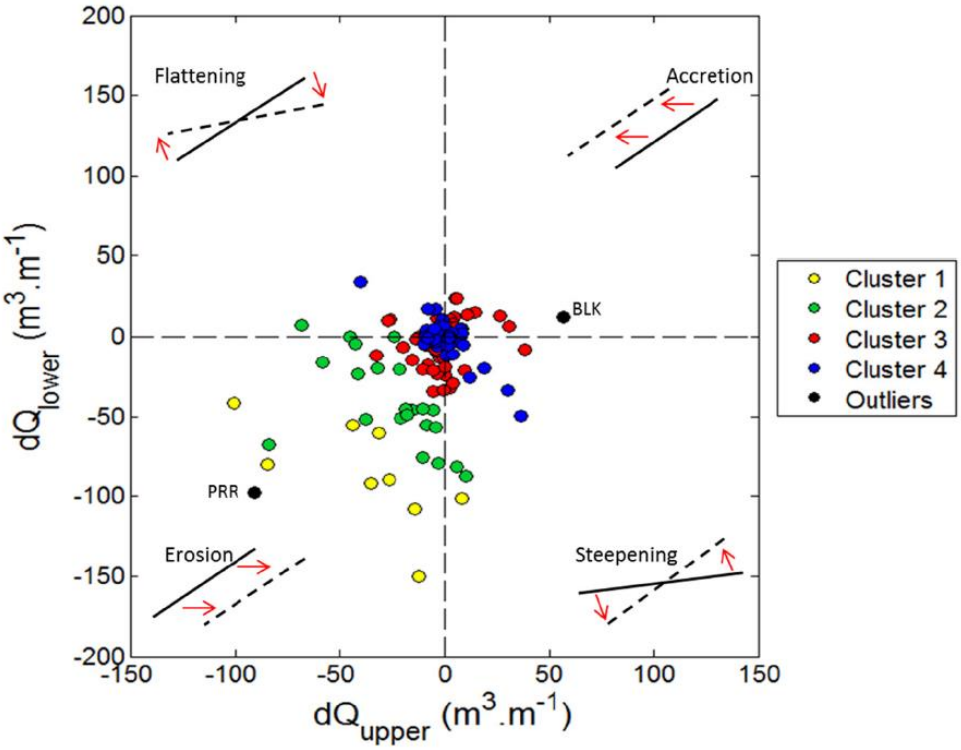

Figure 2.10: Scatter plot of dQ_{upper} and dQ_{lower} with the symbol colour representing the cluster type (Cluster 1 = Yellow; Cluster 2 = Green; Cluster 3 = Red; Cluster 4 = Blue; Outliers = Black with PRR = Perran Sands #46 and BLK = Blackpool Sands #125). The diagrams in the corners of the plot are schematic profile responses typical for each of the quadrants, with solid and dashed line representing the profile before and after the 2013/14 winter storms, respectively.

2.5.3 Role of wave forcing, sand dunes and geology

The cluster analysis is based on the morphological response and does not consider the role of wave forcing or geology. Box plots of three different variables representing wave forcing and geological setting for the four clusters are used to relate these boundary conditions to the different storm response types (Fig. 2.11, top panel).

The parameters used are: incident wave angle (0° angle correspond to shore-normal waves) (Fig. 2.11a); cross-shore wave power (Fig. 2.11b); and the normalized beach length NBL (Fig. 2.11c). Cluster 1 is characterized by the

smallest incident wave angles (c. 10°) and highest values of cross-shore wave power (c. 170 $kW.m^{-1}$), and these beaches are considered 'fully exposed' to the prevailing storm swell. Cluster 2 shows larger incident wave angles (c. 20°) and relatively more moderate cross-shore power (c. 120 $kW.m^{-1}$), also characterised by a higher standard variation for both parameters. Cluster 2 beaches are considered 'semi-sheltered' in comparison to Cluster 1 beaches. Clusters 3 and 4 are characterized by the largest incident wave angles (60 and 55°, respectively) and the smallest cross-shore wave power (30 and 25 $kW.m^{-1}$, respectively). Beaches classified in these two clusters are thus considered 'sheltered' in comparison to Cluster 1 and 2 beaches.

Cluster 1, 2 and 3 show relatively equivalent mean NBL values (4, 3.5 and 3.5, respectively), while Cluster 4 clearly shows higher mean values (8.5) and a larger standard deviation. Cluster 3 and Cluster 4 beaches were therefore separated in two categories: sheltered short and sheltered long beaches, even if some Cluster 4 beaches are also relatively short.

The increase in the wave power during the 2013/14 winter compared to the 2012/13 winter, the longshore wave power and the sediment volume changes over the dunes (dQ_{dunes}) were also parameterised but no clear distinction between the 4 clusters seemed to emerge and were therefore excluded from the analysis.

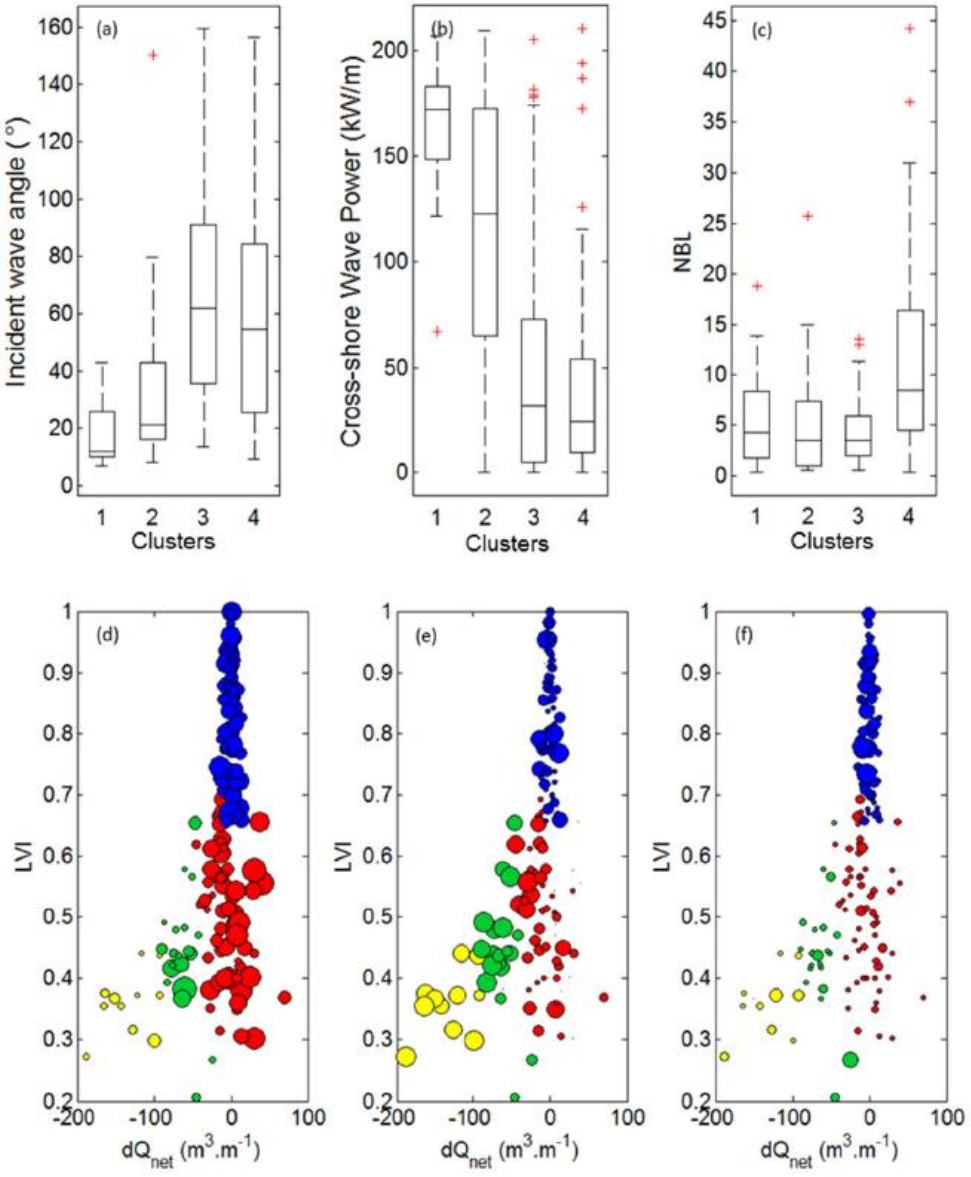

Figure 2.11: Top panel: box plots showing the distribution of (a) incident wave angle, (b) cross-shore wave power, (c) normalized beach length among the four clusters defined by the cluster analysis. Each box plot displays the values of the 25% quantile (bottom line); the median (middle line); the 75% quantile (top line). The maximum whisker length is specified as 1.0 times the interquartile range, and data points beyond the whiskers are displayed using red crosses. Bottom panel: scatter plots of net volumetric change dQ_{net} and longshore variation index *LVI* with the symbol colour representing the cluster type (Cluster 1 = Yellow; Cluster 2 = Green; Cluster 3 = Red; Cluster 4 = Blue). The symbols are scaled according the different variables (a) incident wave angle; (b) cross-shore wave power; (c) normalized beach length.

2.6 Discussion

The wave conditions experienced during the 2013/14 winter along the Atlantic coast of Europe represent the most energetic since at least 1948 and have had a very significant impact on the coastline of Western Europe (Masselink et al., 2016). A limited data set of the 2013/14 winter storm response on 30 beaches in south west England, based on cross-shore profiles, was discussed by Masselink et al. (2015) and highlighted the predominantly cross-shore profile response on the north coast and longshore response on the south coast. Here, we considerably extend this analysis by using LiDAR data to investigate the full-beach storm response of more than 150 beaches. New parameters such as *LVI* and *NBL* were also proposed as proxies for exploring the alongshore variability of storm response to storms and the influence of geological boundaries to control the magnitude of the storm response.

The LiDAR data were used to derive various morphological response variables for each of the beach sites and two of these, the net volumetric change dQ_{net} and the alongshore variability in the beach response *LVI*, were used as the basis for a cluster analysis. Four clusters, each representing distinctive morphological responses during the 2013/4 winter period were identified: (1) fully exposed beaches that experienced large and alongshore uniform sediment losses; (2) semi-exposed beaches that experienced medium alongshore uniform sediment losses; (3) sheltered short beaches that experienced limited alongshore variability in beach response, but insignificant net sediment change; and (4) sheltered long beaches that

experienced considerable alongshore variability in beach response, but insignificant net sediment change. However, this classification applies to the beach response to a sequence of Atlantic storms from the southwest quadrant and is unlikely to be representative for the beach response to less frequent storms coming from any of the other directions. The geographical distribution along the coast of south west England of these beach response types and their main characteristics are presented in Figure 2.12 and Table 2.2, respectively.

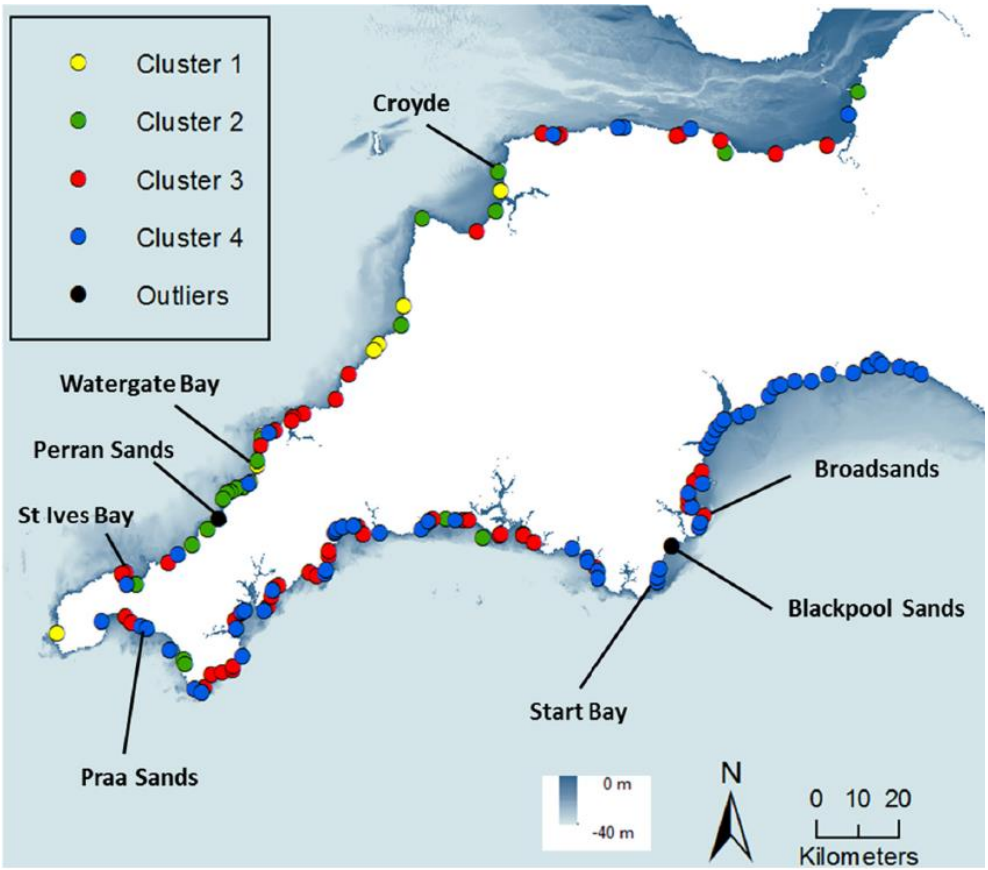

Figure 2.12: Geographical distribution of the 157 beaches in the LiDAR dataset and their cluster type (Cluster 1 = Yellow; Cluster 2 = Green; Cluster 3 = Red; Cluster 4 = Blue; Outliers = Black). The four beach examples presented earlier (Fig. 2.9.) and the two bays presented later (Fig. 2.13) are also located.

Table 2.2: Average values of net volumetric change dQ_{net}, longshore variation index *LVI*, incident wave angle, cross-shore wave power and beach normalized *NBL* for the four beach responses identified: (1) fully exposed beaches; (2) semi-exposed beaches; (3) sheltered short beaches; and (4) sheltered long beaches.

	dQnet ($m^3 \cdot m^{-1}$)	*LVI*	Inc. wave angle (°)	Cross-shore wave power ($kW \cdot m^{-1}$)	*NBL*
Fully exposed beaches	~−100	~0.4	~10	~170	~4
Semi-exposed beaches	~−50	~0.45	~20	~120	~3.5
Sheltered short beaches	~0	~0.5	~60	~30	~3.5
Sheltered long beaches	~0	~0.8	~55	~25	~8.5

On a regional scale, this chapter showed that one of the key factors that discriminates between the different storm responses is the orientation of the beach in relation to the prevailing wave direction, in other words, the degree of exposure to storm waves. This agrees with the findings of Blaise et al. (2015), who investigated beach response along the coastline of Brittany in France during the 2013/14 winter and found that the north and south Brittany coast responded differently to storm waves with varying direction. Furthermore, Castelle et al. (2015) reported dune retreat in excess of 10 m and net volumetric changes > 100 m^3 m^{-1} along the exposed south west coastline of France (Gironde, Landes) and this was similar to the storm response observed along the fully exposed beaches on the north coast of Cornwall. The relatively less-exposed Sefton coast (northwest England) suffered from similar net volumetric changes (c. 40 m^3 m^{-1}; Pye and Blott, 2016), compare to the semi-exposed beaches presented in this chapter. Along the south coast of the study area, the prevailing oblique wave approach due to the predominant W-SW storm tracks is very likely to have induced clockwise beach rotation on many of the beaches, similar to that observed at Slapton Sands #124 by Ruiz de Alegria-Arzaburu and Masselink

(2010). Such rotational behaviour has also been demonstrated in other studies of large embayed beaches (e.g., Ojeda and Guillen, 2008; Turki et al., 2013; Thomas et al., 2015). A second type of beach rotation, not induced by obliquely-incident waves but by an alongshore gradient in the wave energy level (Harley et al., 2015), was also observed at a few sites on the north coast of Cornwall.

However, the degree of wave exposure was not the only factor in controlling the beach response type to extreme storm activity. Several studies (Jackson et al., 2005; Short , 2010; Loureiro et al., 2012) have argued that the presence of physical boundaries can significantly affect sediment transport and morphodynamics. In the present chapter, this is particularly highlighted by the difference in storm response between short and long beaches subjected to similar wave exposure along the south coast. Whereas the short beaches experienced limited beach erosion, or even net accretion, and a largely alongshore-uniform response, the long beaches displayed contrasting responses at opposing ends of the embayment.

The geographical distribution of the different types of beach response along the south west coast of England shows regional coherent behaviour: cross-shore sediment transport is dominant on the north coast, whereas beach rotation largely occurs along the south coast. Studies along the East coast of Australia also showed the existence of regionally coherent behaviour among similar beaches exposed to the same regional-scale wave and climate forcing (Short et al., 2014; Bracs et al., 2016). However, this coherence can be disrupted by significant changes in the shoreline orientation and/or local

factors (e.g., islands, headlands, rock platforms, river outflows). St. Ives Bay, located on the north coast, exemplifies such a spatial change in beach response (Fig. 2.13). Here, the bay includes four sandy beaches, separated from each other by headlands and the Hayle River (Fig. 2.13a), and from north-east to south-west these beaches change in orientation from facing NW to NE. The difference in wave exposure during the 2013/14 winter therefore resulted in neighbouring beaches exhibiting contrasting response types with one Cluster 2 beach (Gwythian #51), two cluster 3 beaches (St Ives #53, Porthgwidden #54) and one cluster 4 beaches (Carbis #52).

The accretion of many of the Cluster 3 beaches during extreme storm conditions also raises the question of the sediment connectivity between adjacent beaches in the same embayment. This is further illustrated by the response of the gravel beaches in Start Bay, located on the south coast (Fig. 2.13b). Each of these gravel beaches are a separate entity over the most of the tidal cycle and they appear to have behaved independently during the 2013/14 winter with three of the four beaches (Hallsands #122, Beesands #123 and Slapton Sands #124) clearly rotating in response to northward littoral drift. However, the northern-most beach (Blackpool Sands #125) demonstrated very considerable accretion (dQ_{net} = 66 m^3 m^{-1}) across its entire length and was in fact one of the two outliers in the cluster analysis. The reason for the large increase in sediment volume on Blackpool Sands is that sediment transported northward on Slapton Sands, bypassed the rocky stretch between the two beaches. This process of headland by-passing (Goodwin et al., 2013; Keshtpoor et al., 2013; Mortlock and Goodwin, 2016;

Vieira da Silva et al., 2016) is considered important along the embayed south west coast of England and is currently the subject of further investigation.

Figure 2.13: DoDs obtained from LiDAR data along (a) St. Ives Bay beach surveyed in April 2012 and April 2014, and (b) Start Bay surveyed in April 2012 and April 2014, illustrating spatial change in beach response and sediment connectivity between adjacent beaches at a local scale. Their location along the south west coast of England is presented in Fig. 2.12. Erosion is coloured in red whereas accretion is coloured in blue.

Several modelling and empirical studies have found an increase in Atlantic storminess over the last few decades (Wang and Swail, 2002; Dodet et al., 2010; Young et al., 2011; Bertin et al., 2013) and this classification of beach response may provide an appropriate framework for considering extreme storm hazards. The classification may also be useful to provide insights into storm recovery. For example, the south embayment of Perran Sands #46, characterized by extensive cross-shore erosion during the 2013/14 winter, has recovered by 50% within 1 year, whereas Slapton Sands #124, which rotated, has not demonstrated any recovery due to the lack of opposing wave direction events (Scott et al., 2016). In 2017, three years after the

2013/14 winter, many exposed and semi-exposed beaches along the southwest coast of England only show partial recovery in comparison to their pre-storm state in 2013, whereas most sheltered long beaches have not recovered at all.

2.7 Conclusions

- During the 2013/14 winter, the south west coast of England was subjected to a sequence of large, storm-induced wave events, representing the most energetic period of waves in the last 60 years. A unique dataset of pre- and post-storm airborne LiDAR dataset for 157 beaches along this coastline was analysed.
- The beach response to these extreme storms was mainly quantified by two parameters: (1) the net volumetric changes over the entire intertidal beach area dQ_{net} which varied between -170 m^3 m^{-1} and +66 m^3 m^{-1}; and (2) a new parameter, the longshore variation index *LVI*, which quantifies the alongshore variability in beach response, and which varied between 0.2 and 1.
- Based on the values of dQ_{net} and *LVI*, a cluster analysis was conducted which resulted in the identification of four different beach response types, largely controlled by wave exposure and normalised beach length: (1) fully exposed beaches; (2) semi-exposed beaches; (3) sheltered short beaches; and (4) sheltered long beaches.
- The geographical distribution among the four different beach responses to extreme storms showed some regional coherence in behaviour. However, several examples demonstrate that this

coherence can be disrupted at a local scale, highlighting the connectivity between beach systems via physical processes like sediment redistribution or/and headland by-passing.

Chapter 3 – Climate forcing of regionally-coherent extreme storm impact and recovery on embayed beaches

3.1 Introduction

Multi-annual and decadal time-series of shoreline and/or beach volume change are becoming increasingly available from around the world (Pye and Blott, 2008; Senechal et al., 2009; Corbella and Stretch, 2012; Barnard et al., 2015; Masselink et al., 2016; Scott et al., 2016; Turner et al., 2016; Castelle et al., 2017a; Phillips et al., 2017). In regions with a seasonal wave climate, these time-series generally show regularly alternating periods of beach erosion and accretion in response to annual variations in incident wave height and period (Wright and Short, 1984; Dubois, 1988; Komar, 1999; Ruggiero et al., 2005). More commonly, however, the temporal coastal behaviour is less regular and governed by processes operating across multiple time scales. Although long-term (100+ years) beach evolution is mainly affected by variations in sea level and sediment supply (Zhang et al., 2002), beach and shoreline behaviour at short- (hours/months) to medium- (months/years) timescales are more impacted by storm events (Ruggiero et al., 2005; Pye and Blott, 2016; Coco et al., 2014; Castelle et al., 2015; Masselink et al., 2015; Scott et al., 2016; Barnard et al., 2017; Harley et al., 2017). Storminess in the North Atlantic, which is characterized by considerable inter-annual and inter-decadal variability was previously shown to be strongly linked to the North Atlantic Oscillation (NAO, Bromirski and Cayan, 2015). However, the NAO index was not correlated to the 2013/14 winter, when a series of extreme storms (H_s > 5.2 m) in the North

Atlantic provided the most energetic winter waves since at least 1948 (Masselink et al., 2016). On the other hand, the West Europe Pressure Anomaly (WEPA), recently proposed by Castelle et al. (2017b), was strongly linked to the 2013/14 winter and therefore serves as a useful proxy for winter wave conditions in this chapter.

Many beaches along the southwest of England were highly affected by the 2013/14 sequence of storms and the morphological impact has been well documented (Masselink et al., 2015; Scott et al., 2016). Using pre- and post-storm airborne LiDAR datasets over that winter, results in Chapter 2 demonstrated the existence of coherent storm response at beaches showing similar exposure to storm waves. This coherent storm response was characterized by medium to large alongshore uniform sediment losses. Short et al. (2014) also showed that synchronous oscillation and rotation were observed over six years at three beaches with the same orientation and length, and exposed to a similar deep water wave climate and tidal regime. This 'regionally representative' behaviour in response to varying and/or changing wave and other climatic forcing, could guide the extent and scope of the ongoing beach monitoring effort required (Bracs et al., 2016). In this chapter, a 10-year dataset of RTK-GPS topographic surveys collected at a regional scale from 10 beaches with similar morphodynamic characteristics (Scott et al., 2011), orientation and wave/tide exposure, but contrasting geomorphological boundaries, will be analysed and discussed. This dataset thus gives an opportunity to address the hypothesis of coherent beach behaviour at a regional scale within a context of extreme storms.

Extreme storms, and the recovery period following these events, are of particular relevance in urbanized coastal areas, since beaches naturally act as a coastal buffer (Stive et al., 2002). Beach recovery processes occur over a wide range of timescales: days (Poate et al., 2015); months (Birkemeier, 1979; Wang et al., 2006; Splinter et al., 2011; Yu et al., 2013; Senechal et al., 2015; Phillips et al., 2017); years (Ruggiero et al., 2005; Choowong et al., 2009; Corbella and Stretch, 2012; Suanez et al., 2012; Castelle et al., 2017a); decades (McLean and Shen, 2006; Thom and Hall, 1991; Houser et al., 2015); or may never fully recover if longshore transport dominated the beach response with permanent sediment losses. Although beach recovery is often associated with small wave conditions (Komar, 1999; Ruggiero et al., 2005; Bramato et al., 2012; Roberts et al., 2013), relatively energetic waves can be essential for mobilisation/recovery of deep offshore storm bar deposits (Scott et al., 2016). Beach morpho-dynamics, including surf zone, beach and foredune interactions, also control beach recovery. Studies showed the importance of the relationship between the beach and the intertidal/subtidal bar (Houser et al., 2015; Scott et al., 2016; Brooks et al., 2017; Phillips et al., 2017; Ge et al., 2017) and/or subaerial dune systems (Suanez et al., 2012; Houser et al., 2015) in beach recovery. The 10 study sites in this chapter were surveyed over 10 years including a period of three years following an extremely energetic winter season, and represent a valuable resource for a better understanding of recovery processes at a regional scale.

Predicting coastline response to storms and longer-term seasonal to inter-annual variability in regional wave climate is an ongoing challenge for coastal zone managers, scientists and engineers. A relatively simple equilibrium shoreline model, ShoreFor, was shown to provide skilful hindcasts of coastal change on coastlines dominated by cross-shore sediment transport (Davidson and Turner, 2009; Davidson et al., 2010; Splinter et al., 2014a). This model primarily encapsulates beach behaviour forced by wave-driven cross-shore sediment transport, including antecedent hydro-/morphodynamic conditions. Based on these skills, the ShoreFor model is one of the best tools to provide a better understanding and interpretation of beach behaviour time series along the exposed and cross-shore dominated 10 beaches presented here.

The aim of this chapter is to study, over a 10-year period, the regional behaviour of 10 beaches in a context of extreme storms. The first objective is to investigate the hypothesis of multi-annual and regionally coherent beach behaviour at beaches exposed to similar wave forcing. The second objective is to contextualize beach response and volume change to a sequence of extreme storms within a 10-year time frame, and to explore the key factors that controlled beach recovery during the 3 years following these extreme storms. The third objective is to use an equilibrium model to provide a better understanding and interpretation of the link between beach behaviour and wave forcing. The fourth objective is to study the link between North Atlantic climate variability and beach volume change using a

climate index controlling winter wave activity along the Atlantic coast of Europe.

3.2 Study area, datasets and methodology

3.2.1 Study area

The 10 study sites, located along the north coast of southwest England (Fig. 3.1), are all high-energy macrotidal sandy beaches that are exposed to swells and wind-waves from the North Atlantic. The wave climate is seasonal with larger waves (mean H_s = 2.2 m, mean T_p = 11 s) in winter from October to March, and smaller waves (mean H_s = 1.4 m, mean T_p = 9 s) in summer from April to September (Fig. 3.1, Table 3.3 and 3.4). The largest waves are generated by extra-tropical storms originating in the mid-latitude westerly wind belt (Lozano et al., 2004), although, occasionally, the coast is also affected by the remnants of tropical cyclones. On average, 17 storm events (peak H_s > 4 m) and 5 severe storm events (peak H_s > 6 m) occur annually (Scott, 2009). The extra-tropical storminess is strongly linked to the North Atlantic Oscillation (NAO; Bromirski and Cayan, 2015) and the West Europe Pressure Anomaly (WEPA; Castelle et al., 2017b), which are both characterized by considerable inter-annual and inter-decadal variability.

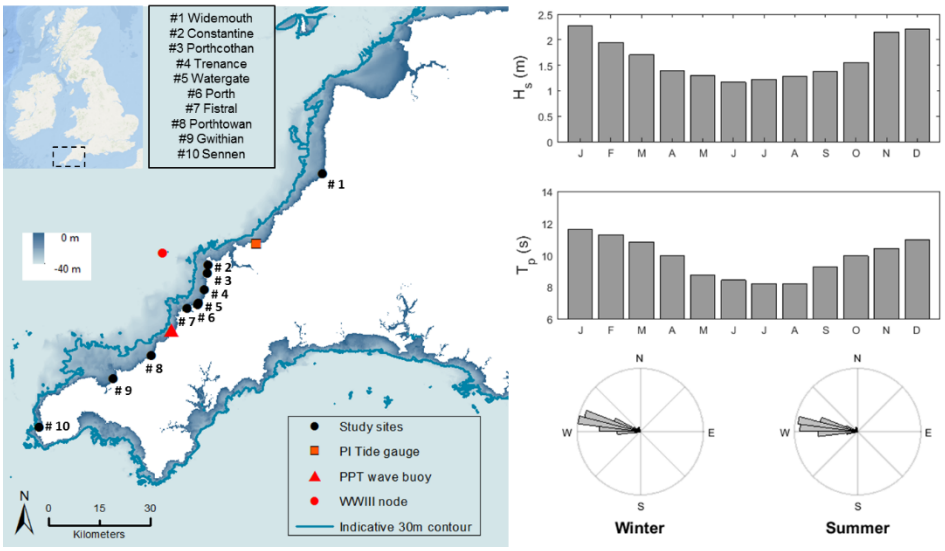

Figure 3.1: Bathymetric map of southwest England with the location of the 10 study sites, Perranporth (PPT) wave buoy, Port Isaac (PI) tidal gauge, the 8-km WWIII modelled wave node and the depth contour representing the 30-m line (left panel). The bar graphs and wave roses represent, respectively, monthly-averaged wave conditions (H_s and T_p) and winter/summer wave direction recorded by the Perranporth wave buoy from 2007 to 2017.

A diverse set of beach systems is represented by the 10 study sites (Fig. 3.2 and Table 3.1) with the median size of the beach sediment ranging from 0.25 to 0.61 mm. Several beaches are backed by dune systems that vary in size and height (Widemouth #1, Constantine #2, Porthcothan #3, Gwithian #9 and Sennen #10) and front high cliffs (Trenance #4 and Watergate #5). Relatively large rocky platforms can be found at Widemouth #1, Constantine #2 and Fistral #7 beaches (Fig. 3.2). All beaches in the data set are constrained by rocky headlands (Fig. 3.2) and can either be considered as very embayed (Porthcothan #3 and Porth #6), semi-embayed (Constantine #3, Trenance #4, Fistral #7 and Porthtowan #8) or relatively open (Widemouth #1, Watergate #5, Gwithian #9 and Sennen #10) with *NBL* values ranging from 3.2 (Porth #6) to 9 (Gwithian #9). Although the studied beaches are characterized by diverse geological settings, Scott et al. (2011)

found them to be similar with respect to beach type and all beaches are considered Low-Tide Bar Rip (LTBR) beaches. The similarity in beach state is explained by the similar hydrodynamic conditions. All beaches are macrotidal, with the mean spring tidal range decreasing from north (6.7 m at Widemouth #1) to south (5.8 m at Sennen #10) (Table 3.1). The beaches also all have a similar SSW-NNE orientation (Fig. 3.2 and Table 3.1) and are, therefore, exposed to similar shore-normal wave conditions. The resulting cross-shore exchange of sediment in response to changing wave conditions is more significant than sediment redistribution alongshore (Buscombe and Scott, 2008), as demonstrated by an analysis of the 2013/14 storm response of all beaches in the southwest of England in Chapter 2.

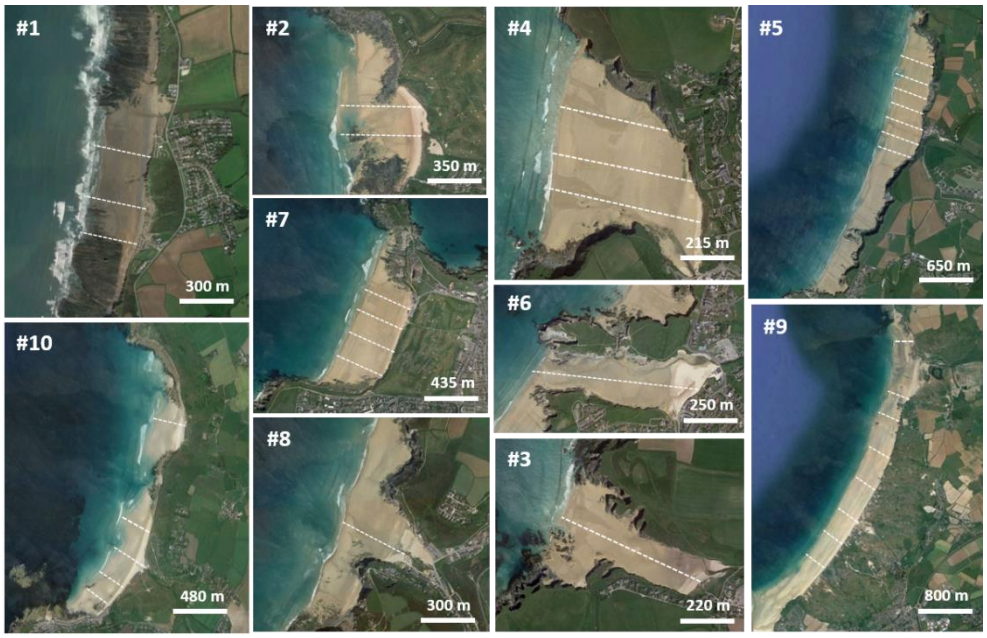

Figure 3.2: Mosaic of Google Earth images showing the geomorphological diversity of the 10 study sites (Widemouth #1, Constantine #2, Porthcothan #3, Trenance #4, Watergate #5, Porth #6, Fistral #7, Porthtowan #8, Gwithian #9 and Sennen #10 beaches). All pictures are oriented according to north-south axis and the beach profile surveyed by the Plymouth Coastal Observatory are located with dashed white lines.

Table 3.1: Key beach characteristics and RTK-GPS profile surveyed at the 10 study sites. *L*: longshore beach length in m; *d50*: beach grain size in mm along the upper/lower part of the beach (Scott et al., 2008); α: clockwise beach angle orientation compare to the north-south axis; number of beach RTK-GPS profiles surveyed; percentage of beach profiles surveyed going through dune system; *MSR*: mean spring tidal range (in m).

Beaches	L (m)	D50 (mm) upper/ lower	α	Number of profiles	Profile with dunes	MSR (m)
Widemouth #1	977	0.55/0.33	10°	3	100%	6.7
Constantine #2	930	0.53/0.30	0°	2	100%	6.4
Porthcothan #3	170	0.61/0.37	30°	1	100%	6.4
Trenance #4	490	0.25/0.29	10°	3	0%	6.4
Watergate #5	3200	0.28/0.29	25°	7	0%	6.4
Porth #6	210	0.28/0.33	5°	1	0%	6.4
Fistral #7	940	0.28/0.41	30°	4	0%	6.3
Porthtowan #8	420	0.38/0.42	30°	1	0%	5.9
Gwithian #9	4500	0.28/0.27	30°	8	50%	5.8
Sennen #10	1730	0.46/0.52	30°	5	80%	5.8

3.2.2 Topographic data

As part as the South West Coastal Monitoring Program, many beaches along the coastline of south west England are surveyed every 6/12 months, and RTK-GPS data sets are provided by the Plymouth Coastal Observatory (http://southwest.coastalmonitoring.org/). The study sites were surveyed twice a year from 2007 to 2017 in spring season (February-March-April) and autumn season (September-October-November), except for Watergate #5 and Gwithian #9 beaches, which were surveyed once a year during spring season (Table 3.2). All beaches are generally surveyed at the same time of the year within a period of 2-3 months (Table 3.2) and because they are fairly dynamic, a difference of 3 months can make the inter-site comparison between beach changes potentially problematic. However, beach behaviour at these 10 study sites is also very seasonal, and the seasonal variations

observed at the beach are more significant than the variations that occur over 2-3 months within the same season. The lag between surveys therefore accounts only for relatively small variations in beach changes and these are discussed later in sections 4.1 and 4.6.

Table 3.2: Survey dates of the RTK-GPS beach profiles from 2007 to 2017 at the 10 study sites. Surveys were carried out by the Plymouth Coastal Observatory.

Dates/beaches	# 1	# 2	# 3	# 4	# 5	# 6	# 7	# 8	# 9	# 10
	01/10/07	25/10/07	28/10/07	28/10/07	26/06/07	27/09/07	27/10/07	30/09/07		14/09/07
	12/02/08	20/03/08	07/04/08	07/04/08	07/02/08	08/02/08	21/02/08	10/02/08	08/02/08	05/04/08
	15/11/08	15/10/08	16/10/08	16/10/08	30/09/08	29/09/08	15/10/08	16/10/08		13/11/08
	26/04/09	12/03/09	11/03/09	11/03/09	12/02/09	10/02/09	29/03/09	13/03/09	12/03/09	24/02/09
	18/10/09	19/09/09	18/09/09	18/09/09	21/09/09	18/09/09	22/09/09	08/09/09		17/10/09
	03/04/10	31/03/10	30/03/10	30/03/10	15/04/10	02/03/10	17/03/10	03/02/10	04/03/10	29/01/10
	05/11/10	08/10/10	07/10/10	07/10/10	07/11/10	08/09/10	11/09/10	08/11/10		24/09/10
	21/04/11	03/04/11	04/04/11	22/04/11	22/03/11	18/02/11	24/03/11	20/03/11	19/03/11	03/02/11
	25/11/11	29/09/11	27/09/11	27/09/11	28/09/11	27/09/11	28/09/11	28/09/11		26/09/11
	19/08/12	09/02/12	08/02/12	11/02/12	23/03/12	20/09/12	21/03/12	10/03/12	10/04/12	22/02/12
	17/10/12	18/10/12	16/10/12	15/10/12	15/11/12	15/12/12	02/09/12	18/09/12		17/09/12
	27/02/13	28/02/13	28/02/13	01/03/13	27/03/13	23/06/13	14/01/13	28/02/13	15/01/13	12/01/13
	03/12/13	05/11/13	21/09/13	21/09/13		05/12/13	19/09/13	20/09/13		20/09/13
	05/03/14	04/03/14	27/02/14	05/03/14	02/03/14	03/03/14	31/01/14	02/02/14	02/03/14	30/01/14
	08/09/14	12/09/14	09/09/14	13/09/14		10/09/14	12/09/14	10/09/14		11/09/14
	22/03/15	22/02/15	21/02/15	21/02/15	20/02/15	19/02/15	18/02/15	20/02/15	21/02/15	22/03/15
	02/09/15	01/09/15	29/08/15	29/08/15		01/10/15	30/08/15	31/08/15		30/08/15
	12/03/16	08/04/16	14/03/16	14/03/16	06/05/16	09/02/16	13/03/16	12/03/16	10/03/16	05/05/16
	20/10/16	15/10/16	17/10/16	17/10/16		18/10/16	17/10/16	19/10/16		17/10/16
	27/06/17	29/04/17	02/03/17	13/02/17	28/04/17	28/02/17	12/02/17	10/02/17	26/05/17	12/07/17

Individual datasets consist of a site-specific number of 2D cross-shore profiles that were surveyed at the exact same location throughout the 10 years and that often stretch along the entire longshore length of the beach

(Fig. 3.2 and Table 3.1). The surveys are carried out during spring tides to maximise beach coverage and extend vertically from around mean low water spring level (MLWS) to the top of the backshore, or dunes when present.

Beach sand volume per unit metre width, $V_{profile}$ in $m^3\ m^{-1}$, is integrated for every cross-shore profile based on the shortest profile over the 10-year period (Equation 3.1).

$$V_{profile} = \int_{z_{min}}^{z_{max}} z dz \tag{3.1}$$

where z corresponds to the topographic values interpolated every metre, and z_{min} and z_{max} are the lowest and the fixed backshore topographic points, respectively (Fig. 3.3). These volumes are computed for every survey to create a beach volume time series, V in $m^3\ m^{-1}$, relative to the first survey (V *(Autumn 2007) = 0*). Beaches are also represented by either one or several cross-shore profiles (N) that are approximatively equally-spaced and spread over the entire beach (Figure 3.2). As these beaches are cross-shore dominated, the profile volume time series can be averaged to obtain longshore-averaged beach volume time series V (Equation 3.2).

$$V = {}^{1}/_{N} \sum_{1}^{N} V_{profile} \tag{3.2}$$

The cross-shore profiles stretching from z_{min} to z_{max} (fixed backshore topographic) point were also vertically divided in two zones if dunes are present, with the dunes area extending from the dune foot to the z_{max} (Fig. 3.3). For the sediment volume computations, the distinction between the elevation of the top of the beach and the base of the dunes (the dune foot)

was estimated by adding the vertical storm runup computed using Stockdon et al. (2006), for a typical beach gradient of 0.02 and average storm wave conditions characterised by H_s = 5.2 m and T_p = 11 s, to the MHWS level. This storm runup elevation is 1.2 m and is representative of a storm event and was coherent with the few dune foot measurements present in the dataset.

In the following sections, beach volume changes, *dV* in $m^3\ m^{-1}$, are used to express the longshore-averaged beach volume changes between surveys. Beach recovery from erosion, expressed as a %, is defined as:

$$Recovery = 100 * \frac{V_{last} - V_{post}}{V_{pre} - V_{post}} \quad (3.3)$$

where V_{last} is the profile for which the recovery is being computed, and V_{pre} and V_{post} represent the beach volumes associated with pre- and post-storm surveys, respectively.

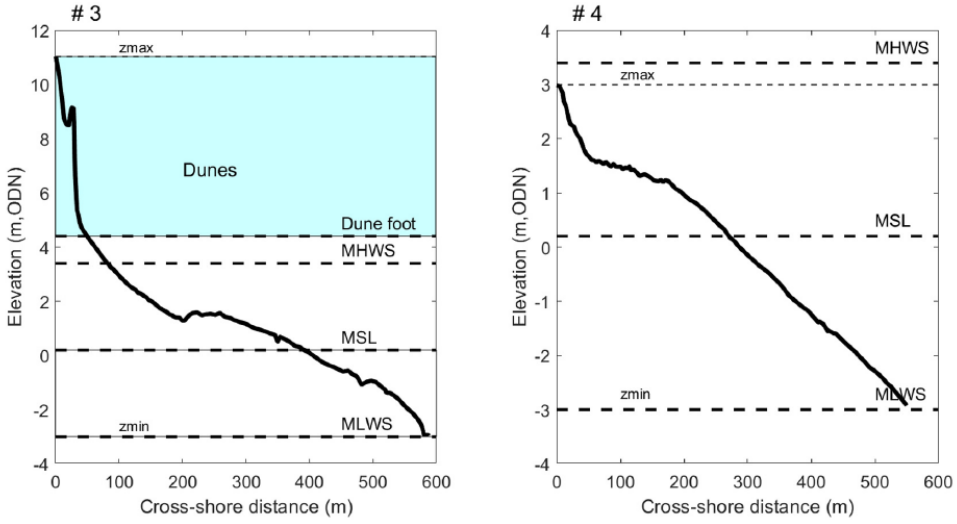

Figure 3.3: RTK-GPS cross-shore profiles of Porthcothan #3 (left panel) and Trenance #4 (right panel) beaches, where vertical beach and dune areas are highlighted according to the different topographic and water levels (z_{max}: fixed backshore topographic point; z_{min}: lowest topographic point; *MHWS*: mean high water spring; *MSL*: mean sea level; *MLWS*: mean low water spring).

3.2.3 Wave, tidal and climate index data

Modelled wave data were obtained from the Met Office 8-km WAVEWATCH III model; data were validated by Saulter (2017). Three-hourly values of significant wave height H_s and peak wave period T_p were extracted from 1 January 1980 to 31 December 2016 at a 50-m deep grid point located half-way along the study region (Fig. 3.1). This time-series was extended to 30 June 2017 using H_s and T_p values measured at a nearshore directional wave buoy located 1.4 km offshore of Perranporth beach in 16-m water depth deep (50.35379°N, 5.17497°W, Fig. 3.1), deployed since December 2006 by the Channel Coastal Observatory. Least-squares regression between the measured (averaged every 3 hours) and modelled datasets for the period 2006–2016 reveals that the H_s time-series are significantly correlated (r = 0.93, p = 0.000), despite the fact that the model node is located further offshore. There is more scatter in the T_p time series (r = 0.84, p = 0.000) (Fig. 3.4). The linear regression models obtained (refer to Fig. 3.4) were used to extend the modelled H_s and T_p time series to 30 June 2017 to maximise the overlap between wave forcing and beach profile observations. Wave directions measured at the Perranporth wave buoy were also used to produce the wave rose in Fig. 3.1 Measured tidal water levels, from an Etrometa step gauge deployed in July 2010 at Port Isaac (Fig. 3.1), were also provided by the Channel Coastal Observatory. The WEPA winter index values from 1980 to 2017 were provided by Bruno Castelle (University of Bordeaux, France). This index was computed using the variations of the sea level pressure gradient between the stations Valentia (Ireland) and Santa Cruz de

Tenerife (Canary Islands) located in the North Atlantic Ocean (Castelle et al., 2017b). These variations were averaged and normalized each year over the months of December, January, February and March (Boreal winter) to obtain the time-series presented in Figure 3.5c.

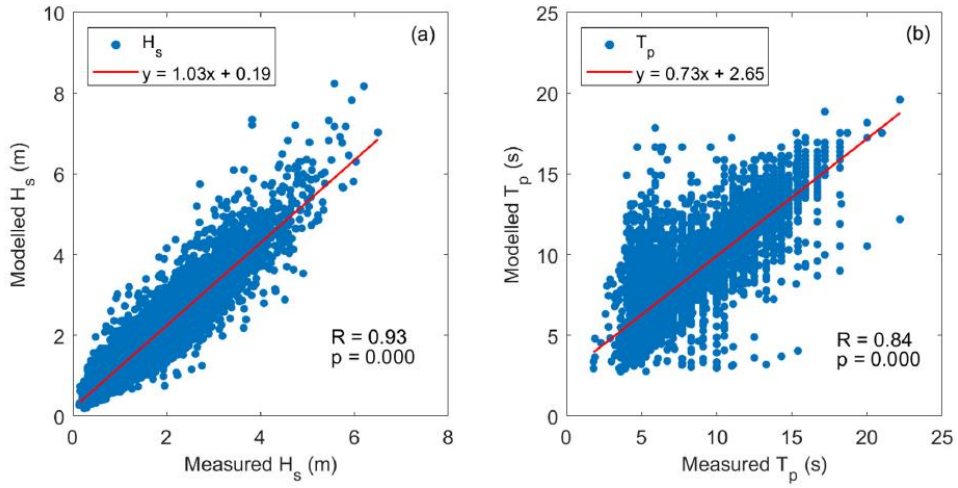

Figure 3.4: Scatter plots of measured and modelled (a) significant wave height, H_s, and (b) peak wave period, T_p, from 2007 to 2017. Measured wave data were obtained from the Perranporth wave buoy (16 m deep) managed by the Channel Coastal Observatory, and 8-km WaveWatch III modelled wave data (50 m deep) were provided by the MetOffice.

3.2.4 ShoreFor model

To test whether any coherent responses between the study sites are coherently related to the offshore wave forcing, and importantly whether this variability is potentially predictable, observations are compared with a subtle variant of the equilibrium shoreline ShoreFor model proposed by Davidson et al. (2013). This variant predicts beach volume variability rather than shoreline change, the results proposed in this chapter are thus comparable with other recent studies using beach volume changes to describe the 2013/14 storm response (Castelle et al., 2015; Masselink et al., 2016; Scott et al., 2016) and no significant differences should be observed in

terms of model predictions. This equilibrium model is based upon the principle that cross-shore-dominated shorelines migrate toward a time-varying equilibrium position (Wright et al., 1985). Here we give a very brief description of the model and the reader is referred to Davidson et al., (2013) for a more detailed description of the model.

The change in beach volume per metre coastline, *dV*, with time is computed using Equation 3.4 where *P* is the incident wave power expressed in W, *c* is a rate parameter expressed in $m^{2.5}\ s^{-1}\ W^{-0.5}$, and Ω is the dimensionless fall velocity which is a simple function of local wave conditions and sediment grain size ($\Omega = H_b/wT_p$ where H_b is the significant breaking wave height, *w* is the settling velocity, and T_p is the spectral peak wave period).

$$\frac{dV}{dt} = cP^{0.5}\left(\Omega_{\phi} - \Omega\right) \tag{3.4}$$

The first model free parameter, *c*, controls the magnitude of the volume change and is optimized by direct comparison between the model prediction and observations, while the use of a temporally varying equilibrium condition Ω_{ϕ}, which is based on a weighted average of the antecedent dimensionless fall velocity over a time-scale ϕ, describes the "memory" of a beach to antecedent conditions. The second model free parameter, ϕ, is called the response factor and it controls the window-width (in days) of the weighted antecedent average. This weighting function has a centre of mass at 0.41 ϕ, thus seasonal variation have ϕ-values of order 10^3 days, whilst more storm dominated site are characterised by ϕ-values $<10^2$ days.

The numerical tests on ShoreFor by Splinter et al. (2013) suggested that bi-annual measurements of coastal change utilised in the present chapter would not be of sufficient temporal resolution to adequately optimise the second model free parameter, ϕ. Thus, here we use the parameterisation proposed by Splinter et al. (2014b), to compute an appropriate value of ϕ.

This parameterisation, based on shoreline changes at eight sites spread over three continents, show that an increase of the normalized values of dimensionless fall velocity coincides with an increase of the response factor values. This result indicates that the shorelines along dissipative beaches tend to respond to the seasonal changes in wave climate and are more resilient to individual storms, while the shorelines of lower energy, more reflective beaches rapidly respond to changes in wave energy. The parametrisation, best represented by an exponential fit can be subdivided into three main categories of shoreline response, where reflective beach states have near constant ϕ values, while an exponential increase in ϕ values can be observed between intermediate and more dissipative states. The shoreline is again observed to be more stable for highly dissipative beaches with ϕ values becoming independent of the dimensionless fall velocity, and optimizes at the order of 1000 days.. Based on an average grain size value of 0.37 mm and the average of the dimensionless fall velocity mean values for our study sites, the Splinter et al., (2014a) parameterisation yielded a value for ϕ ≈1000 days, which typifies dissipative environments with a strong seasonal variability, such as other exposed open coastlines (e.g., Gold Coast, AUS; Truc Vert, FR; and North Head, USA).

The ShoreFor model has been shown to have high skill at forecasting coastal recession and progradation on exposed energetic coastlines dominated by cross-shore sediment transport (Davidson et. al, 2013; Splinter et al., 2014; Davidson et al., 2017); however, it takes no account of the longshore sediment transport process. For the current study sites, this model restriction is not thought to be particularly severe since sediment transport at the 10 beaches is dominated by cross-shore processes (Buscombe and Scott, 2008).

3.3 Wave forcing

3.3.1 Multi-annual wave conditions time-series

The time series of modelled significant wave height H_s, peak energy period T_p and winter WEPA index from 1980 to 2016 are presented in Fig. 3.5. The 8-week block-averaged H_s and T_p time series clearly highlight the seasonal variability in wave conditions between winter and summer. Over the last 36 years, six very energetic winters can be observed from the H_s time series (Fig. 3.5a and 3.5b). The 'Great Storm' of 1987 and the 'Burn's Day Storm' in 1990 were reported (McCallum, 1990) for the strength of wind gusts recorded, and caused widespread damage and the dramatic loss of 18 and 47 lives in the UK, respectively. Three years later, the 'Braer Storm' of 1993 had one of the lowest-ever recorded central pressures (914 mb) in the North Atlantic (McCallum and Grahame, 1993; Burt, 1993) and the 1994/95 winter was reported as 'very cyclonic' (Hulme, 1997). More recently, the 2013/14 winter wave conditions associated with storms were the most energetic since at least 1948 along the southwest coast of England (Masselink et al.,

2015), followed by the 2015/16 winter that was as energetic as 1993 and 1994/95 mentioned previously (Fig. 3.5a).

The winter WEPA time-series show that the high H_s values during the 1993/94, 1994/95, 2013/2014 and 2015/2016 winters are all synchronous with positive peaks along the winter WEPA index time-series (Fig. 3.5c). However, only average wave conditions occurred during the 2001 winter when WEPA was strongly positive. The relationship between the winter-mean significant wave height H_s and the winter WEPA index was analysed and showed that the two time-series were strongly correlated over the 1980–2017 and the 10-year study period ($r = 0.76$, $p = 0.000$ and $r = 0.80$, $p = 0.006$, respectively) (Fig. 3.6).

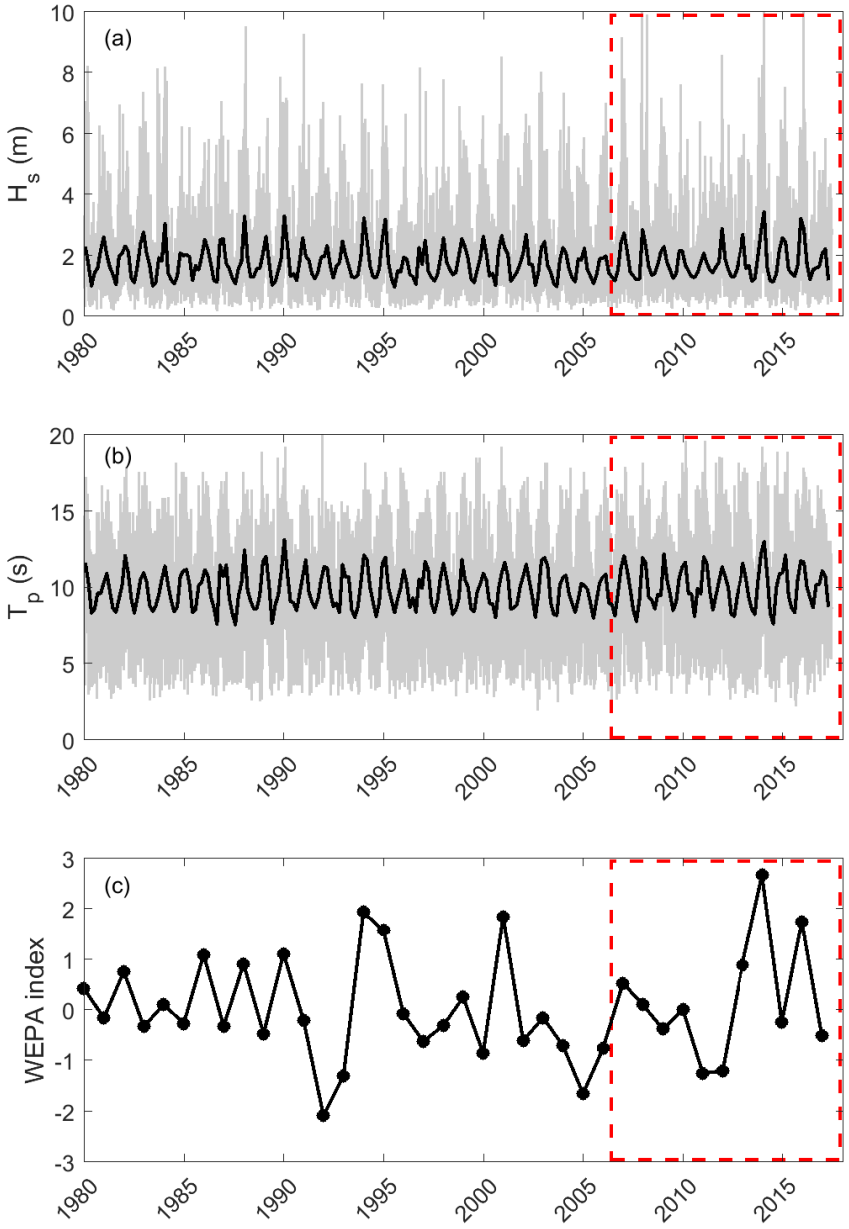

Figure 3.5: Time series from 1980 to 2017 of: (a) 3-hourly modelled significant wave height H_s (grey) and 8-weeks block-averaged wave significant wave height (black); (b) 3-hourly modelled peak wave period T_p (grey) and 8-week averaged peak wave period (black) at modelled grid point; and (c) winter WEPA index (DJFM). The red dashed-square represent the 10-year study period for which beach topographic surveys are available and for which mean values are provided in Tables 3.3 and 3.4.

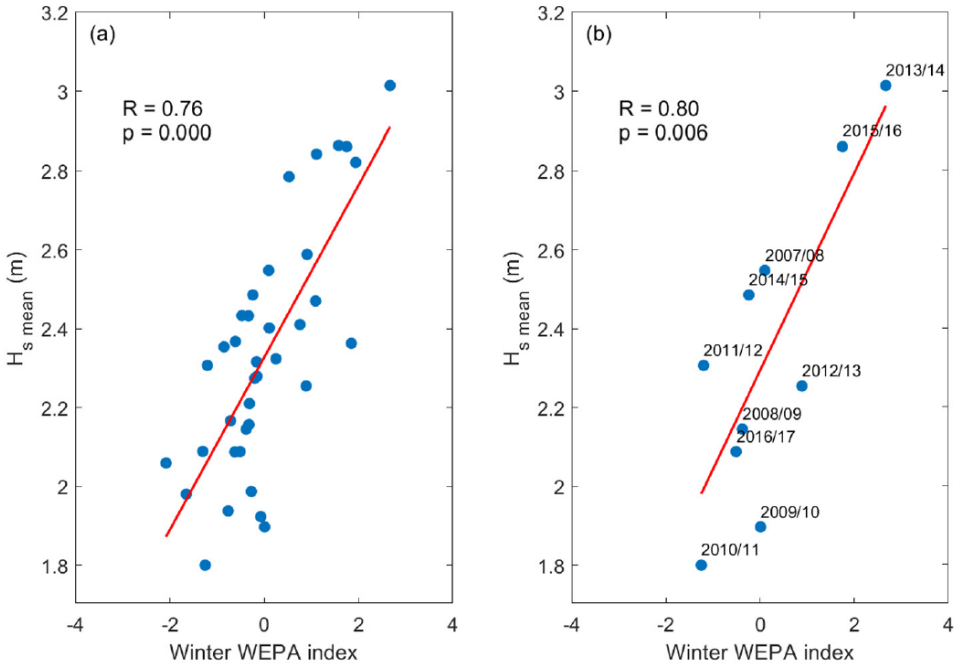

Figure 3.6: Scatter plots of the winter-mean (DJFM) modelled significant wave height, $H_{s\ mean}$, and the winter WEPA index (a) from the 1980/81 to the 2016/17 winter; and (b) from the 2007/08 to the 2016/17 winter.

Based on the 6-monthly topographic surveys carried out around spring and autumn months, and the monthly-averaged wave conditions (H_s and T_p) presented in Fig. 3.1, each year is divided into a winter and summer season spanning the 6 months between October-March (ONDJFM), and April-September (AMJJAS), respectively. The addition of October and November to the Boreal winter (December, January, February, March), used to calculate winter WEPA index values, did not alter the relationship between winter WEPA index and winter-mean significant wave height over the study period, which show an even better correlation coefficient (r = 0.84, p = 0.000). Over the 2007–2017 period, for which RTK-GPS survey data are available, H_s and T_p winter-mean values ranged from 1.80 m to 2.73 m, and 10.6 s to 11.9 s, respectively (Table 3.3), with the highest winter-mean values exceeding 2.5 m and 11 s during the 2013/14 and 2015/16 winters. Summers

are characterized by lower H_s and T_p mean values, ranging from 1.30 to 1.54 m and 8.6 to 9.1 s (Table 3.4), respectively, with the least energetic months corresponding to the 2014 summer (1.18 m and 8.8 s). As observed in Fig. 3.5, H_s and T_p values also show a strong seasonal signal, in addition to inter-annual variability.

Table 3.3: Winter-mean values (from October to March) of significant wave height H_s (m), wave peak period T_p (s), number of storms, mean duration of storms (h), cumulative storm duration (h) and energetic rank based on wave energy level, from the 2006/07 to the 2016/17 winter.

Season	Mean H_s (m)	Mean T_p (s)	Number of storms	Mean storm duration (hours)	Cumulative storm duration (hours)	Rank
Winter 2006/2007	**2.41**	**11.3**	**9**	**17**	**100**	**3**
Winter 2007/2008	2.13	10.7	9	13	75	5
Winter 2008/2009	2.11	10.6	7	13	75	7
Winter 2009/2010	1.99	11.2	3	12	37	9
Winter 2010/2011	1.80	10.9	2	7	13	11
Winter 2011/2012	2.13	10.9	4	18	55	6
Winter 2012/2013	2.09	10.8	3	15	44	8
Winter 2013/2014	**2.73**	**11.9**	**17**	**12**	**187**	**1**
Winter 2014/2015	2.36	11.2	6	14	86	4
Winter 2015/2016	**2.58**	**11.5**	**12**	**11**	**123**	**2**
Winter 2016/2017	1.93	10.7	1	5	5	10

Table 3.4: Summer-mean (from April to September) values of significant wave height H_s (m), wave peak period T_p (s), number of storms, mean duration of storms (h), cumulative storm duration (h) and energetic rank based on wave energy level, during summer months from 2007 to 2016.

Season	Mean H_s (m)	Mean T_p (s)	Number of storms	Mean storm duration (hours)	Cumulative storm duration (hours)	Rank
Summer 2007	1.31	8.8	0	0	0	8
Summer 2008	1.37	9.1	0	0	0	6
Summer 2009	1.39	9.1	0	0	0	4
Summer 2010	1.30	9.1	0	0	0	9
Summer 2011	**1.54**	**9.4**	**1**	**5**	**5**	**1**
Summer 2012	1.39	8.6	1	8	8	5
Summer 2013	1.35	8.8	0	0	0	7
Summer 2014	1.18	8.8	0	0	0	10
Summer 2015	**1.42**	**8.9**	**0**	**0**	**0**	**3**
Summer 2016	**1.44**	**9.2**	**1**	**10**	**10**	**2**

3.3.2 Multi-annual storminess

The peaks-over-threshold (POT) method is commonly used to identify coastal storms from significant wave height time series (Houser and Greenwood, 2005; Almeida et al., 2012; Corbella and Stretch, 2012; Castelle et al., 2015; Masselink et al., 2015). Ciavola and Coco (2017) identified three parameters to specify when using the POT method: (1) the storm threshold; (2) the minimum storm duration; and (3) the meteorological independence criterion. Based on the time series of modelled significant wave height H_s

and similarly to Masselink et al. (2015), a storm is defined here as a wave event during which the maximum H_s exceeds the 1% exceedance offshore wave height (5.2 m), and where the start and the end of the storm event is when H_s exceeds or falls below the 5% exceedance wave height (3.8 m). These wave exceedance values were calculated using the modelled H_s wave time-series over the last 10 years only, to avoid the influence of long-term trends in winter-mean wave height (Castelle et al., 2018). Given that the southwest coast of England is mostly exposed to extra-tropical storms, a meteorological independence criterion of 24 hours is used to distinguish storm events, as suggested by Ciavola and Coco (2017). The numbers of storm events during winter and summer months from 2006 to 2016 are reported in Table 3.3 and 3.4. The number of storms shows a high seasonal variability and only three of the 76 storm events identified between October 2006 and June 2017 occurred during summer months (Table 3.3 and 3.4). The highest number of storm events are associated with the 2013/14 and 2015/16 winters (17 and 12 storms, respectively) while only one storm occurred during the 2016/17 winter, representing the lowest number among the last 10 years (Table 3.3 and Fig. 3.7). The number of winter storms varies from one year to another, ranging from 1 to 17 over the 10-year study period. Mean storm durations are also highly variable from one winter to another, ranging from 5 to 18 hours (Table 3.3), justifying the use of an independence meteorological criterion of 24 hours. Although the role of storm surge is limited and rarely exceeds 1 m along this open coast (Masselink et al., 2015), the coincidence of the peak storm with spring tides has a particular importance since 5 of the macro-tidal study sites have a

supra-tidal dune system (Table 3.1). During the 2013/14 winter, for the 17 storms recorded, 7 storms occurred at approximatively the highest stage of the spring tides, while 6 of the 12 storms occurred at that stage during the 2015/16 winter (Fig. 3.7).

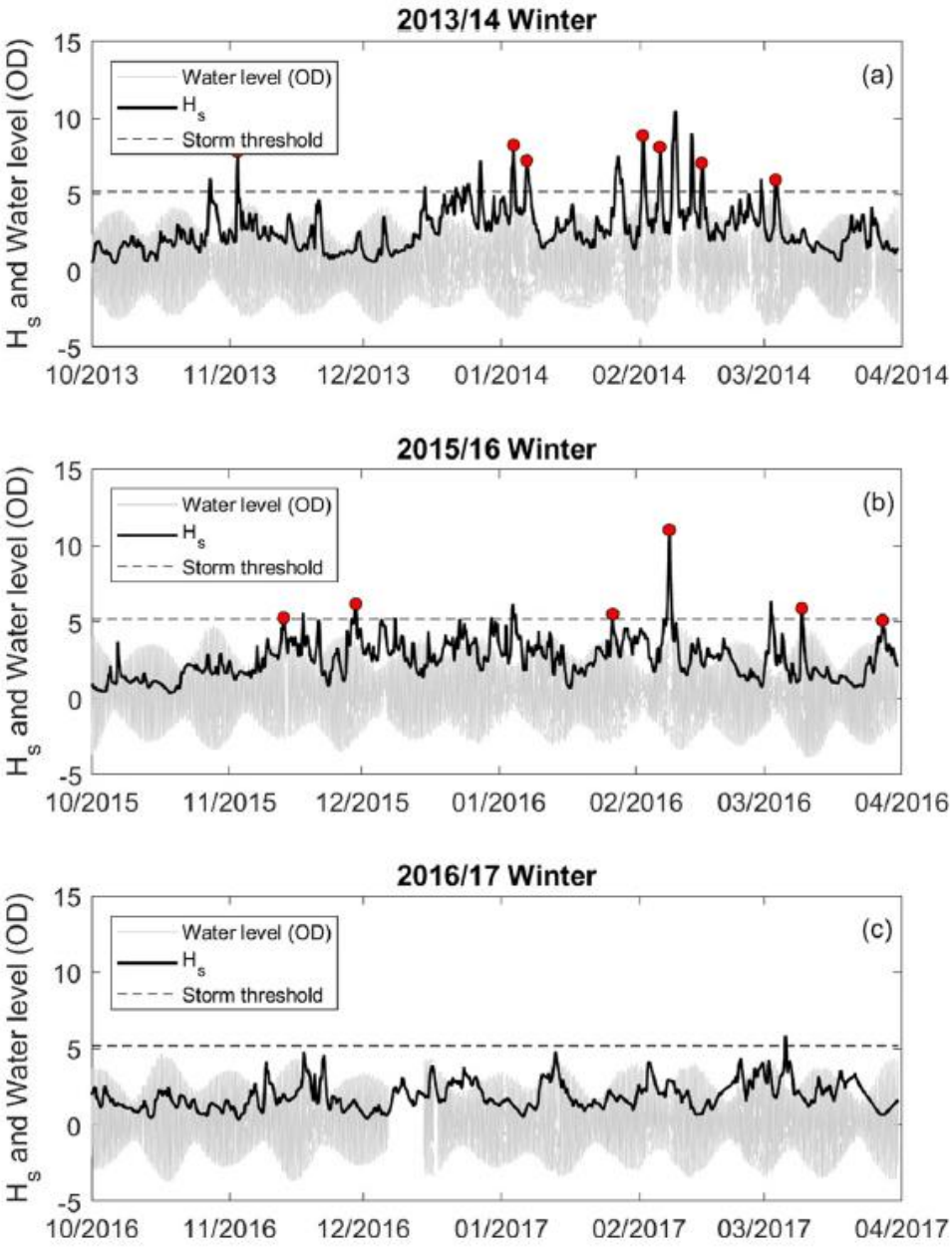

Figure 3.7: Time series of significant wave height H_s (m), water level (m above Ordnance Datum, OD) and storm threshold ($H_{s\ 1\%\ exceedance}$) during the winter of: (a) 2013/14; (b) 2015/16; and (c) 2016/2017. Storms that occurred during spring tides are highlighted by red dots.

3.4 Regionally coherent beach behaviour, storm response and recovery

3.4.1 Influence of wave forcing in beach behaviour

In the previous section, results showed that the 10 study sites were exposed to temporally-varying seasonal wave conditions over the last 10 years. The 6-monthly or yearly topographic changes in response to this variability in wave forcing can be observed along individual RTK-GPS beach profiles (Fig. 3.8). Observations at Constantine #2, Trenance #4 and Fistral #7, used as three representative examples for all study sites, showed that beach response is temporally and spatially coherent. Overall, few morphological changes were observed at the three representative study sites over the 2011/12 winter while beach erosion and accretion were observed over the 2013/14 winter and the 2016 summer, respectively (Fig. 3.8). However, the magnitude of the morphological changes differs from one site to another. All beach profiles surveyed over the last 10 years are bounded by the Autumn 2013 and Spring 2014 profiles, suggesting that the 2013/14 winter corresponds to the most erosive event for at least 10 years, and the three beach profiles corresponding to Autumn 2016 suggest that beach recovery from that winter was not complete 2.5 years later (Fig. 3.8).

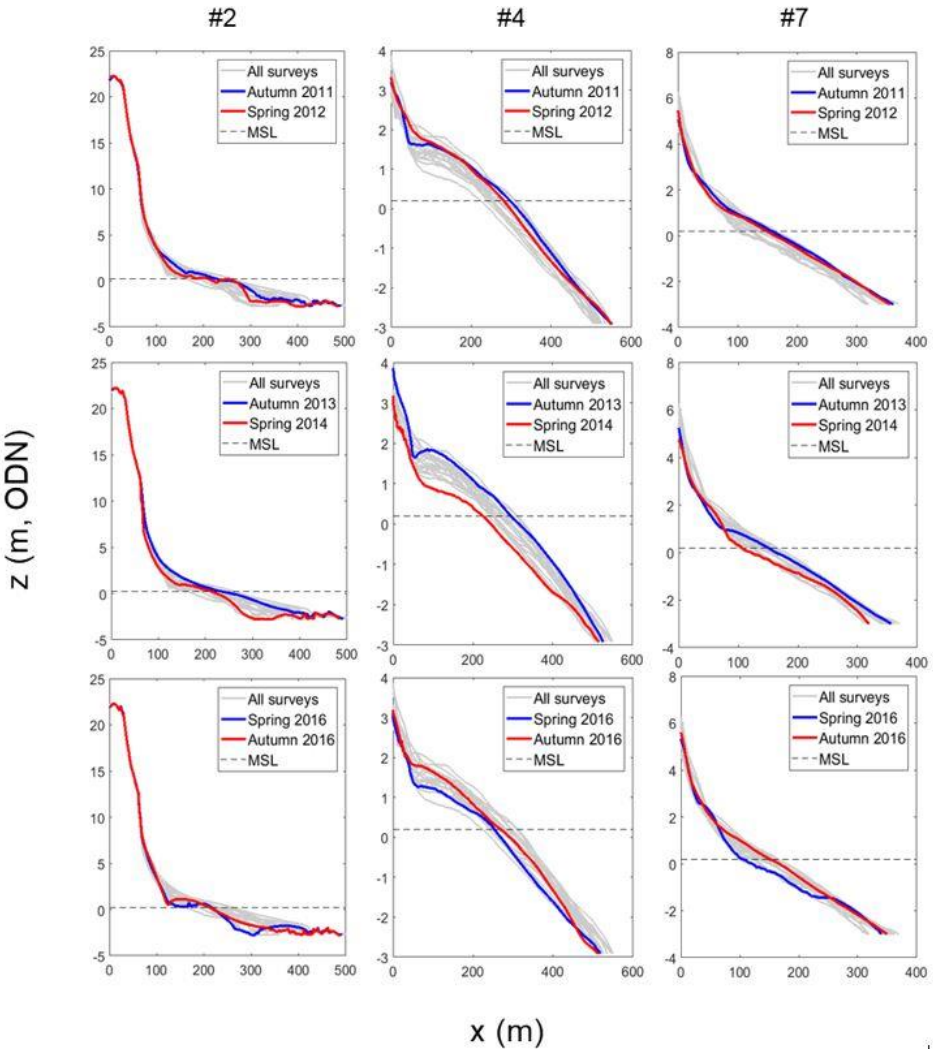

Figure 3.8: Three representative examples of RTK-GPS cross-shore profiles showing the 2011/12 winter (top panels), 2013/14 winter (middle panels) and the 2016 summer (bottom panels) beach responses at Constantine #2, Trenance #4 and Fistral #7 beaches. Antecedent and subsequent profiles are, respectively, coloured in blue and red, while all other profiles from Autumn 2007 to Spring 2017 are coloured in grey. Beach profiles are also presented on a variable vertical scale to give a better visualization of the morphological changes at beaches where dunes are not present.

To capture and study the temporal volume changes observed along these cross-shore profiles, the longshore-averaged beach volume time-series, *V*, were computed from 2007 to 2017, using the methodology presented in section 2.2 (Equation 3.2). All the 10 longshore-averaged beach volume time-series over the last 10 years, presented in Fig. 3.9, showed that: (1) beaches presented a seasonal behaviour with most winters characterised by

erosion while most summers were associated with accretion; and (2) beaches showed a coherent behaviour, although volume change magnitude can differ (Fig. 3.9). These differences in magnitude can be partly explained by the differences in beach characteristics, and also by the different dates at which beaches were surveyed, as mentioned in section 2.2.

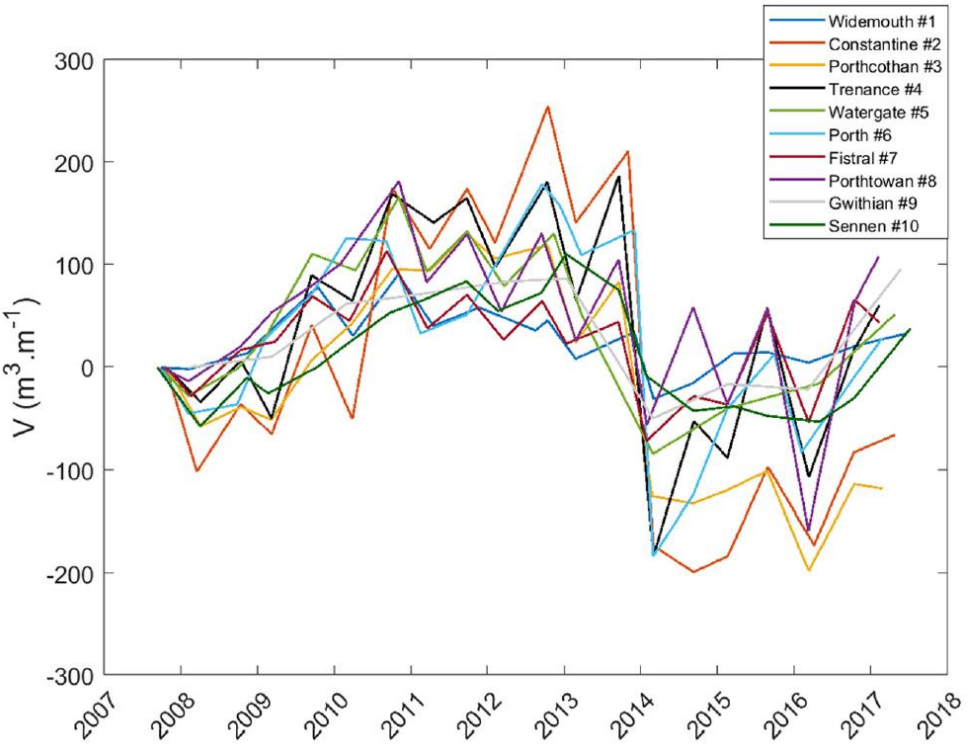

Figure 3.9: Time series from 2007 to 2017 of the longshore-averaged beach volume time-series V (m^3 m^{-1}) for the 10 study sites.

When considering the average of the 10 beach volume time-series, V_{avg}, and its bounded standard deviation, representing inter-site variability, four different phases can be identified (Fig. 3.10a). During the first phase, from autumn 2007 to autumn 2010, the 10 beaches accreted with an average rate of volume change of 3.6 m^3 m^{-1} per month (Fig. 3.10a). During this phase, winter periods were ranked as 5th, 7th and 9th most energetic and corresponded to the recovery phase following the energetic 2006/07 winter

ranked as the 3rd most energetic over the last 10 years (Table 3.3). Accordingly, the yearly WEPA index gradually decreased from 0.5 to -1.25 during this 3-year phase (Fig. 3.10c). The second phase, spanning the three years between autumn 2010 and autumn 2013, was characterized by an equilibrium in beach volume change (- 7 m^3 m^{-1}) where seasonal sediment exchange was dominant over inter-annual exchange (Fig. 3.9). This suggests that the beaches reached an equilibrium as recovery from the 2006/07 winter was complete. This phase was associated with a relatively stable WEPA index from 2010 to 2012 followed by a rapid increase from -1.20 to 1 during 2013 which did not seem to influence the volume changes (Fig. 3.10c). Phase 3, corresponding to the 2013/14 winter, was the strongest erosive event over the last 10 years as previously observed along the three cross-shore profiles in Fig. 3.8. Between autumn 2013 and spring 2014, the 10 beaches lost from 80 to 384 m^3 m^{-1} (Fig. 3.9), resulting in an average erosion rate of 34 m^3 m^{-1} per month. These large losses of sand occurred during the most energetic winter of the study period (Fig. 3.10b), where 17 storms were recorded (Fig. 7a and Table 3.3), associated to the WEPA index 10-year maximum value of 2.7 (Fig. 3.10c). Although the increase in WEPA values between 2013 and 2014 is similar to the increase observed between 2012 and 2013, the wave conditions and associated beach responses were much stronger, suggesting a threshold effect in the WEPA control on wave climate. Phase 4, which corresponded to the following three years from spring 2014 to spring 2017, was related to the recovery period from the extreme storms of phase 3. From spring 2014 to autumn 2015, the beaches slowly recovered with an average accretion rate of 3.5 m^3 m^{-1} per month

(Fig. 3.10a). The smaller wave conditions during the 2014/15 winter compared to the 2013/14 winter (Fig. 3.7a and 3.7b) were associated with a decrease of the WEPA index through 2015 (Fig. 3.10b and 10c). However, that winter was still relatively energetic (ranked 4th, Table 3.3) and resulted in variable response among the 10 study sites with both erosion or accretion depending on the beach (Fig. 3.9). Most of the sand recovered over this 1.5 years was lost during the energetic 2015/16 winter (Fig. 3.7c), which ranked as the second most energetic period over the last 10 years (Table 3.3) and paired with the second highest value of WEPA index (Fig. 3.10c), adding to the hypothesis of a threshold effect observed in phase 3. These losses were quickly recovered the next summer in 2016 (Fig. 3.10a), and accretion (36 m^3 m^{-1}) even occurred during the 2016/17 winter when calm wave conditions prevailed and no storms occurred (Fig. 3.7c and 3.10b). This winter also had a reduced WEPA index (Fig. 3.10c). When considering the volumes lost between spring 2013 and spring 2014, these losses were recovered on average by 77% in spring 2017. However, recovery percentages were highly variable between the 10 study sites (from 5 to 200%), as testified by the increase in standard deviation along the average volume time-series during phase 4 (Fig. 3.10a).

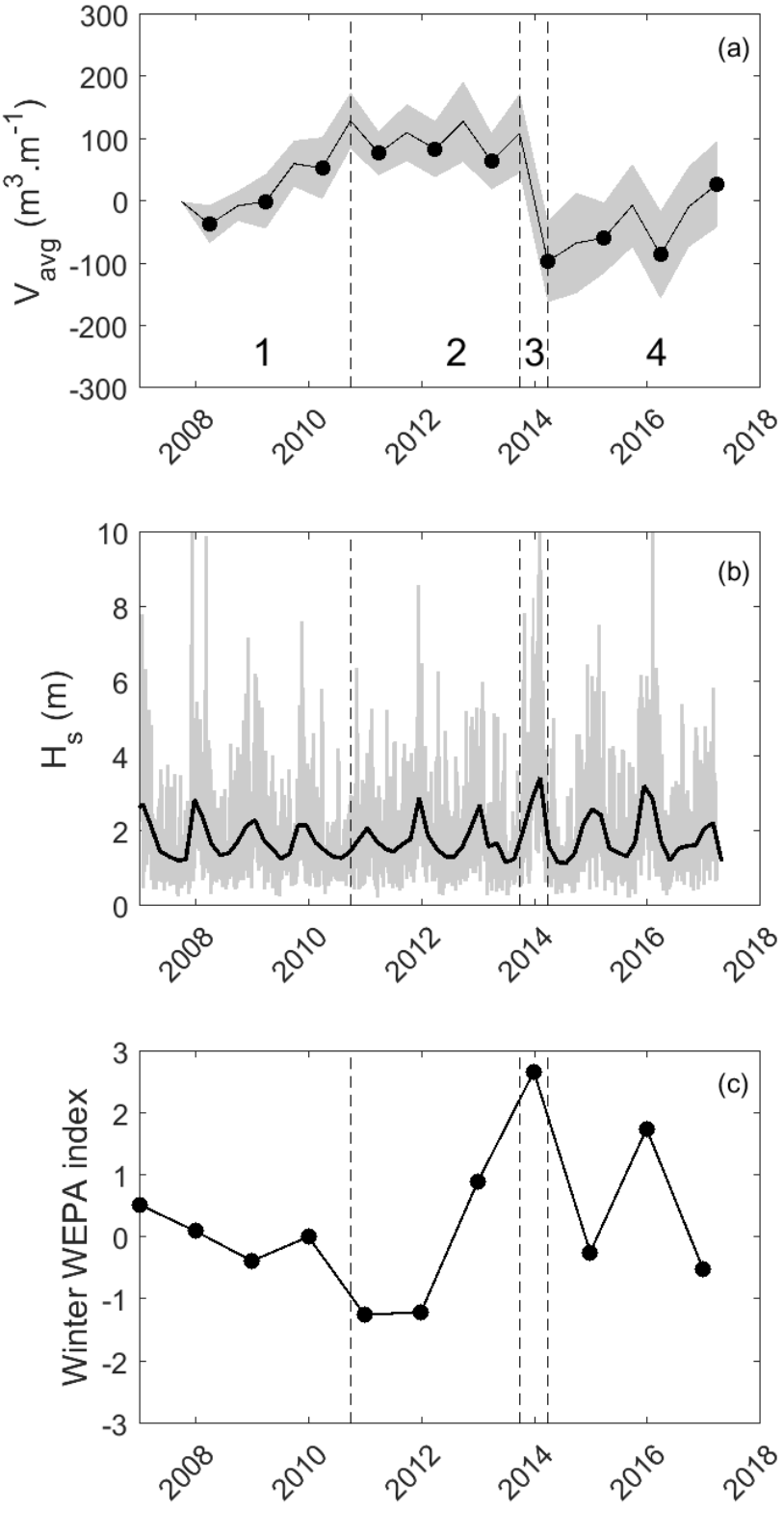

Figure 3.10: Time series from 2007 to 2017 of: (a) the average of the 10 beach volume time-series, V_{avg} (m^3 m^{-1}) in black bounded by its standard deviation in grey; (b) 3-hourly modelled significant wave height H_s (grey) and 8-week block-averaged significant wave height (black); and (c) winter WEPA index. Surveys in spring (end of winter) each year are indicated with black dots to highlight seasonal variations in the beach volume time-series.

The volume changes observed during the 3-year recovery period (phase 4) suggested that summer conditions contribute to beach recovery but, above all, the recovery trajectory is largely and mainly forced by winter waves. The mean of the 6-monthly volume changes, dV_{mean}, over winter and summer months, and the associated 6-monthly significant wave height, H_s, were therefore computed and compared. Results showed that both volume changes and wave conditions during summer months represent rather small inter-annual variability compared to winter months (Fig. 3.11). For example, the 58 m^3 m^{-1} gained during the 2015 summer was rapidly lost during the subsequent energetic winter (-97 m^3 m^{-1}) while the 96 m^3 m^{-1} gained during the 2016 summer were supplemented by the subsequent calm winter (+36 m^3 m^{-1}). Results also showed that inter-site variability in volume change, represented by the error bars, was larger during winter months than summer months over the study period, especially when wave conditions were energetic (Fig. 3.11). The 10 beaches average standard deviation of 6-monthly volume changes from 2007 to 2017, dV_{std}, which represents the inter-site variability in volume change, was therefore computed and plotted against the corresponding 6-monthly significant wave height mean values (Fig. 3.12). Over winter months, the increase of deviation in volume changes between the 10 study sites was strongly correlated with the increase of significant wave height ($r = 0.83$), while no significant correlation was found between these two variables over summer months (Fig. 3.12).

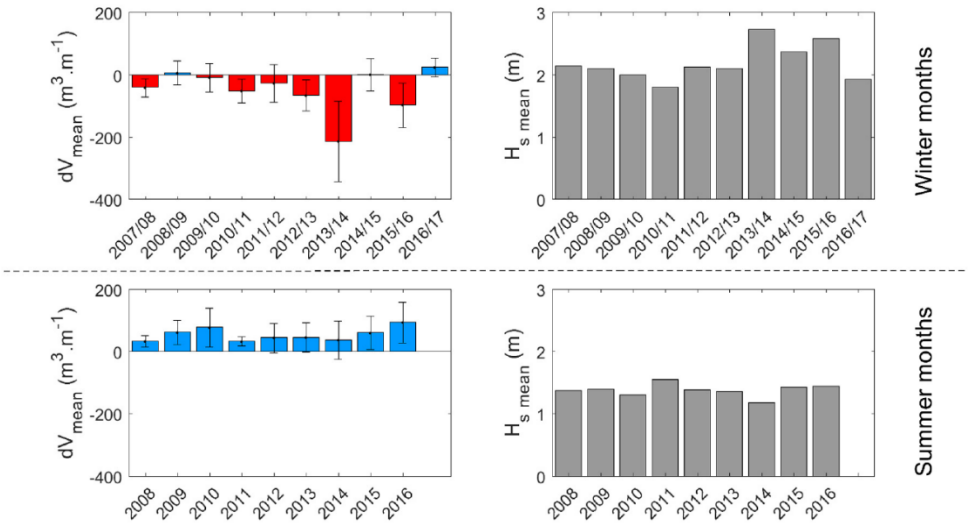

Figure 3.11: Time series of 6-monthly average of longshore averaged beach volumes changes dV_{mean} ($m^3\ m^{-1}$) and 6-monthly average significant wave height $H_{s\ mean}$ during winter (upper panel) and summer (lower panel) months, from 2007 to 2017. The error bars represent the standard deviation in volume change. Watergate #5 and Gwithian #9 were not incorporated because they were only yearly surveyed.

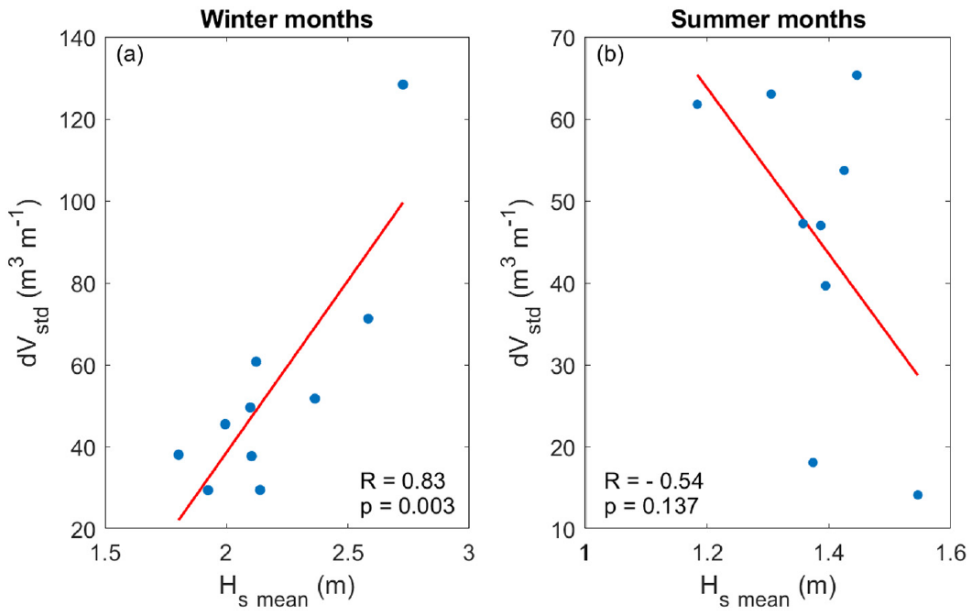

Figure 3.12: Scatter plots of the 10 beaches average standard deviation of 6-monthly volume changes, dV_{std}, and the corresponding 6-monthly significant wave height mean values, $H_{s\ mean}$, over (a) winter months, and (b) summer months from 2007 to 2017.

The longshore-averaged beach volume time-series showed that the 10 study sites located along the north coast of Cornwall presented a coherent and synchronous behaviour from 2007 to 2017. For each beach, the volume changes were partly controlled by intra-annual variability due to the strongly seasonal wave climate, but largely controlled by the inter-annual variability in wave forcing during winter months, especially when sequences of extreme storms were recorded. This variability in winter wave forcing was also shown to create some variability in volume change between study sites and to have a large influence on recovery processes. Furthermore, the average of the 10 beach volume time-series was shown to be fairly well correlated with North Atlantic climate variations illustrated by the yearly WEPA index, although similar variations in WEPA index values were not associated with the same beach response, suggesting the existence of a threshold in WEPA control or the influence of other processes.

3.4.2 Influence of geomorphological and geological boundaries in beach behaviour

In the previous section, the 10 beaches showed a coherent and synchronous behaviour over the last 10 years. However, some variability in the magnitude of volume change was observed between the 10 study sites, which increased when waves become more energetic. Accordingly, the percentages of sand volume recovered following the extreme events of the 2013/14 winter highly varied between the 10 beaches. This variability could be partly explained by small differences in coastline orientation that influence inshore wave conditions, which were not addressed here because a generalised

offshore wave forcing was used for all study sites, rather than a beach-specific inshore wave forcing. It could also be explained by other intrinsic beach characteristics that vary between the 10 study sites (Table 3.1). The influence of dune systems on multi-annual beach behaviour is investigated here.

In the present chapter, five sites have dune systems that vary in alongshore extent (from 160 to 2400 m) and height (from 11 to 22 m). The role of storm surge is limited along the open coast of North Cornwall, and rarely exceeds 1 m (Masselink et al., 2015); however, the coincidence of events of energetic and long-period waves with spring high tides can induce strong dune erosion. The influence of coastal dune systems on beach volumetric changes over the last 10 years was investigated by quantifying the longshore-averaged dune volume time series, as mentioned in section 3.2. The volume time series associated with the dunes, V_{dunes}, at Widemouth #1, Constantine #2, Porthcothan #3, Gwithian #9 and Sennen #10, show that dunes were variably active over the last 10 years (Fig. 3.13). The contribution of dune volume changes over intertidal beach volume changes was highly variable between the different study sites, being either insignificant at Widemouth #1, small at Constantine #2, Gwithian #9 and Sennen #10, or significant at Porthcothan #3. Being relatively stable during phases 1 and 2, larger dune volume changes are observed during the third and fourth phases (Fig. 3.13). The largest losses of dune sand were observed during the 2013/14 winter at Constantine #2, Porthcothan #3, Gwithian #9 and Sennen #10 (-48, -40, -35, and -23 $m^3\ m^{-1}$, respectively), while very little volume change was observed

at Widemouth #1 (-9 m^3 m^{-1}). The 2015/16 winter was also responsible for strong and significant dune erosion at Porthcothan #3 and Sennen #10 (-41 and -16 m^3 m^{-1}, respectively). Moreover, the cross-shore RTK-GPS profiles showed that the way dunes eroded was also variable between study sites. At Constantine #2, and Sennen #10, which have relatively steep and high dunes, sand was mostly eroded from the fore dunes or/and the toe of the dunes during the 2013/14 winter, while much larger dune scarping and steepening was observed at Porthcothan #3 (Fig. 3.13). Cross-shore RTK-GPS profiles of the dunes at Widemouth #1 and Gwithian #9 was not presented here because no significant dune erosion was observed at Widemouth and only yearly beach profiles are available at Gwithian. The rate of dune recovery between these study sites was also site-specific; between their pre-storm state in spring 2013 and spring 2017, dunes completely recovered (Constantine #2), partly recovered (Gwithian #9 and Sennen #10) or remained in an erosive state (Porthcothan #3).

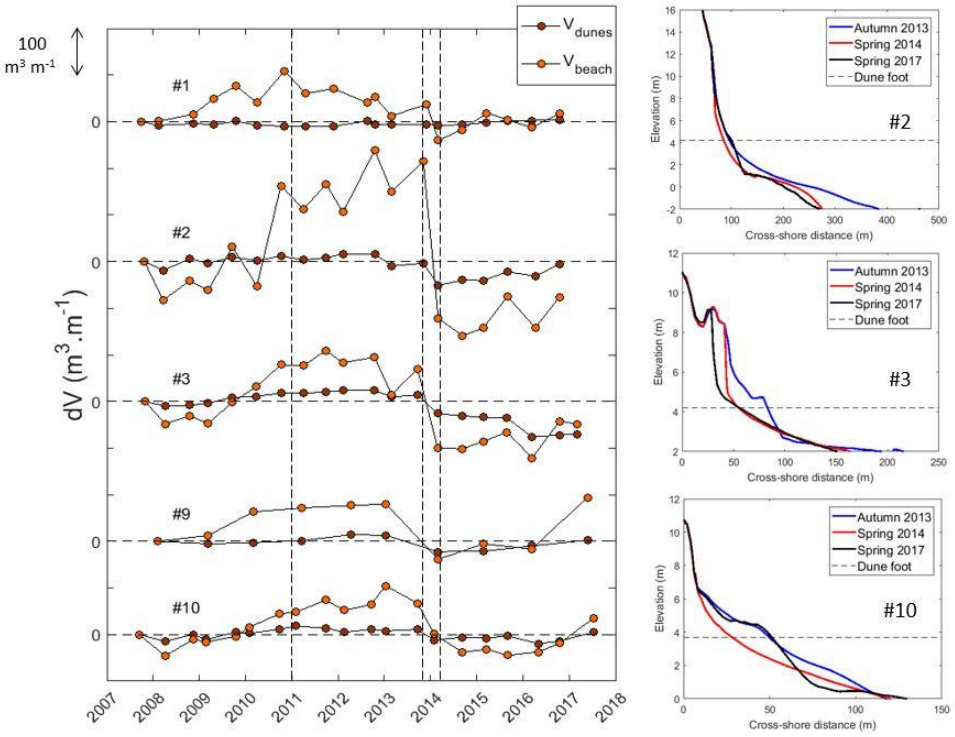

Figure 3.13: Longshore-averaged dunes and intertidal beach volume time series (V_{dunes}, V_{beach}) from 2007 to 2017 at Widemouth #1, Constantine #2, Porthcothan #3, Gwithian #9 and Sennen #10 beaches (left panel). The vertical scale between each tick mark represents a 100 m^{-3} m^{-1} volume change. Pre-storm (Autumn 2013), post-storm (Spring 2013) and last (Spring 2017) RTK-GPS cross-shore profiles showing dune erosion and recovery at three representative beaches: Constantine #2, Porthcothan #3, and Sennen #10 (right panel). Autumn 2013, Spring 2014 and Spring 2017 profiles are respectively coloured in blue, red and black and the beach profiles have been vertically cropped for a better visualization of the area of interest (dunes).

Dune systems can therefore represent a source of temporal and spatial variability when comparing the magnitude of volume change from one site to another. Over the last 10 years, dunes along the north coast of Cornwall were only significantly impacted during the 2013/14 winter, and were likely to be one of the factors that contributed to the increase of inter-site variability in volume change during that period. Furthermore, some variability in the way dunes responded to the 2013/14 extreme storms was also observed between the 5 sites that have dunes, which consequently

influenced storm response and beach recovery over the whole beach system.

3.5 Modelling of multi-annual beach behaviour

In the previous section, the longshore-averaged beach volume time series was strongly controlled by seasonal and inter-annual wave forcing. The 6-monthly volume changes, *dV*, for each study site were plotted against the corresponding 6-monthly significant wave height mean values $H_{s\ mean}$, and the 6-monthly cumulative storm duration (Fig. 3.14). Trends of decrease in beach sand volumes with increase in wave height (Fig. 3.14a) and storm duration (Fig. 3.14b) can be observed. Erosion was systematically observed at the 10 study sites when waves exceed 2.5 m and the cumulative storm duration exceeds 100 hours (Fig. 3.14). These two thresholds were only exceeded during the 2013/14 and 2015/16 winter, and could be used to define extremely energetic winter seasons.

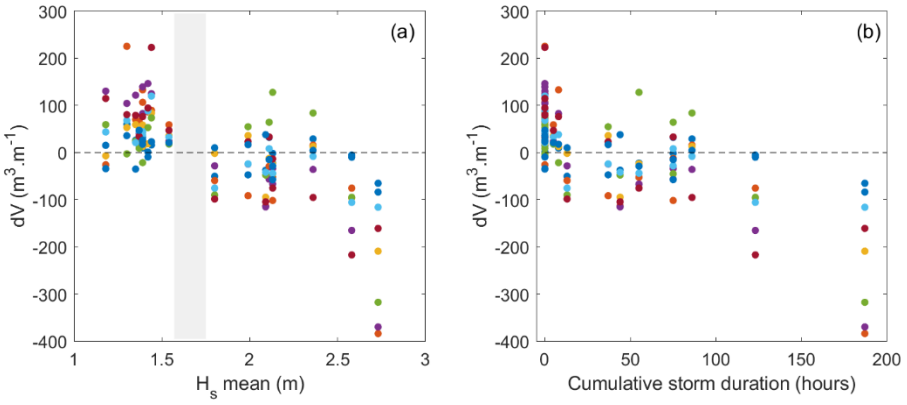

Figure 3.14: Scatter plot of 6-monthly beach volumes changes, *dV*, with (a) the corresponding 6-monthly significant wave height mean values $H_{s\,mean}$, and (b) the 6-monthly cumulative storm duration, at the 10 study sites represented by different colours (same code of colours relative to Fig. 3.9). Interpreted threshold of $H_{s\,mean}$ is indicated by the grey band. For every beach, each 6-monthly volume change *dV* value is attributed to a 6-monthly wave height mean H_s or storm duration value, a same value of wave height/storm duration can therefore correspond to several summer or winter periods. Watergate #5 and Gwithian #9 were not incorporated because they were only yearly surveyed.

The trends between volume changes and wave forcing storms depicted in Figure 3.14 do not take into account antecedent wave conditions, while previous results suggested that they have a significant role in beach behaviour. For this purpose, the ShoreFor model was used to explore in more detail the relationship between wave forcing and beach response. Considering the largely coherent beach behaviour dominated by cross-shore sediment transport across the study region, the time series representing the average beach volume time series for the 10 beaches was used (Fig. 3.15).

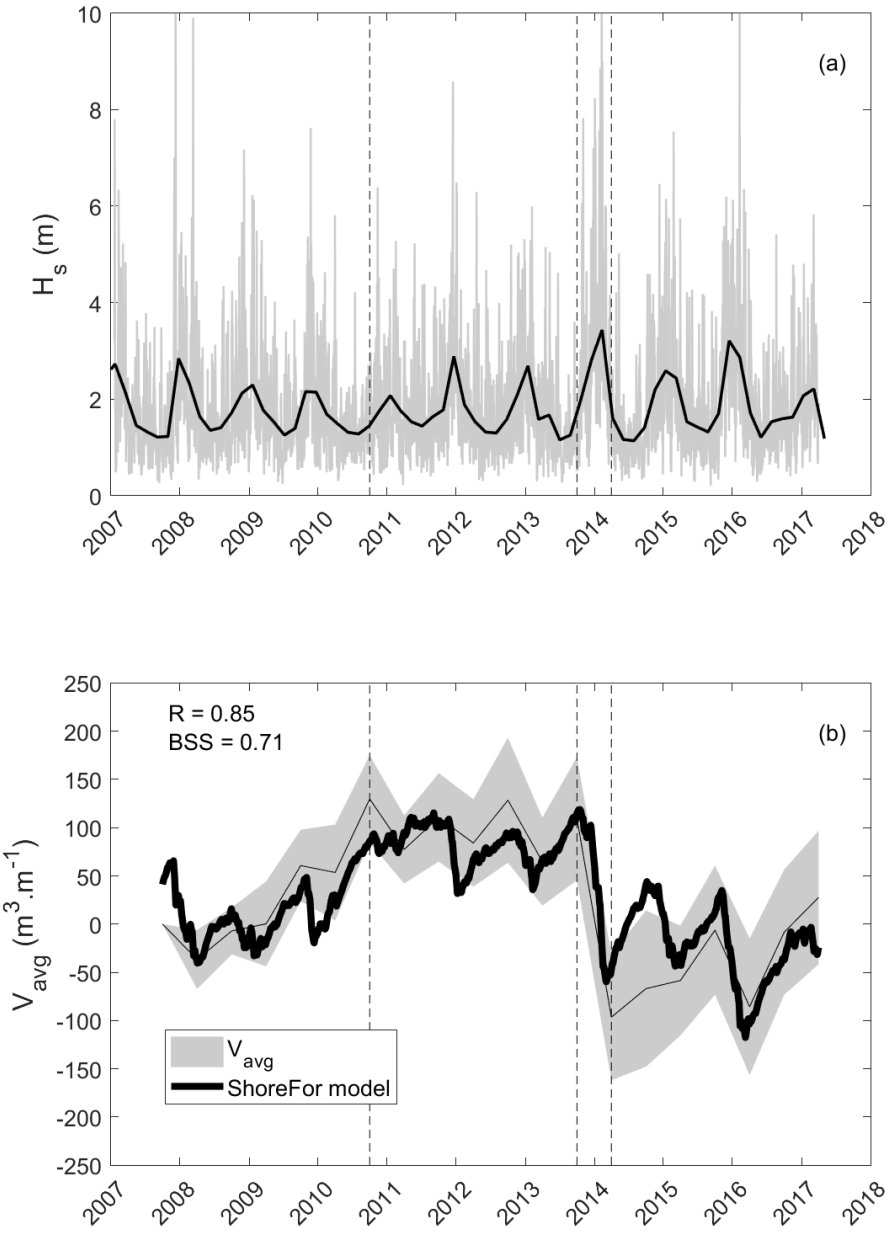

Figure 3.15: Time series from 2007 to 2017 of: (a) 3-hourly modelled significant wave height H_s (grey) and 8-week block-averaged significant wave height (black); and (b) the average of the 10 longshore-averaged beach volume time-series, V_{avg} ($m^3\ m^{-1}$), in thin black line bounded by its standard deviation in grey and ShoreFor model results represented by the thick black line.

Pearson's correlation coefficient, R, and the Brier Skill Score, BSS (Sutherland et al., 2004) calculations suggested that the model provides a good hindcast of the average of the 10 beach volume time-series (r = 0.85 and BSS = 0.71, respectively). In general, the model predicts quite well both the seasonal and

inter-annual variability in volume change. While apparent overestimations of the eroded volumes can be observed in phase 1 and 2 (e.g. 2007/08 winter, 2009/10 winter, 2011/12 winter), the erosive impact of the extreme 2013/14 storms (phase 3) is slightly under-estimated, and the recovery during the following 6 months (Summer 2014) is largely over-estimated if the previous underestimation is not considered (Fig. 3.15). The increase of inter-site variability in the magnitude of volume change over that period partially dilutes the skill of the model. Indeed, less accretion occurred during the 2014 summer at most of the study sites than the model suggests. Because most of the beaches were still in a very-much depleted state by the end of the 2014 summer, the 2014/15 winter was accretionary. The ShoreFor model predicts erosion during the 2014/15 winter because of the over-prediction for the accretion during the preceding summer. However, the energetic 2015/16 winter storm response and its subsequent recovery was very well captured by the model. The good ShoreFor model results demonstrate that the observed coherent regional variability in sand volume is linked to incident wave forcing. Consideration of antecedent conditions through their inclusion in the model also demonstrates the importance of antecedent conditions on future volume change in comparison to the simple correlations with significant wave height (Fig. 3.14).

In the previous section, the average of the 10 beach volume time-series was shown to be fairly well correlated with North Atlantic climate variations illustrated by the WEPA index (Fig. 3.10). Based on these results, winter volume changes, *dV*, for each study site were plotted against values of the

winter WEPA index (Fig. 3.16a). Results showed that these two variables were well and negatively correlated (r = -0.78) over the last 10 years. Similarly, modelled winter volume changes obtained using ShoreFor were plotted against values of the winter WEPA index (Fig. 3.16b), and also showed a good correlation (r = -0.80). Although the thin line between an accretive and an erosive winter was difficult to observe within the variability in WEPA index values, these negative correlations were particularly verified for the extreme values of the datasets (e.g. 2013/14 and 2015/16 winters), implying the use of strong positive WEPA index values as extremely energetic winters and a possible threshold effect as mentioned in section 3.4. Since the volume time series were shown to be mainly shaped by the temporal occurrence of these extreme events, these results suggest that the WEPA index values and the ShoreFor model predictions could be used as proxies for wave conditions and measured beach volume changes, respectively, in studies focusing on beach dynamics over multi-annual timescales.

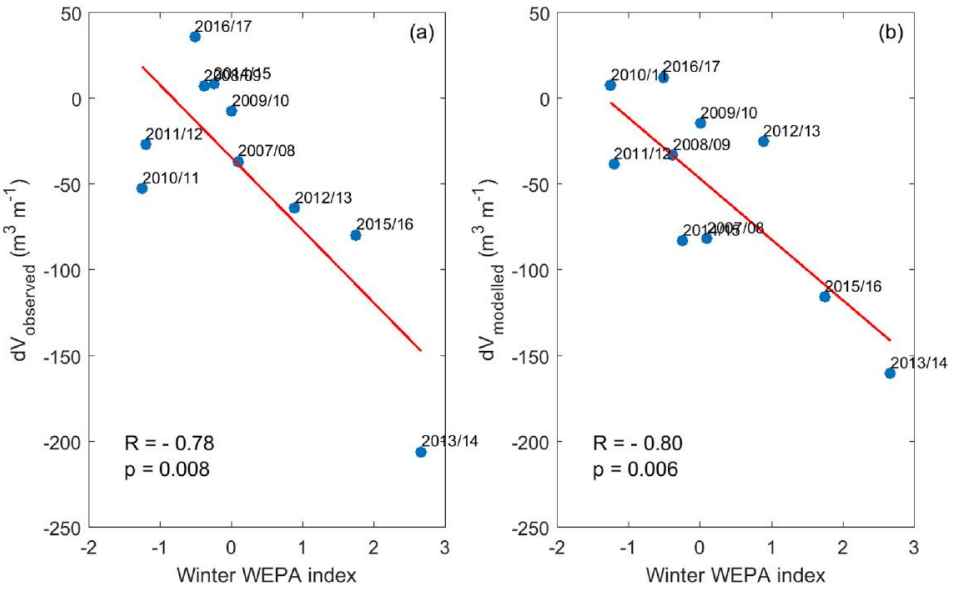

Figure 3.16: Scatter plots of the winter WEPA index with (a) the average of the 10 beach observed winter volumes changes, and (b) the average of the 10 beach modelled winter volumes changes from the 2007/08 to the 2016/17 winter.

3.6 Discussion

From 2007 to 2017, the north coast of Cornwall experienced highly variable wave conditions on seasonal and inter-annual temporal scales. This variability in wave conditions, which was fairly well correlated to a new climate index proposed for the Atlantic coast of Europe (WEPA; Castelle et al., 2017b), drove a synchronous and coherent beach response, dominated by cross-shore sediment transport, for the 10 studied beaches along this coastline. Such regionally-coherent coastal response has also been demonstrated for the east coast of Australia, where it was found that beaches of similar orientation had synchronous oscillation and rotation over a 6-year period (Short et al., 2014; Bracs et al., 2016). However, the three beaches along the east coast of Australia have similar size while, here, the 10 study sites represent a wide variety of beach size and length. As also

observed for Perranporth beach (Poate et al., 2014; Masselink et al., 2016 ; Scott et al., 2016), a well-studied beach located along the north coast of Cornwall not included in the present data set, beach volume time series of all 10 studied beaches showed seasonal variations superimposed on inter-annual variations coupled to winter wave activity. Such multi-scale variation in wave conditions is generally observed on storm-dominated coastlines with a seasonal wave climate (Ruggiero et al., 2005; Pye and Blott, 2008; Castelle et al., 2015; Barnard et al., 2017; Harley et al., 2017a).

The 10-year study period includes the 2013/14 winter, which was the most energetic winter since, at least, 1948 and caused significant morphological changes all along the west coast of Europe (Masselink et al., 2016). Results showed that these extreme wave conditions to which our 10 study sites were fully exposed (Chapter 2), were responsible of the most erosive event over, at least, the last decade. The antecedent morphological beach state being a controlling factor of beach response to storm (Voudoskas et al., 2012a; Harley et al., 2016), the dramatic response of the beaches to the 2013/14 winter is partly attributed to the fact that the beaches were in their most accreted state after the 2013 summer, enhancing the disequilibrium between beach state and wave forcing during the 2013/14 winter. Furthermore, these extreme events drove an increase of variability in the magnitude of volume change between the 10 study sites. Many factors can account for this increase of spatial variability. First, as shown in Table 3.2, the dates for which the cross-shore profiles were surveyed vary from one beach to another. A late winter survey could possibly not include one or

several storms, while a late spring survey would and could even capture some of the recovery processes. This issue has, however, only minor consequences on the results since seasonal variations in beach volume change are much larger than the changes measured by 2-month-spaced surveys carried out within the same season. Second, the 10 study sites present different geological settings. Beach morphological response to storms was demonstrated to be strongly controlled by local coastline orientation relative to storm wave direction (Harley et al., 2017a). The small differences in coastline orientation among our study sites, resulting in differences in inshore storm wave conditions, not accounted for here, could have been enhanced during storm conditions and may explain the increase of variability in volume change magnitude among the 10 beaches following the 2013/14 winter. Moreover, this chapter also showed that, after being relatively stable from 2007 to 2013, dunes shifted from swash to collision regime (Sallenger, 2000) during the 2013/14 winter, highlighting the episodic and irregular nature of beach-dune interactions (Pye and Blott, 2008; Castelle et al., 2015). The spatial variability of dune response to storm waves can be accounted for by the increased variability in volume change magnitude among the 10 beaches; likewise, other intrinsic beach characteristics could also have played a role, such as sediment size and availability (Prodger et al., 2016), headland by-passing (Valiente et al., in prep.; Wiggins et al., in prep.) or the presence of large rocky platforms.

Three years after the 2013/14 extreme storms, beach recovery is variable (from 5 to 200%) between study sites covering the four beach recovery

stages defined by Morton et al. (1994). Recent studies have also shown that substantial beach recovery following storm events can occur after days (Angnuureng et al., 2017) or between one and two years (Castelle et al., 2017a; Harley et al., 2017b). In our 10-beach dataset, only six beaches showed a percentage of recovery close or superior to 100% after 3 years, while four beaches are still recovering (between 5 and 70%). The belated post-storm beach recovery along the north coast of Cornwall appears to be mainly controlled by the winter wave conditions over the years following extreme storms, with the wave height variability in summer only playing a minor role. Indeed, only one energetic winter, such as the 2015/16 winter, nullified the total recovery that occurred over the previous 18 months. Summer conditions consistently contribute to modest beach recovery, but substantial recovery over a year only takes place when a mild and therefore accretionary winter occurs. Over the 10-year study period, the 2008/09, 2014/15 and 2016/17 winters were all accretionary and they also followed intense erosive periods during the 2006/07, 2013/14 and 2015/16 winters that left the beaches in a depleted state. These results re-emphasise the importance of the antecedent wave conditions, as well as the actual wave forcing in driving beach response. It should be noted that this conclusion concerning beach recovery is valid only for beaches with prevailing cross-shore sediment transport; recovery of beaches dominated by longshore sediment transport processes (Scott et al., 2016) is not simply dictated by the difference between antecedent and actual wave steepness, and requires a consideration of the wave direction.

Building on the coherent and synchronous beach behaviour at all study sites and the strong correlation between wave forcing and beach response, the ShoreFor equilibrium model (Davidson et al., 2013) was used to hindcast the average beach volume time series taking into account all 10 beaches. The good skill of the model indicates that the observed regionally-coherent variability in sand volume is linked to incident wave forcing and is, importantly, potentially predictable. Consideration of antecedent conditions through their inclusion in the model improves the skill of predictions, highlighting the importance of antecedent conditions on future beach volume/shoreline change, as demonstrated in previous field studies (Wright et al., 1985; Plant et al., 1999; Miller and Dean, 2004) and applications of the model to other exposed sites (Splinter et al., 2014a). In agreement with the results of Splinter et al. (2014), application of the ShoreFor model to the average beach volume time series for the 10 Cornish beaches yields a response factor $\phi \approx 1000$ days. This illustrates the strong seasonal signal with larger-winter (small-summer) waves driving beach erosion (accretion) superimposed on inter-annual variability in winter wave height driving extreme storm-erosion during energetic winters and stability, or even recovery, during mild winters. These results also show that the ShoreFor model explains most of the variability in 10 beaches when only modelled wave data were provided to force the model; this reinforces the conclusion that coherent behaviour is mainly controlled by offshore wave climate and is highly sensitive to the antecedent conditions, while beach intrinsic factors only act as secondary control factors. These findings illustrate that in regions with coherent coastal response, a relatively simple shoreline model based

on the difference between actual wave conditions and the equilibrium conditions can be successfully applied for the whole region. This has further implications for the management of beaches in terms of both predicting the impact of storms and assessing potential rates of beach recovery following severe erosion (Davidson et al., 2017). Moreover, the significant correlations between the climate index controlling winter wave activity along the Atlantic coast of Europe (WEPA) especially during very energetic winters, and observed/modelled beach annual volume changes is a promising result for the development of weather regime-driven beach/shoreline models, as suggested by Robinet et al. (2016). The recent skilful predictability of the winter North Atlantic Oscillation (Dunstone et al., 2016), which is the primary mode of atmospheric variability in the North Atlantic region, and its implication on coastline change along the western coast of Europe is worthwhile exploring.

3.7 Conclusions

1. Regionally-coherent and synchronous behaviour over the decadal time scale was observed at 10 cross-shore dominated and energetic beaches exposed to similar wave conditions, but having different sediment characteristics, beach lengths and degrees of embaymentisation. Some inter-site variability in the magnitude of volume change was observed and was shown to increase with winter significant wave height.

2. The sequence of extreme storms during the 2013/14 winter corresponded to the most erosive event over, at least, the last 10 years along the southwest coast of England. Three years later, 60% of the beaches fully or

over-recovered, while the remaining 40% only showed partial or almost non-existent recovery. Many factors accounted for this inter-site variability, such as the variability in dune erosion and recovery. Despite this spatial variability, beach recovery was shown to be mainly controlled by winter wave conditions over the years following extreme storms, in comparison to summer wave conditions that consistently contribute to modest beach recovery.

3. Skilful hindcasts of regional changes in beach volumes were obtained using an equilibrium-type shoreline model (ShoreFor), demonstrating that beach changes are coherently linked to changes in the offshore wave climate and highly sensitive to the antecedent conditions. This finding also illustrates that, in regions with cross-shore dominated beaches and coherent coastal response, the ShoreFor model can successfully be applied for the whole region.

4. Over the last 10 years, good correlations were also found between winter beach volume changes and climate index values controlling winter wave activity along the Atlantic coast of Europe (WEPA), opening up the opportunity for the development of weather regime-driven beach/shoreline models.

Chapter 4 – The relative role of antecedent beach state, tidal stage and dunes in beach response to extreme storms

4.1 Introduction

Storm events are characterised by energetic wave and wind conditions, and cause significant sediment erosion along many coastal areas of the world (Ruggiero et al., 2005; Pye and Blott, 2016; Coco et al., 2014; Castelle et al., 2015; Masselink et al., 2016; Scott et al., 2016; Barnard et al., 2017; Harley et al., 2017). These events are often defined using specific wave height thresholds obtained through different statistical methods, such as the peak-over-threshold method (Lemm et al., 1999; Dolan and Davis, 1992; Houser and Greenwood, 2005; Mendoza et al., 2011; Almeida et al., 2012; Armaroli et al., 2012; Corbella and Stretch, 2012; Plomaritis et al., 2015). Depending on wave data availability, statistical indices are calculated over long (multi-annual or multi-decadal) measured and/or modelled significant wave height time series (Masselink et al., 2015; Castelle et al., 2018). Wave height is a key factor in determining the way in which a beach responds to extreme storm activity; however, the peak wave period, the wave direction and the tidal stage coinciding with the storm peak are also important factors. Together with the wave height, the peak wave period determines the wave power (e.g. Lee et al., 1998; Karunarathna et al., 2014; Splinter et al., 2014b), while wave direction and coastline orientation influence the ratio between cross-shore and longshore sediment transport such as demonstrated In Chapter 2. The tidal stage controls the active zone of the beach affected by storm waves and this affects beach morphodynamics under storm conditions especially along meso- and macro-tidal coastal areas (Coco et al.,

2014; Dissanayake et al., 2014, Masselink et al., 2015, Guisado-Pintando and Jackson, 2018).

Along with the dynamic forcing conditions (waves and water level), other static controlling conditions (e.g., beach morphology, active/inactive dunes) are independent of storm characteristics and also influence beach response to storms. The antecedent beach state has been previously shown to control beach morphodynamics under storm conditions (Splinter et al., 2014; Harley et al., 2016). Beach morphology changes as a function of the disequilibrium between antecedent and current wave conditions (Wright and Short, 1985). A beach exposed to constant wave conditions would therefore tend to reach an equilibrium state, explaining why among a sequence of storms, beach is less responsive during the latter storm (Dissanayake et al., 2015; Masselink et al., 2015; Angnuureng et al., 2017). Other beach characteristics, such as the presence of coastal dunes, can also play a significant role in beach response to storms (Houser, 2009; Pye and Blott, 2008; Castelle et al., 2015). The variable strength of the forcing processes with regards to the dune characteristics (e.g. dune height) control the magnitude of impact (Sallenger, 2000), and the exchange of sediment between the dunes and the beach accordingly.

The process-based and open source model XBeach developed by Roelvink et al. (2009) was created with the purpose of modelling storm impact at exposed and sandy beaches. Over the past couple of years, this model has been extensively calibrated and validated for many field or laboratory experiments (McCall et al., 2010; Bolle et al., 2010; Splinter and Palmsten,

2012; Voudouskas et al., 2012b; Karunarathna et al., 2014; Dissanayake et al., 2014). XBeach models both inshore wave and tide hydrodynamics and the resulting sediment transport along a beach profile by solving shallow water equations. The model therefore offers the possibility to study beach response to extreme storms using varying beach state and hydrodynamic setting inputs.

Many beaches along the southwest coast of England are exposed to winter extra-tropical storms travelling from west to east across the North Atlantic Ocean. Perranporth beach is one of the most exposed sites along the southwest coast of England to these NW-W storm waves and experienced very severe erosion during the 2013/14 winter (Masselink et al., 2015; Scott et al., 2016). Four main clusters of beach response were classified among 157 beaches along the southwest coast of England in Chapter 2, in response to this sequence of extreme storms, categorised as 1:60 year event (Masselink et al., 2015). The two first clusters represent exposed beaches that respectively experienced large and moderate offshore sediment transport, while the third cluster represents sheltered beaches that experienced minimal erosion or even accretion during the storms and the fourth cluster represents beaches dominated by longshore transport and a rotational response. Perranporth is representative of the first two clusters, but with, compared to the other cross-shore dominated beaches, an extremely large amount of erosion experienced with some alongshore variability due to its geological settings (e.g., headland) and dune

characteristics. This fully exposed beach therefore represents a pertinent study site to examine beach response to extreme storms.

The aim of this chapter is to investigate the relative roles of hydrodynamic forcing (i.e., waves and tides), beach antecedent state and beach-dune morphology in beach response to extreme storms. Since these different factors are difficult to isolate independently or to measure in the field during storm conditions, we used a numerical modelling approach, similar to Splinter et al. (2014b) and Dissanayake et al. (2014) who addressed the role of storm clusters. The first objective is to calibrate the XBeach model using the observed and measured beach-dune response to the 2013/14 storms at Perranporth beach. The second objective is to analyse the relative role of the tidal conditions, the antecedent beach state and the presence of dunes in beach response to an extreme storm using modelled beach volume changes and hypothetical hydrodynamic scenarios. The third objective is to propose a conceptual model of beach response to extreme storms taking into consideration the tidal conditions, the antecedent beach state and the presence of dunes.

4.2 Methods

4.2.1 Study area and datasets

Perranporth beach is located in north Cornwall along the southwest coast of England (Fig. 4.1). This stretch of coastline is fully exposed to near-normally incident, energetic and highly seasonal swell waves mainly generated by extra-tropical storms tracking across the northern Atlantic Ocean during the

winter months. This macrotidal beach (MSR = 6.5 m) is 3.5 km long (Fig. 4.1), and is comprised of quartz sand (D50 = 0.33 mm; Prodger et al., 2016). It is classified as a Low-Tide Bar Rip (LTBR) beach (Scott et al., 2011), but can also be considered as dissipative during energetic winter months (Davidson et al., 2017).

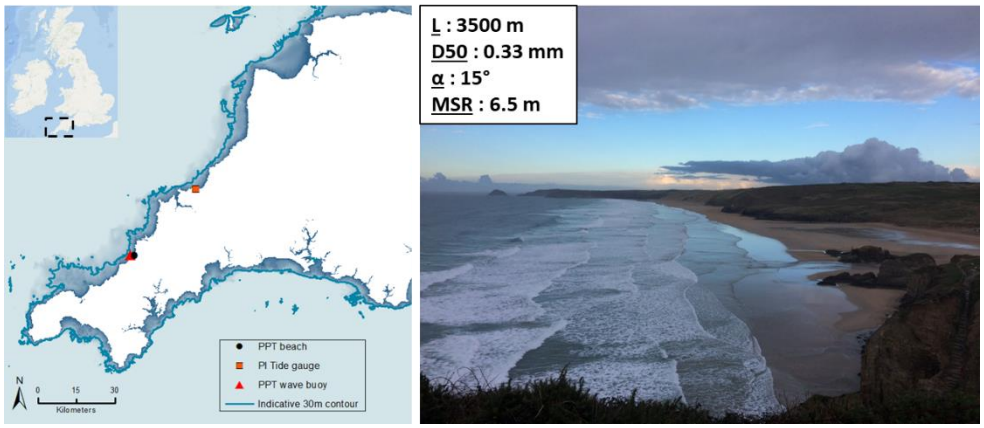

Figure 4.1: Bathymetric map of southwest England with the location of Perranporth (PPT) beach, Port Isaac (PI) tidal gauge, Perranporth (PPT) wave buoy, and the depth contour representing the 30-m line (left panel). Picture and key characteristics of Perranporth beach (right panel). L: longshore beach length in m; D50: beach grain size in mm (Prodger et al., 2016); α: clockwise beach angle orientation compare to the north-south axis; MSR: mean spring tidal range (in m).

The beach can be divided into a 2.5-km northern section (Perran sands) and a 1-km southern section (Perranporth), separated by a short rocky headland (Fig. 4.2). Using RTK-GPS equipment, the intertidal area and dunes of the southern section of the beach have been surveyed every month by the Coastal Processes Research Group at Plymouth University, while nine cross-shore profiles spread over the entire longshore length of the beach have been surveyed every year around spring time (March-April) by the Plymouth Coastal Observatory. These profiles cover the intertidal and supratidal (including dunes) areas of the beach (from -3 to 25 m). Covering the same

area of the beach, airborne LiDAR surveys were also carried out every two years since 2010 along the north coast of Cornwall where Perranporth beach is located. Bathymetric surveys of the subtidal beach area are also carried out every couple of years along the southern section (Fig. 4.2), using a RTK-GPS and single-beam echo-sounder mounted on an Arancia inshore rescue boat (IRB). Significant wave height, H_s, and peak wave period, T_p, and wave direction values are obtained every hour from a nearshore directional wave buoy located 1.4 km offshore of Perranporth beach in 16-m water depth (50.35379°N, 5.17497°W, Fig. 4.1 and 4.2). The wave buoy has been deployed since December 2006 and data are available from the Channel Coastal Observatory (https://www.channelcoast.org/southwest/). Measured water levels, from an Etrometa step gauge deployed in July 2010 at Port Isaac Harbour (Fig. 4.1), are also provided by the Channel Coastal Observatory.

These measured wave and tide conditions and the associated measured beach changes encompass the 2013/14 sequence of storms and therefore represent a unique dataset to model beach response to extreme storms using XBeach model.

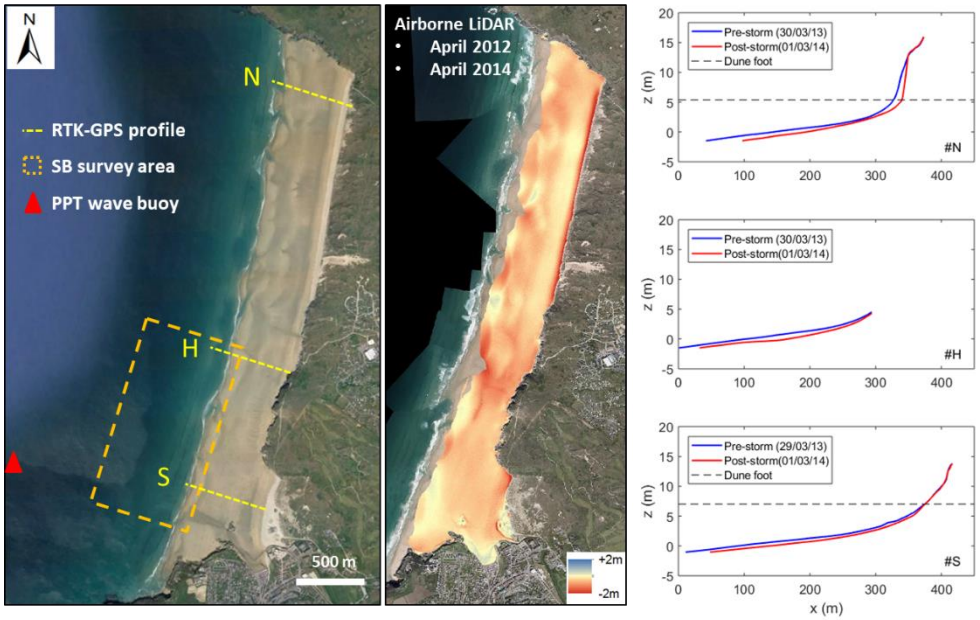

Figure 4.2: Google Earth aerial image of Perranporth beach with: the location of the RTK-GPS cross-shore profile line, the single-beam echo-sounder bathymetric survey area and the Perranporth (PPT) wave buoy (left panel); the overlapped difference of Digital Elevation Models (DEMs) between the pre- and post-storm airborne LiDAR collected in April 2012 and April 2014, respectively (middle panel); and RTK-GPS cross-shore beach profiles surveyed in March 2013 and March 2014 at the northern section (N), in front of the headland (H), and at the southern section (S) of the beach (right panel).

4.2.2 The 2013/14 storm response

The 2013/14 winter was defined as the most energetic winter recorded along the southwest coast of England (Masselink et al., 2016), and extreme storm waves caused significant erosion at Perranporth beach during that period (Scott et al., 2016).

The difference between pre- and post-storm airborne LiDAR data Digital Elevation Models (DEMs) collected in April 2012 and April 2014, and three representative RTK-GPS profiles of the south, headland and north parts of the beach surveyed in March 2013 and March 2014 are presented in Fig. 4.2. These LiDAR and RTK-GPS pre- and post-storm surveys are respectively 2

years and 1 year apart and therefore do not exactly represent the 2013/14 winter storm response. However, monthly time series of beach volume change show that most of the significant changes happened during that winter (Masselink et al., 2015; Scott et al., 2016). Furthermore, only limited post-storm recovery is encompassed within the measured storm response since the post-storm survey was carried out only a few days after the last storm of the 2013/14 winter. Both LiDAR and RTK-GPS results reveal c. 1 m vertical erosion over most of the intertidal area along the full length of the beach, with the largest erosion observed along rip currents, especially the one located in front of the headland (Fig. 4.2). LiDAR and RTK-GPS results also reveal moderate dune erosion along the southern section of the beach, often limited to the dune foot, and significant dune erosion along the northern section for which horizontal retreat was up to 14 meters (Fig. 4.2).

Two bathymetric surveys were carried out on 26/07/2012 and 10/04/2014 along the southern section of the beach covering the area shown in Fig. 4.2. The alongshore-averaged cross-shore profiles of these two surveys showed a seaward migration of a nearshore sand bar, with the bar crest migrating c. 100 m, the crest of the sandbar culminating respectively at -5 m and -9 m deep before and after the storms (Fig. 4.3a). Although these two surveys are 20 months apart, the topographic changes observed here were assumed to be mostly caused by the 2013/14 winter storm waves as discussed earlier.

The subtidal, intertidal, supratidal and dune response are needed to calibrate XBeach model. Considering that (1) no bathymetric data are available for the northern section of the beach before 2015; and (2) the

dunes along the southern section of the beach did not show significant erosion and are, furthermore, frequently reshaped; the only way to obtain a profile that can be used to calibrate the XBeach model with the current data set was to combine the southern subtidal response (Fig. 4.3a) to the northern intertidal, supratidal and dune response (Fig. 4.3b). Both datasets were merged at a depth of 3 m (relative to Mean Water Level), which corresponds to Mean Low Water Spring level (MLWS), resulting in a pre-storm and post-storm profile from the top of the dunes (20 m) to the depth of closure (-13 m; Valiente et al., submitted). These two profiles were also artificially extended to a depth of 20 m (Fig. 4.3c), for XBeach calibration purposes (Roelvink et al., 2015). Merging these two datasets represent a fair assumption since both LiDAR and RTK-GPS results show that the 2013/14 storm response at Perranporth beach was cross-shore dominated. Furthermore, only the changes over the intertidal and dune sections of the profiles are considered in the following analyses, while the subtidal part of the profile is only used for modelling purpose. The inclusion of a subtidal sand bar, although measured at the other end of the beach, provides a more realistic profile for the modelling of inshore wave dynamics and represents a step forward in comparison to previous studies where bathymetric data are not presented (Splinter and Palmsten 2012; Dissanayake et al., 2014).

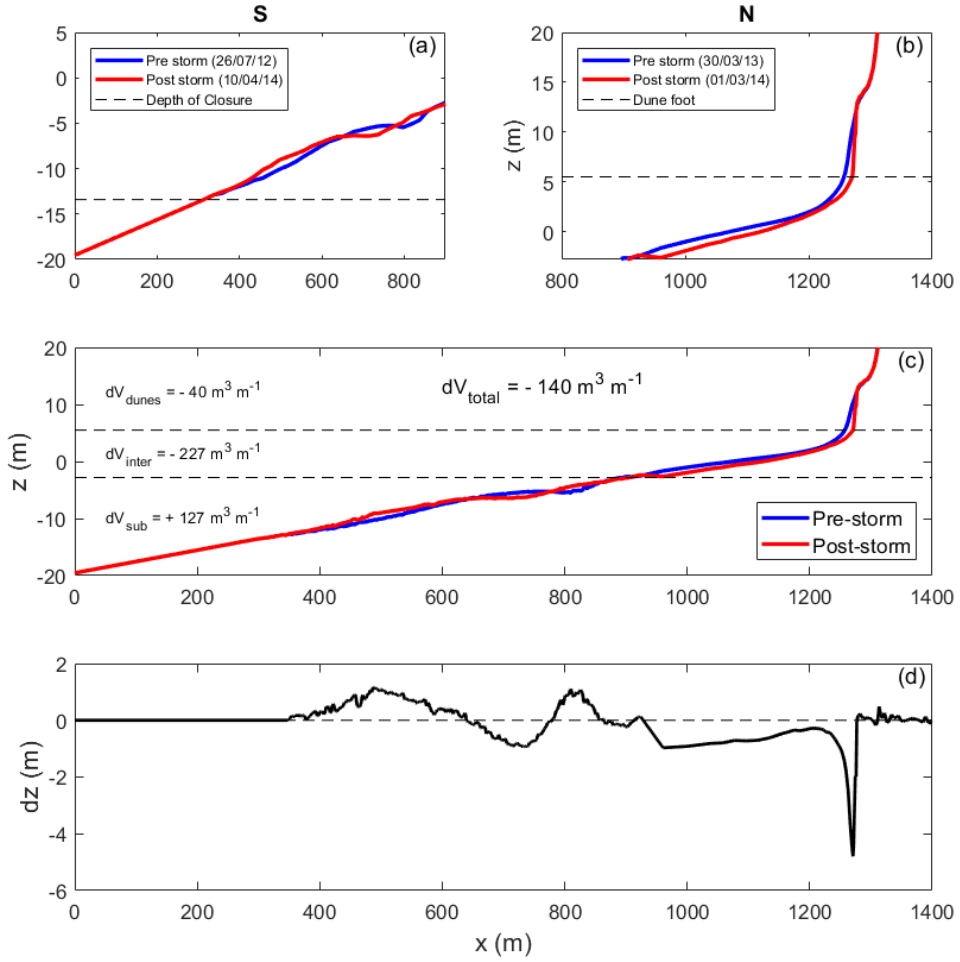

Figure 4.3: Cross-shore profiles of (a) pre- (26/07/2012) and post-storm (10/04/2014) single beam data collected by the Coastal Processes Research Group from Plymouth University along the south part of the beach; (b) pre- (30/03/2013) and post-storm (01/03/2014) RTK-GPS data collected by the Plymouth Coastal Observatory along the north embayment (p97); (c) both single beam and RTK-GPS data merged artificially extended to a 20 m depth for modelling purpose. (d) Plot of the topographical difference, *dz*, between the pre- and post-storm profiles presented in (c). The dune foot was recorded during the pre-storm RTK-GPS survey while the depth of closure was proposed by Garcia Valiente et al. (submitted).

4.2.3 Beach volume changes and wave power

Beach volume changes are used in this chapter to assess the cross-shore dominated beach response to extreme storms. Sand volume per unit metre width, V in $m^3\ m^{-1}$, was integrated along both pre- and post-storm profiles:

$$V_{profile} = \int_{x_{min}}^{x_{max}} z dx \quad (4.1)$$

where *z* corresponds to the topographic values interpolated every metre, and x_{min} and x_{max} are the cross-shore coordinates of the lowest and the fixed backshore topographic points *z*, respectively. The sand volume change between the two profiles, *dV* in $m^3\ m^{-1}$, was obtained by subtracting $V_{pre\text{-}storm}$ to $V_{post\text{-}storm}$ (Equation 4.2). To compare the subtidal, intertidal and subaerial volume changes, the cross-shore profiles were vertically divided in three zones (Fig. 4.3c): the subtidal area from the depth of closure (-13 m, Garcia Valiente et al., submitted) to Mean Low Water Spring level (-3 m); the intertidal area from Mean Low Water Spring to the dune foot recorded during the pre-storm survey (5.5 m); and the dune area from the dune foot to z_{max} (20 m). The sand volume changes between the pre- and post-storm over the subtidal, intertidal and dune areas were also calculated using Equation 4.2 and were respectively noted dV_{sub}, dV_{inter} and dV_{dunes}.

$$dV = V_{post-storm} - V_{pre-storm} \quad (4.2)$$

The comparison between the pre- and post-storm for the combined/merged cross-shore profile showed that the intertidal and dunes area eroded by 227 and 40 $m^3\ m^{-1}$, respectively, while the subtidal area accreted by 127 $m^3\ m^{-1}$ (Fig. 4.3c). Not surprisingly the sand mass is not conserved along the whole profile (-140 $m^3\ m^{-1}$), because changes over the intertidal and dune area were measured along the northern section while the changes of the subtidal area were measured along the southern section of the beach, and both sections were shown to have responded to the 2013/14 storms differently (Fig. 4.2).

In section 4.3, modelled changes are expressed as a function of variable significant wave height H_s and peak wave period T_p. To combine the effect on these two forcing parameters, deep water wave power, *P*, was calculated using an adapted version of the offshore wave equation proposed by Herbich (2000) where wave energy period T_e was replaced by peak wave period T_p :

$$P = \frac{1}{64\pi} \rho g^2 H_s^2 T_p \quad (4.3)$$

and where ρ and g corresponds to water density and gravity, respectively. However it must be taken into consideration that the peak wave period is entirely defined by the most energetic wave component, and can lead to overestimation of the wave power in comparison with other parameters such as of the mean wave period or the wave energy period.

4.2.4 XBeach model

4.2.4.1 Model description

To estimate beach erosion under storm events, the process-based and open-source numerical model XBeach (Roelvink et al., 2009), designed for this purpose, was used in this chapter. This model simulates both hydrodynamic and morphodynamic processes on sandy coasts.

XBeach uses a coordinate system where the computational x-axis is always oriented towards the coast, and the y-axis is alongshore (Roelvink et al., 2015). The 1D version of the model along the cross-shore beach profile was used in this chapter. Wave angles with relation to the computational x-axis are represented by the symbol Θ. The phase-averaged mode named

'surfbeat' was used because this study focused on extreme events along intermediate/dissipative beaches. In this mode, the short wave envelope (wave group scale) and the associated long waves are resolved. Variations of the short wave groups are solved using the short wave action balance formulation (Holthuijsen et al., 1989):

$$\frac{\partial A}{\partial t} + \frac{\partial c_{gx} A}{\partial x} + \frac{\partial c_{\theta} A}{\partial \theta} = -\frac{D_w + D_f}{\sigma} \quad (4.4)$$

Wave propagation is represented by the wave group velocity, c_g, and the wave action, A, is expressed as a function of the wave energy density and the wave frequency σ (Equation 4.4). Wave decay is represented by three wave dissipation terms that describe short wave dissipation processes due to wave breaking D_w (Roelvink, 1993; Baldock et al., 1998; Janssen and Battjes, 2007; Daly et al., 2010), bottom friction D_f (Ruessink et al., 2001). Momentum stored at the surface after wave breaking is solved using a roller model (Svendsen, 1984; Nairn et al., 1990; Stive and de Vriend, 1994), while radiation stress exerted by the short wave action (Longuet-Higgins and Stewart, 1964) is evaluated using linear wave theory.

The variations of the short wave envelope drive, through radiation stress gradient, infragravity waves and unsteady currents. These long waves and currents are solved by the XBeach model using nonlinear shallow water equations (Phillips, 1977). A depth-averaged Generalized Lagrangian Mean formulation (Andrews and McIntyre, 1978; Walstra et al., 2000) is used to calculate Lagrangian velocities as a function of wave induced stress, bed

shear stress (Ruessink et al., 2001), water level, horizontal viscosity (Smagorinsky, 1963), and the Coriolis force.

In the morphodynamic part of the model, sediment transport is modelled using a depth-averaged advection-diffusion scheme based on equilibrium sediment concentration calculations (Galappatti and Vreugdenhill, 1985):

$$\frac{\partial hC}{\partial t} + \frac{\partial hCu^E}{\partial x} + \frac{\partial}{\partial x}\left[D_h h \frac{\partial C}{\partial x}\right] = \frac{hC_{eq} - hC}{T_s} \quad (4.5)$$

where h is the local water depth, C is the sediment concentration in the water column, u^E is the eulerian velocity, D_h is the sediment diffusion coefficient, T_s is the adaptation time meant to represent the entrainment of the sediment, and C_{eq} is the equilibrium sediment concentration for both bed and suspended loads which is expressed as a function of the velocity magnitude, the orbital velocity and the fall velocity. Two sediment transport formulations are proposed in the model, the Soulsby-Van Rijn (van Rijn, 1985; Soulsby, 1997) and Van Thiel-Van Rijn (van Rijn, 2007; van Thiel de Vries, 2009), that differ by the absence of drag coefficient and the separation between currents and waves critical velocities in the latter formulation. Hindered erosion by dilatancy and bed slope effect expressions are included. The effects of wave nonlinearity (e.g. skewness and asymmetry) on sediment transport are accounted for in the advection-diffusion equation (Equation 4.5). Bottom updating is calculated based on sediment fluxes including expressions for dune avalanching and bed composition.

4.2.4.2 Model Calibration

The recommended maximum simulation time of the XBeach model is restricted to approximately 11 days (Roelvink et al., 2015). Given that the January month caused the largest beach changes at Perranporth (Masselink et al., 2015), the period of 11 days from 27/12/2013 to 07/01/2014 was selected to calibrate the model.

Cross-shore profile of the beach was provided with an horizontal resolution of 1 m. Sediment grain size was set at 0.33 mm and was assumed to be homogeneous over the entire length of the profile although some variation are expected, especially between the intertidal and dune areas. Measured time series of the significant wave height, peak wave period and water level over these 11 days were used to force the model (Fig. 4.4). Similarly to Masselink et al. (2015), a storm was defined as a wave event during which the maximum H_s exceeds the 1% exceedance offshore wave height (5.2 m), based on a 10-year time series of significant wave height recorded from the Perranporth wave buoy and such as demonstrated in Chapter 3. This threshold was exceeded three times over the 11 selected days (Fig. 4.4a), overtaking the minimum number of storms required for XBeach calibration suggested by Simmons et al. (2017). Storm 1 showed the highest significant wave height of the three (H_s = 6.8, 5.9 and 5.7 m respectively, Fig. 4.4a), but this storm occurred over neap tides while Storm 2 and 3 occurred during spring tides (Fig. 4.4c). Storm 3 was also characterized by a large wave period in comparison to the first and second storm (T_p = 14.3, 16.7 and 20 s respectively, Fig. 4.4b). However, there was no significant difference in wave

direction between the three storms (293, 294 and 284° respectively, Fig. 4.4d). During the model simulation, water levels (*TWL*) were updated every 10 minutes while wave conditions (H_s and T_p) were updated every 60 minutes. Wave groups were generated using a parametric Jonswap spectrum with a peak enhancement factor, γ, of 3.3 (Hasselmann et al., 1993), based on the concept of a fully developed sea proposed by Pierson and Moskowitz (1964). Considering the coastline orientation (285°), and the averaged wave direction (290°) of the three storms used for calibration, incident wave approach in the XBeach model was considered as almost orthogonal to the beach profile (< 5°).

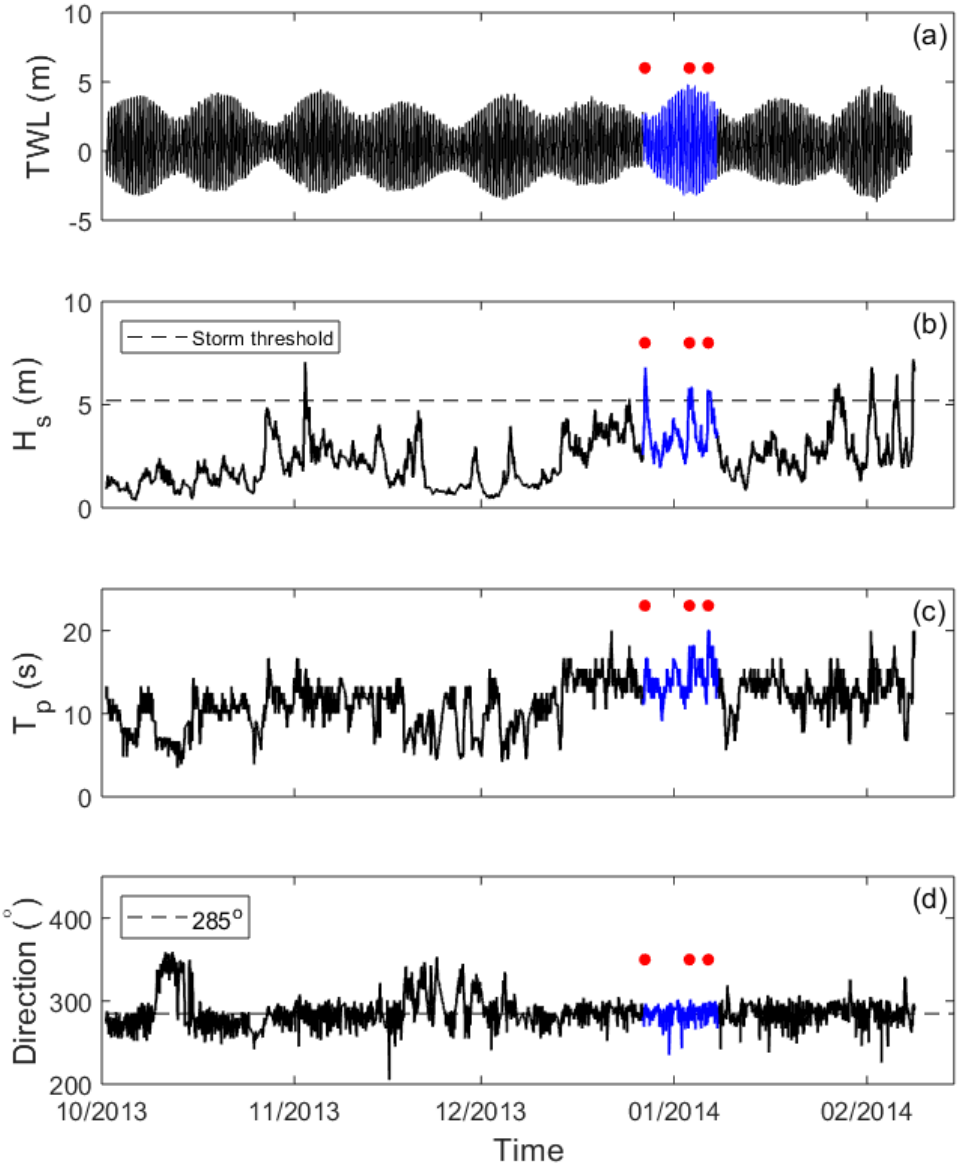

Figure 4.4: Time series from 01/10/2013 to 08/02/14 of (a) total water level, *TWL*, measured by the Port Isaac (PI) tidal gauge; (b) significant wave height H_s (m); (c) peak wave period T_p (s); and (d) wave direction (°) measured by the Perranporth (PPT) wave buoy. The 11 selected days for Xbeach calibration are coloured in blue, while Storm 1, 2 and 3 are highlighted by a red dot. The storm threshold (H_s = 5.2 m) and shore-normal waves (Direction = 285°) are represented by a dashed line in (b) and (d), respectively.

The model was first run over the 11 selected days using the default settings of the model proposed by XBeach developers (Roelvink et al., 2015). The output of this model run, presented in Fig. 4.5a, resulted in very large overestimation of the eroded volumes along the dunes (+640 %), an

underestimation of the eroded volumes over the intertidal area (-52 %), and an overestimation of the accreted volumes along the subtidal area (+219 %). Modelling morphological changes captured by 1-year apart beach-dune surveys using only 11 days of hydrodynamic forcing can be questionable. However, monthly topographic changes monitored at the south end of Perranporth beach showed that most of the changes over the 2013/14 winter at were caused by the three extreme storms encompassed in the 11 days used to force the model (Masselink et al., 2015). Although one purpose of this calibration is to reduce the overestimation and underestimation of volume changes, the main objective was to successfully describe beach and dune behaviour at Perranporth beach under different hydrodynamic scenarios. Furthermore, these large errors in topographic change, mostly over the dune area, also show that XBeach model requires a site specific calibration, such as demonstrated in other studies (Splinter and Palmsten, 2012; Vousdoukas et al., 2012; Pender and Karunarathna, 2013; Dissanayake et al., 2014; Elsayed and Oumeraci, 2017; Harter and Figlus, 2017).

The emphasis was on requiring as little deviation from the default parameter values of the model where possible, and only three parameters were modified (Table 4.1). Among the literature, many parameter modifications are proposed according to specific study sites ranging from a meso-tidal steeply sloping beach (Voudoskas et al., 2012b) to a very mild sloping (1:100) mega-tidal beach (Dissanayake et al., 2014). The model performance over the whole profile was the most sensitive to the eps parameter, which corresponds to the vertical threshold water depth above which grid cells are

considered wet (Roelvink et al., 2015). During storm conditions over spring tides, infragravity waves travel over the upper part of the beach and are likely to reach the dune foot, the wet sand located at the base of the dunes thus can be remobilised and trigger dune slumping. This dune slumping is likely to be overestimated by XBeach model by considering grid cells wet when they are not since, in reality, these infragravity waves reaching the dune foot are temporally spaced and sand can dry in between. Increasing the eps parameter value reduces the number of cells considered wet by the model and therefore reduces the overestimation of dune slumping and erosion. Dune erosion is best predicted using *eps* = 0.4 (default value = 0.05). Default wave dissipation values were used as no wave transformation data was available. However, to reduce the intertidal topographic and volume change errors, and similarly to Splinter and Palmsten (2012), the default dissipation formulation break (Roelvink, 1993, Eq. (3)) in which wave dissipation is proportional to H_{rms}^3/h, was changed for another formulation (Roelvink, 1993, Eq. (2)), in which wave dissipation is proportional H_{rms}^2/h (where H_{rms} is the local *rms* wave height in m, and *h* is the local water in m). The *morfac* parameter is a morphological acceleration factor of O(1-10) that speeds up the morphological time scale relative to the hydrodynamic timescale (Reniers et al., 2004). McCall et al. (2010) demonstrated that this factor had no significant impact on the model outputs, and its maximum value (10) is commonly used to reduce the simulation computational time (Splinter and Palmsten (2012); Voudouskas et al., 2012b; Schambach et al., 2018). However, a *morfac* factor greater than four was shown to increase model errors in our simulations, which is a similar finding to other XBeach

simulations run for macrotidal (Poate, 2011) and mega-tidal (Dissanayake et al., 2014) environments.

Table 4.1: Default and calibrated values of Xbeach model free parameters and the associated model scores. The *break* parameter corresponds to the wave breaking formulation. The *eps* parameter corresponds to the threshold water depth above which cells are considered wet, and the *morfac* parameter is a morphological acceleration factor that speeds up the morphological time scale relative to the hydrodynamic timescale (Roelvink et al., 2015). Default values were used for the other Xbeach model free key parameters. The Brier Skill Score (*BSS*, Sutherland et al., 2004) and the root mean square error (rmse) in m were used to assess the model skill during the calibration process.

Parameters	Default	Calibration
break	Roelvink, 1993 (eq. 3)	Roelvink, 1993 (eq. 2)
eps (m)	0.05	0.4
morfac	1-10	4

Scores	Default	Calibration
BSS	0.92	0.99
rmse (m)	1.48	0.39

This calibration resulted in a better performance of the model as it can be observed in Fig. 4.5b, with a Brier Skill Score (*BSS*, Sutherland et al., 2004) increasing from 0.92 to 0.99, and a root mean square error decreasing from 1.48 to 0.39 m (Table 4.1). The overestimation of the eroded volumes over the dune area was reduced from +640 to +33%, the underestimation of the eroded volumes over the intertidal area was reduced from -52 to -23%.

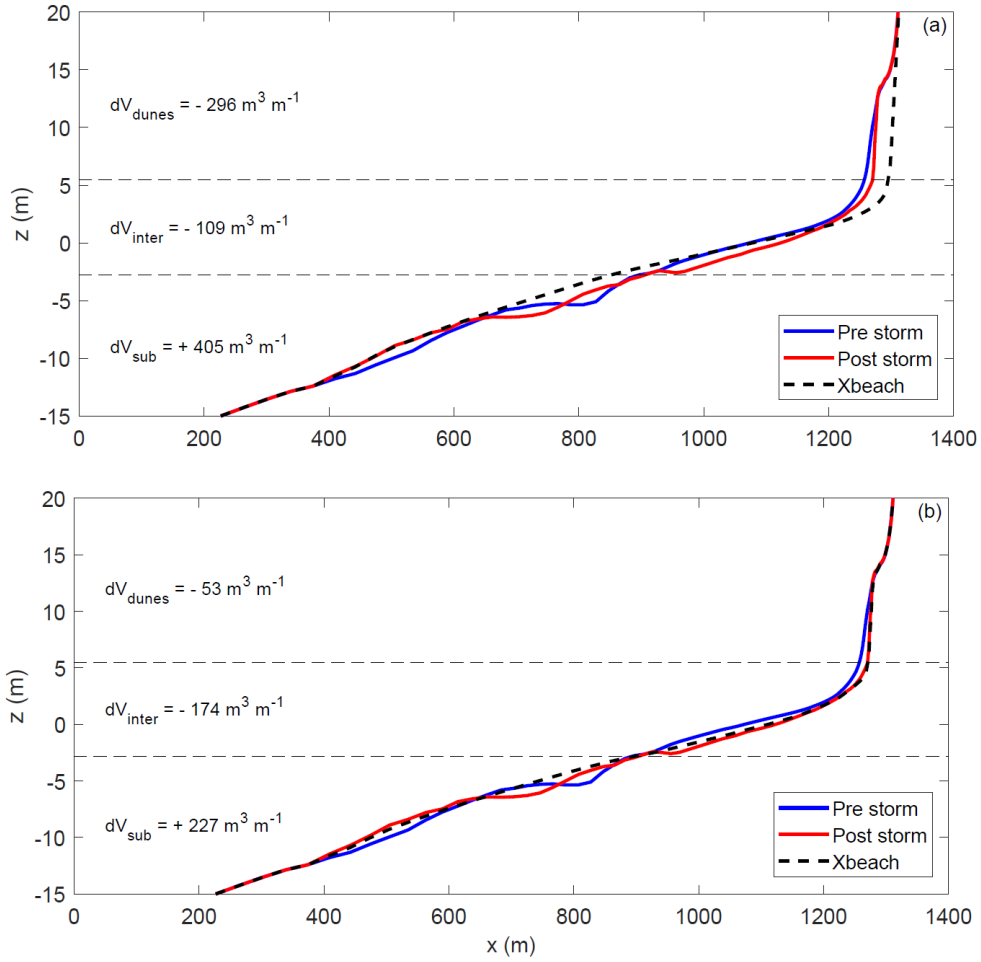

Figure 4.5: Pre-storm, post-storm and XBeach cross-shore profiles using (a) the default values and (b) modified values of the model free parameters. All profile were cut at -15 m deep and + 20 m because no changes were observed outside these vertical limits.

To analyse the impact of each of the three storm events that were recorded within the 11 days used to calibrate the model, the time series of the volume change are presented in Figure 4.6. Modelled results showed strong erosion along the whole profile (V_{total}) during the first storm and that erosion mainly occurred across the intertidal area of the beach (V_{int}). Significant erosion was observed along the dunes (V_{dune}) during the second storm, which was associated with spring tides. Erosion of the intertidal area was limited due to the sediment supply from the eroding dunes. However, during the third

storm, which was after the peak spring tides, no further dune erosion was observed while extensive erosion took place along the intertidal section of the beach. The instantaneous volume change (dV_t) time series also show the existence of opposite volume changes between the intertidal area and the dune during the second storm, demonstrating that the eroding dunes are feeding the beach (Fig. 4.6). These results highlight that the intertidal beach can either erode or accrete as a function of dune activity, which is itself controlled by synchronous large wave and spring tide levels.

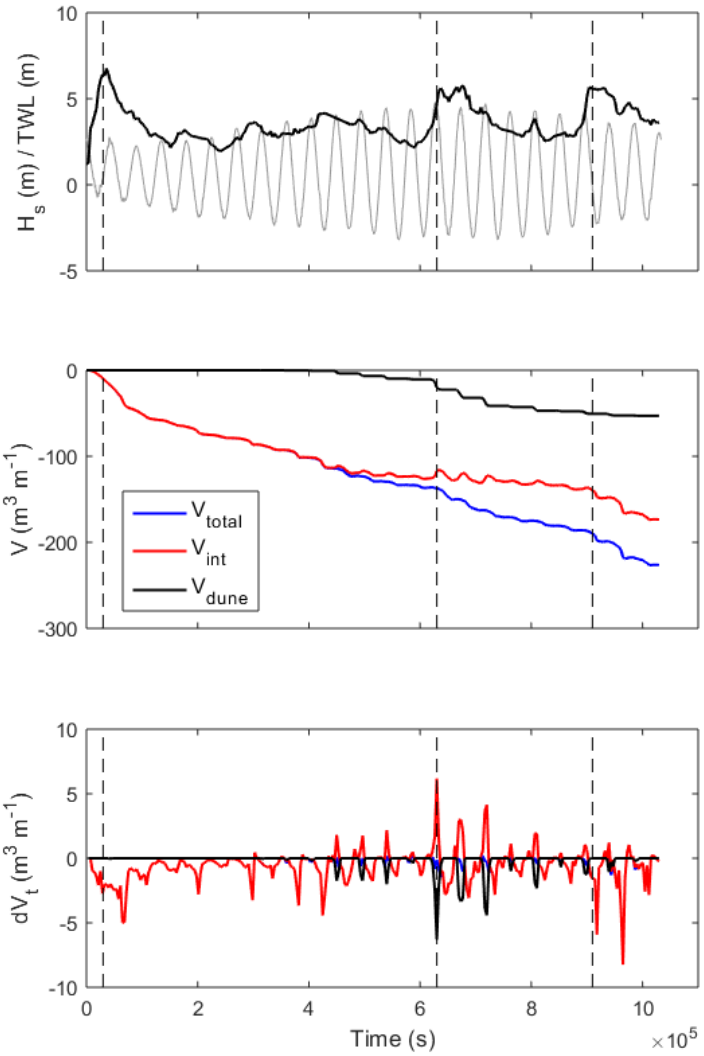

Figure 4.6: Time series of (a) measured significant wave height H_s and measured total water level *TWL* used for the calibration of the model; (b) the modelled sediment volume over the whole profile (V_{total}), the intertidal area (V_{int}) and the dune (V_{dune}); and (c) the instantaneous modelled volume change (dV_t) over the beach, the intertidal area and the dune using the same colour code than in (b). The three vertical dashed lines represent the time of storms 1, 2 and 3.

4.3 Results

4.3.1 Hypothetical hydrodynamic and morphological scenarios

To estimate the relative role played by the significant wave height, the peak wave period, the tidal stage and the antecedent beach state, hypothetical scenarios combining all these parameters were created. Varying wave

heights and periods were used to force the XBeach model during two tidal cycles at either spring or neap tides, and over either an 'accreted' or an 'eroded' beach profile. These two tidal cycles (24 hours) correspond to the average duration of large waves from an extra tropical storm (Ciavola and Coco, 2017) and the pre- and post-storm profiles presented in section 4.2 were used as the 'accreted' and 'eroded' beach profiles, respectively. Modelled volume changes over the whole beach, the intertidal area and the dunes were used as a proxy for beach response in all these scenarios.

To select realistic combinations of significant wave height, H_s, and peak wave periods, T_p, hourly measured values of these two variables recorded by the Perranporth wave buoy from 2007 to 2017 were plotted against each other (Fig. 4.7). Two bands were defined around these measured values (Fig. 4.7), and were exploited to determine the ranges of the H_s and T_p values used to force XBeach model. Significant wave significant heights were therefore divided in 15 bins ranging from 0 to 7.5 m with an interval of 0.5 m, while peak wave periods were divided in 25 bins ranging from 0 to 25 s with an interval of 1 s, resulting in 375 wave combinations. Although the probability of each wave height and period combination is variable, all combinations were considered the same way.

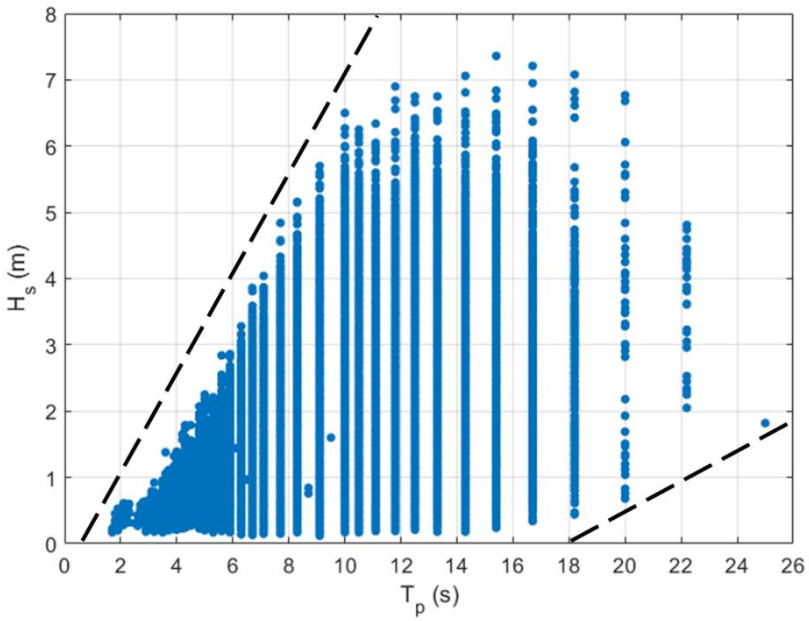

Figure 4.7: Scatter plot of hourly measured significant wave height, H_s, and peak wave period, T_p, recorded by the Perranporth wave buoy from 2007 to 2017. The two dashed lines represent the boundaries of the H_s and T_p values used to force the model.

First, to assess the role of the tidal stage in beach response, the 375 wave combinations were used to force the model for two tidal scenarios where water levels, *TWL*, correspond to spring (ST) and neap tides (NT) water levels. The water levels were obtained from measured *TWL* time series by the tidal gauge at Port Isaac (Fig. 4.1), during the spring (-3.05 m < *TWL* < 4.80 m) and neap (-1.37 m < *TWL* < 2.2 m) tides that occurred between 15/12/13 and 15/01/14 (Table 4.2). Second, to assess the role of antecedent beach state in beach response, each tidal scenario were run with the model using either an accreted profile (AP), or an eroded profile (EP). The accreted profile corresponds to the profile measured in March 2013 (Fig. 4.3b) when Perranporth beach volume was approximatively at its late winter/spring maximum over the last 10 years (Scott et al., 2016), while the eroded profile corresponds to the profile measured in March 2014 (Fig. 4.3b) when

Perranporth beach volume was at its extreme minimum over, at least the last 10 years (Scott et al., 2016). A difference of 267 m^3 m^{-1} were calculated between the two profiles, as presented in section 4.2.3. These four scenarios (ST-AP, NT-AP, ST-EP and NT-EP) resulted in four sets of model runs, which are presented in Table 4.2 for more information.

Table 4.2: Ranges of the significant wave height, H_s, peak wave period T_p, total water level *TWL*, used to force XBeach model and the selected initial beach profile chosen to run the model in the four scenarios (ST-AP: spring tides and accreted profile; NT-AP: neap tides and accreted profile; ST-EP: spring tides and eroded profile; NT-EP: neap tides and eroded profile).

	ST-AP	**NT-AP**	**ST-EP**	**NT-EP**
H_s (m)	[0 : 0.5 : 7.5]	[0 : 0.5 : 7.5]	[0 : 0.5 : 7.5]	[0 : 0.5 : 7.5]
***T_p* (s)**	[0 : 1 : 25]	[0 : 1 : 25]	[0 : 1 : 25]	[0 : 1 : 25]
***TWL* (m)**	[-3.05 , 4.80]	[-1.37 , 2.2]	[-3.05 , 4.80]	[-1.37 , 2.2]
Initial profile	Pre-storm 30/03/2013	Pre-storm 30/03/2013	Post-storm 01/03/2014	Post-storm 01/03/2014

4.3.2 Modelled beach response and volume changes

The modelled storm-induced volume changes for the four hypothetical scenarios are presented in Figure 4.8, and were calculated for the whole profile (dV_{total}), the intertidal area (dV_{inter}) and the dune region (dV_{dune}), using the methodology presented in section 4.2.2. The volume changes over the subtidal area of the beach (dV_{sub}) are not presented here because they are equivalent to the opposite values of the sum of dV_{inter} and dV_{dune} since mass conservation is applied in XBeach model. Regardless of the spring or neap tide scenarios, the intertidal area extends from Mean Low Water Spring (MLWS) to the dune foot elevation that was recorded during RTK-GPS

surveys. For this analysis, the vertical offshore boundary and landward boundaries of the intertidal zone and dunes are therefore assumed to be fixed. This assumption is fair since beach and dune volume changes are calculated over model runs that simulate beach and dune response to 24 hours of forcing conditions, which represent the averaged time window of energetic wave conditions caused by one extra-tropical storm (Ciavola and Coco, 2017). However, this assumption is not applicable to analyses where the impact of storm clustering on beach and dune morphological changes are considered, since the cross-shore position of the boundaries will be significantly modified and cannot be considered as fixed. Furthermore, the landward boundary condition is assumed to be closed since the dunes located at the north end of Perranporth beach are very high (approximatively 35 m) and largely vegetated, limiting the transport of sediment outside of the beach area due to aeolian processes.

Most of the plots presented in Figure 4.8 show an increase of erosion with increasing wave height and period, regardless of the area of the beach. However, strong variability in the magnitude of these eroded volumes can be observed among the four scenarios along the intertidal area of the beach and dune. Depending on the scenario, erosion can reach 100 m^3 m^{-1} over the intertidal area (Fig. 4.8f) and 76 m^3 m^{-1} over the dune (Fig. 4.8k) when the model is forced with the most extreme wave conditions (H_s > 6 m and T_p > 23s).

There is only small difference in total volume change (dV_{total}) between the spring tide and neap tide scenarios for a same beach state (Fig. 4.8a compare

to 4.8b, and 4.8c compare to 4.8d). The total volume of erosion was on average slightly larger by 2 ± 5 m^3 m^{-1} in the neap tide scenario compare to the spring tide along an accreted profile, and slightly smaller by 4 ± 5 m^3 m^{-1} along an eroded profile. However, the spatial partition of erosion along the accreted profile varies strongly, with the total volume erosion being made up of contributions from the intertidal beach (c. 79% in average) and the dune (c. 21%) for the spring tide scenario, whereas for the neap tide scenario all erosion comes from the intertidal area of the beach.

Much more erosion was observed along an accreted profile compared to an eroded profile (Fig. 4.8a compare to 4.8c, and 4.8b compare to 4.8d). The total erosion was larger by 25 ± 21 m^3 m^{-1} in the neap tide scenario, and by 18 ± 17 m^3 m^{-1} in the spring tide scenario. This result supports the notion of beach equilibrium since the disequilibrium between the antecedent and present wave conditions is larger along an accreted profile than an eroded profile.

The dune was not eroded, even under the most extreme H_s and T_p conditions, in the two neap tide scenarios (Fig. 4.8j and 4.8l), as waves do not reach the dune foot. However, dune erosion was observed in the two spring tide scenarios, delivering sediment from the dune to the beach that resulted in an average intertidal beach erosion reduction of 14 ± 15 m^3 m^{-1} (Fig. 4.8e compare to 4.8f), or even induced intertidal beach accretion up to 50 m^3 m^{-1} (Fig. 4.8g).

Dune erosion is enhanced by 6 ± 7 m^3 m^{-1} during spring tide when extreme wave conditions act on an eroded profile compare to an accreted profile (Fig.

4.8i compare to 4.8k). This result confirms that the dune is more active/exposed on a spring tide with an eroded profile so dunes will erode more in this scenario.

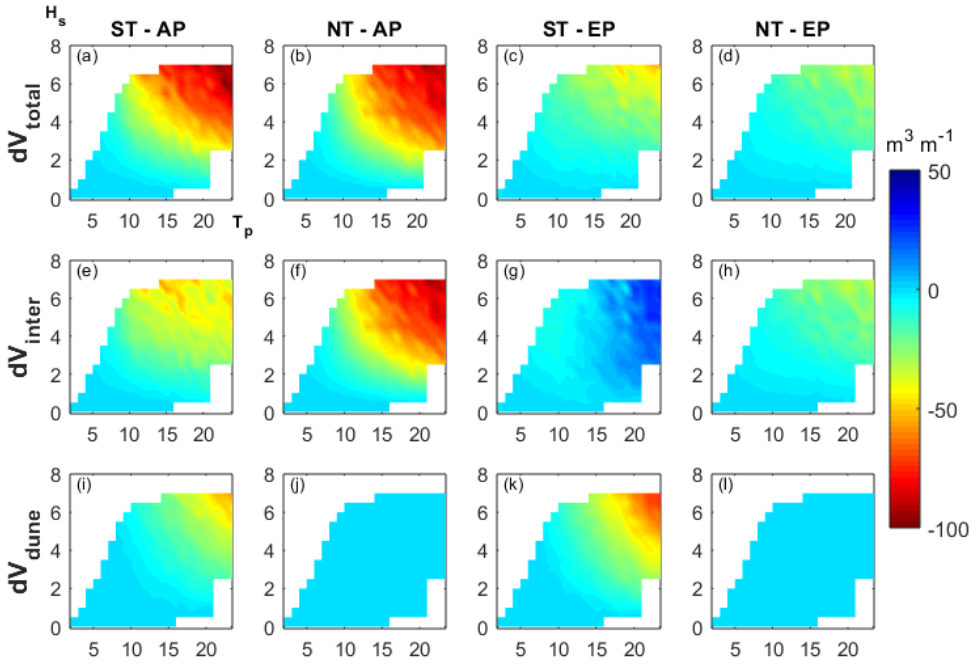

Figure 4.8: Modelled volume changes over the whole profile (dV_{total}), the intertidal area (dV_{inter}), and the dune (dV_{dune}) in function of the significant wave height H_s and the peak wave period T_p in the four scenarios (ST-AP: spring tides and accreted profile; NT-AP: neap tides and accreted profile; ST-EP: spring tides and eroded profile; NT-EP: neap tides and eroded profile).

4.3.3 Relative role of tidal stage, beach antecedent state and the presence of dunes in beach response

To compare the relative role of the tidal stage and the antecedent beach state, the modelled beach volume changes for the four scenarios were plotted together (Fig. 4.9). The combined effect of the wave significant height and the peak wave period was integrated by calculating wave power, *P*, such as presented in section 4.2.1. Results clearly show that the beach antecedent state has a larger control on the total volume change compared

to the tidal stage coinciding with storm waves, reinforcing the observations made above. In our case, erosion was on average 1.9 ± 0.9 and 2.9 ± 0.1 times higher along an accreted profile compare to an eroded one in the spring and nep tide scenarios, respectively (Fig. 4.9). Whereas erosion was in average almost equivalent (1.01 ± 0.4) in both spring and neap tide scenarios along an accreted profile, and in average 1.5 ± 0.3 times higher during spring tide compare to neap tide along an eroded profile (Fig. 4.9). This last point also confirms that, even though the beach state is close to an equilibrium with storm conditions, its lower level leaves the dune more exposed which enhances overall erosion.

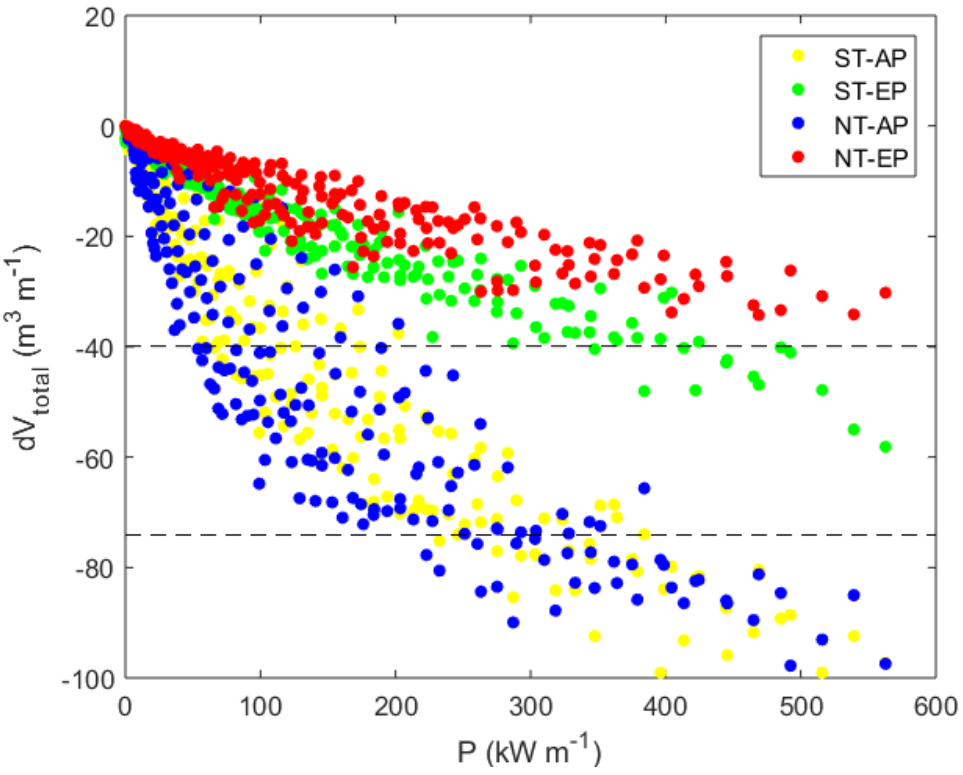

Figure 4.9: Scatter plot of the modelled volume change over the whole profile (dV_{total}) and the wave power (P) in the four scenarios (ST-AP: spring tides and accreted profile in yellow; ST-EP: spring tides and eroded profile in green; NT-AP: neap tides and accreted profile in blue; NT-EP: neap tides and eroded profile in red).

4.4 Discussion

Knowledge and understanding of beach response to extreme storms have increased over the recent years. Field-based studies showed that large scale (>100 km) beach response was strongly influenced by the coastline orientation relative to the storm track (Harley et al., 2017). On a smaller scale (km), other studies showed that variability in the storm response could be caused by the tidal conditions (Coco et al., 2014; Masselink et al., 2015; Guisado-Pintado and Jackson, 2018), the antecedent beach state (Splinter et al., 2014a; Harley et al., 2016), beach characteristics such as the presence of dunes (Houser, 2009), or geological boundaries (Loureiro et al., 2012). However, field data do not necessarily give the opportunity to assess the relative importance of all the factors that control beach response to extreme storms, justifying the use of hydrodynamic and sediment transport modelling.

In this chapter, the XBeach model was successfully applied for modelling beach and dune response to storms. As already demonstrated in other studies (Splinter and Palmsten, 2012; Vousdoukas et al., 2012; Pender and Karunarathna, 2013), a site-specific calibration was needed to find the best fit between measured and modelled data. Similarly to Poate (2011) and Dissanayake et al. (2014), high values of the acceleration factor *morfac* was shown to increase XBeach model errors when mean tidal range exceeds four meters (e.g. macrotidal). The parameter called *facua* (γ_{ua}), often modified to counter the commonly observed overestimation of erosion in the XBeach model (Splinter and Palmsten, 2012; Voudouskas et al., 2012b; Callaghan et

al., 2013; Dissanayake et al., 2014; De Santiago et al., 2017; Schambach et al., 2018) was also investigated here. This parameter control the skewness and asymmetry of waves which dictate the relative influence of onshore versus offshore wave driven sediment transport. In our case, the intertidal and subaerial erosion overestimation was effectively reduced by gradually increasing values of the *facua* parameter which enhances the onshore sediment transport. However, this enhanced onshore sediment transport also resulted in the formation of an unrealistic sand bar close to the shore while the actual sand bar position was relatively well modelled when using the default value. Instead, the parameter *eps*, used to differentiate if the sand is either wet or dry within one grid cell (Roelvink et al. , 2015), was found to be the main parameter responsible of the model errors by enhancing dune slumping. This calibration help to decrease errors in the model topographic outputs, but modelled beach volume changes were still underestimated or overestimated, depending on the beach area considered, by approximatively 30%. These approximations would probably be reduced with the use of a better dataset since the pre- and post-storm surveys dates here do not exactly match with the time-series of wave conditions used to force the model.

Significant wave height, used as the sole parameter to define a storm event (Dolan et al., 1988; Corbella and Stretch, 2012; del Rio et al., 2012), or coupled with peak wave period through the calculation of wave power (Lee et al., 1998; Haerens et al., 2012; Karunarathna et al., 2014; Splinter et al., 2014b), plays a key in beach response to extreme storms. Although wave

forcing is the main factor driving storm response, this study has shown that this response could also be significantly affected by the antecedent beach state and, in a secondary manner, by other factors such as the tidal conditions and the presence of dunes. Using one of the most accreted and the most eroded post-winter profiles recorded over the last 10 years at Perranporth beach, modelled beach response showed that volumes of erosion were on average up to three times higher for the same wave conditions along an accreted profile in comparison to an eroded profile. Moreover, knowing that the most accreted profile at Perranporth in any given year is end-summer (Scott et al., 2016), much more erosion can be expected when comparing an end-winter eroded profile and an end-summer accreted profile. Sediment volume of erosion due to individual storm is therefore strongly controlled by the antecedent state of the beach (Splinter al., 2014; Harley et al., 2016; Guisado-Pintado and Jackson, 2018), and explains why, among a cluster of storms, the first one often causes the most significant beach changes (Dissanayake et al., 2015; Masselink et al., 2015; Angnuureng et al., 2017). Such as demonstrated by Wright and Short (1985), the disequilibrium between antecedent and present wave conditions will decrease and the beach will reach an equilibrium state. However, the second storm can also cause further erosion, such as evidenced by Castelle et al. (2007) who observed that the seaward displacement of the outer bar due to the first storm left the beach unprotected and enhanced erosion during the second storm.

Similar results were found here with regards to the dunes, since dune erosion was enhanced (by 6 ± 7 m^3 m^{-1} in average) when the dune was unprotected by a low and narrow beach compared to when it was protected by a healthy beach (Hallermeier and Rhodes, 1988). Results also showed that dunes were only significantly eroding when storm conditions were synchronous to spring tides (Pye and Blott, 2008; Suanez et al., 2015; Karunarathna et al., 2018). Large sediment exchange between the dune and the beach caused by this dune erosion also caused beach accretion (Karunarathna et al., 2018) which highlights the protective aspect of the presence of dunes, such as demonstrated by Houser (2009) who observed that areas with larger foredunes and dunes along a back barrier have smaller rates of historical shoreline erosion. Furthermore, dune toe elevation was defined as the predominant determinant of maximum dune erosion by Splinter et al., (2018), drawing a parallel between the mutual importance of beach and dune antecedent states. Dune growth and post-storm recovery depend on effective winds, sediment inputs from the beach, and the binding effect of vegetation (Davidson-Arnott et al, 2018). Although Perranporth dunes are densely vegetated, their growth require strong onshore winds, and these winds are the strongest in winter when beaches are in their most depleted state, limiting sediment input from the beach.

Considering given storm wave conditions, the overall sediment volume of erosion or accretion caused by this storm along a cross-shore dominated and macrotidal energetic beach is controlled by (1) the beach antecedent state; and (2) the tidal conditions that control beach-dune interaction. These key

findings described above were used to build a conceptual model of beach response to extreme storm (Fig. 4.10). This model relates 24 hours of storm wave conditions with the resulting beach erosion/accretion in function of the different associations between the beach antecedent state, the tidal conditions and the dune activity. Four scenarios are presented: (1) a storm hits a healthy beach during neap tide where dunes are not active resulting in strong beach erosion (≈ 100 m^3 m^{-1}); (2) a storm hits a healthy beach during spring tides where dunes are slightly eroded resulting in moderate beach erosion (≈ 50 m^3 m^{-1}); (3) a storm hits an eroded beach during neap tides where dunes are not active and resulting in relatively small beach erosion (≈ 20 m^3 m^{-1}); (4) a storm hits an eroded beach during spring tides where dunes are strongly eroded resulting in beach accretion (≈ 50 m^3 m^{-1}). In terms of beach resilience, a sequence of storm coinciding with spring tides over a depleted beach represent the least hazardous scenario, for which beach is accreting. However, this accretion is caused by the loss of large dune sediment volumes, thus a sequence of storm coinciding with neap tides over a depleted beach can be considered as the least hazardous scenario in terms of coastal (beach and dune) resilience. The results presented in this chapter also highlight the importance of beach monitoring before every winter season for coastal management purposes, and the need to include these parameters in early warning systems (Poelhekke et al., 2016; Plomaritis et al., 201) to avoid discrepancies between anticipated coastal storm impacts and those actually observed (Guisado-Pintado and Jackson, 2018). Knowledge about the tidal fluctuations, that are highly predictable, should

also be coupled with beach antecedent state information for dune management purposes.

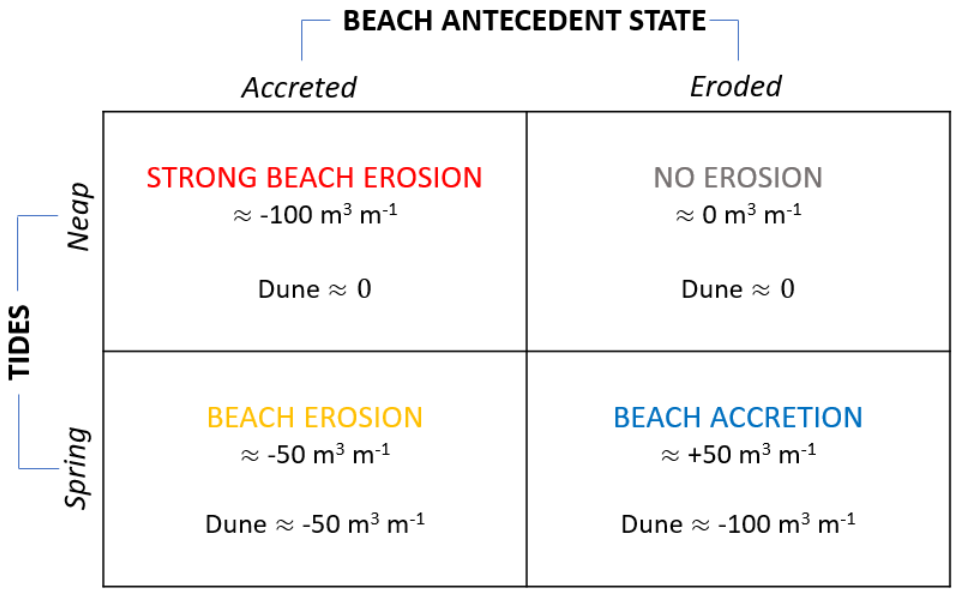

Figure 4.10: Conceptual model of a macrotidal and cross-shore dominated beach response to 24 hours of extreme storm wave conditions as a function of the beach antecedent state, the tidal stage and dune activity.

4.5 Conclusions

- The 2013/14 sequence of extreme storms recorded along the southwest coast of UK was responsible of strong morphological change and erosion (>200 m^3 m^{-1}) on fully exposed and cross-shore dominated beach. XBeach model was successfully applied to model the intertidal and dune erosion caused by the 2013/14 sequence of extreme storms.
- A method of modelling beach response to extreme storms for hypothetical scenarios with varying hydrodynamics conditions and beach state was proposed and is applicable for any coastal system where pre- and post-storm beach surveys datasets are available.

- Beside significant wave height and peak wave period, the beach antecedent state was shown to be the dominant factor in controlling the volumes of sediment erosion and accretion along a cross-shore dominated beach. Eroded volumes were, on average, up to three times higher along an accreted beach compared to an eroded beach for the same wave conditions. This increase in beach erosion volume was explained by the large disequilibrium between the antecedent and present wave conditions.
- The presence of a dune, being only significantly active during spring tides and storm conditions along this macrotidal beach, represents a natural reservoir of sand that can reduce erosion or even cause accretion along the beach. However, this natural barrier can be exposed to severe erosion when the beach is low. Volumes of dune erosion were higher when beach was in an eroded state compare to an accreted state for the same wave conditions.
- The monitoring of beach state before each winter season, along with measured/modelled tidal conditions are essential for effective beach/dune management and the development of early warning systems.

Chapter 5 – Synthesis and conclusions

5.1 Synthesis

In Figure 6.1, the key forcing and controlling factors of storm response and beach recovery acting at different spatial and temporal scales are presented. This synthesis highlights how storm response and beach recovery are related to some of these key factors in this thesis, and the results are discussed using other studies from the literature.

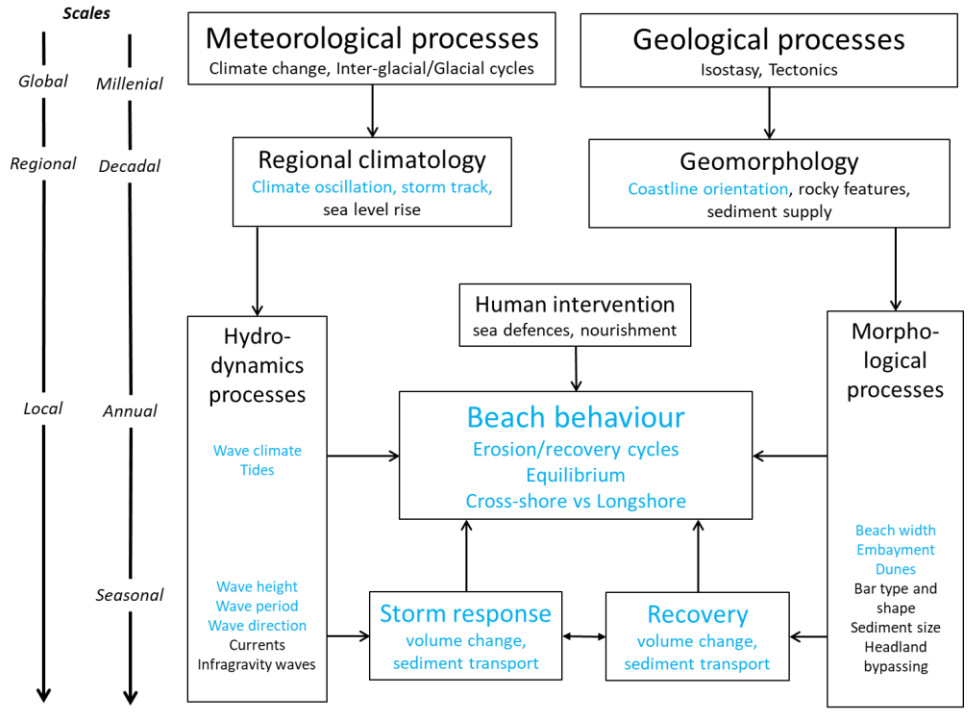

Fig. 6.1: Conceptual model of the key processes and factors involved in storm response and recovery over different temporal and spatial scales. The processes and parameters presented in this thesis are coloured in blue.

Coastline changes over millennial and global scales are controlled by climate and atmospheric variations (Petit et al., 1999) and geological processes, such as isostatic and tectonic land movements (Kiden et al., 2002). Beaches, which represent the interface between water and land, are particularly

influenced by variations in sea level and sediment supply (Zhang et al., 2002). While glacial and interglacial periods alternate at a millennial scale, decadal or annual atmospheric variations can be described by climatic oscillations observed around the globe, for example by the El Niño Southern Oscillation (ENSO; Trenberth and Hoar, 1997) and the North Atlantic Oscillation (NAO; Hurrell, 1995). The North Atlantic Oscillation (NAO) index was shown to control winter-averaged significant wave height off north west Britain (Bromirski and Cayan, 2015), while the Western Europe Pressure Anomaly (WEPA; Castelle et al., 2017b) was shown to explain the winter-averaged significant wave height variability along the Atlantic coast of Europe southward of 52^{o}. In Chapter 3 (section 3.5) , it is shown that beach volumes at cross-shore dominated beaches in south west England are correlated to the WEPA index at multi-annual timescales (Fig. 3.16), with large values of WEPA equating to large volume losses (erosion). Other studies have suggested correlations between the North Atlantic Oscillation index and nearshore bar variations (Masselink et al., 2014), beach erosion/accretion phases (Suanez et al., 2015) and shoreline change (Robinet et al., 2016) along the western coast of Europe. Similarly, Barnard et al. (2015) demonstrated that coastal change for 48 beaches throughout the Pacific Ocean basin varies most closely with El Niño/Southern Oscillation.

Decadal atmospheric and climate variability can also induce regional shifts in storm tracks (Harley et al., 2017) and/or increases in wave energy (Castelle et al., 2018), causing enhanced coastal erosion. At a regional scale, the results showed in Chapter 2 demonstrated the importance of storm tracks

and the associated storm wave incidence relative to the coastline orientation. Along the coast of south west of England, which offers a high diversity of beach orientations, four main types of storm response were defined (Fig 2.7), and their differences were mainly explained by two key factors: (1) wave exposure, essentially defined by the wave significant height and the peak wave period; and (2) the angle of storm wave approach in relation to the shoreline orientation (Fig. 2.11). Here, beaches were considered as: fully exposed when incident offshore wave angle was between 0 to 25°, semi-exposed when incident offshore wave angle was between 25 to 45°, and sheltered when this angle was exceeding 45°. The large variability in wave exposure resulted in different storm responses (Fig. 2.9) that ranged from large and alongshore uniform offshore sediment losses at exposed and cross-shore dominated sites (Castelle et al., 2015; Masselink et al., 2015), to considerable alongshore sediment redistribution (i.e., rotation), but limited net sediment change at more sheltered sites with oblique waves (Costas et al., 2005; Ruiz de Alegria-Arzaburu and Masselink, 2010). Such differences in beach response were also observed during the 2013/14 winter along the north and south coast of Brittany (Blaise et al., 2015), where beaches were alternatively fully exposed or semi-sheltered from storm waves because of two extreme storms having different tracks (i.e., north of 50° and south of 50° latitude). Harley et al. (2017) also showed that regional spatial variability in morphological response along the south east coast of Australia was predominantly controlled by local coastline alignment relative to storm wave direction, as well as by alongshore gradients in storm wave energy flux. Furthermore, the geographical

distribution of the different types of beach response along the south west coast of England shows regionally coherent beach behaviour at beaches with a similar shoreline orientation (Fig. 2.12). In Chapter 3 (section 3.4), this regional coherence was shown to be consistent over multi-annual timescales since coherent and synchronous variations in sediment volumes, albeit at different magnitudes, were observed for 10 cross-shore dominated beaches over a 10-year period (Fig 3.9). Regionally coherent beach behaviour was also highlighted by Short et al. (2014) and Bracs et al. (2016) along the south east coast of Australia, where synchronous rotation was observed over six years at three beaches with the same orientation and length, and exposed to a similar deep water wave climate and tidal regime.

Along rocky and embayed coastlines, such as the south west of England, headlands represent lateral boundaries that exert a control on beach morphodynamics and sediment transport. In this thesis, embayed beaches were characterized as short (long) when their alongshore lengths bounded by headlands was shorter (longer) than their cross-shore length (from MLWS to MHWS). In Chapter 2 (section 2.5), the length of the embayment was shown here to control beach response, and particularly limit horizontal beach rotation at shorter beaches (Fig 2.11). Loureiro et al. (2012) also showed that these natural geological boundaries constrain the morphological behaviour of embayed beaches; longshore sediment transport and beach rotation being restrained within short embayments. However, the influence of these lateral boundaries can decrease during storm conditions. In Chapter 2, it was shown that within a large bay (>10 km

long) (south east facing Start Bay, Fig. 2.13), strong erosion was observed at beaches located at the south west (updrift) end of the bay (Hallsands, Beesands, Torcross), while strong accretion was observed at beaches located at the downdrift end (Strete, Blackpool Sands). This redistribution of sediment along the large bay, between adjacent beaches within the bay, suggests the presence of subaqueous headland by-passing of the smaller headlands within the bay, such as observed at other embayed beaches exposed to oblique waves (Goodwin et al., 2013; Vieira da Silva et al., 2016). Recent studies also showed strong correlations of beach rotation and headland bypassing with climate oscillations indices, like the ENSO along the south east coast of Australia (Mortlock and Goodwin, 2016) and the NAO and WEPA along the south west coast of England (Wiggins et al., 2018).

On a regional spatial scale where beaches are exposed to similar wave conditions, strong correlations were found between beach volume changes and wave energy on both seasonal and multi-annual timescales in Chapter 3 (section 3.4). Offshore significant wave height and peak wave period are negatively correlated with beach volume changes and positively correlated with WEPA index values (Fig 3.16), while offshore wave direction influences the alongshore variability of the response. At cross-shore dominated beaches, beach volume time series showed a strong seasonal signal with larger-winter (small-summer) waves driving beach erosion (accretion) superimposed on inter-annual variability in winter wave height driving extreme storm-erosion during energetic winters and stability, or even recovery, during mild winters (Fig. 3.10). Three years after the 2013/14

extreme storms, beach recovery was shown to be variable (from 5 to 200%) at cross-shore dominated beaches. Recent studies have also shown that substantial beach recovery following storm events can occur after days (Angnuureng et al., 2017) or between one and two years (Castelle et al., 2017a; Harley et al., 2017). In our 10-beach dataset, only six beaches showed a percentage of recovery close or superior to 100% after 3 years, while four beaches are still recovering (between 5 and 70%). The belated post-storm beach recovery along the north coast of Cornwall appears to be mainly controlled by the winter wave conditions over the years following extreme storms, with the wave height variability in summer only playing a minor role.

In Chapter 3 (section 3.5), the skilful hindcasts of the beach volumes time series (Fig. 3.15) using an equilibrium-type shoreline model (Davidson et al., 2013) demonstrated that the magnitude of the storm responses and recovery rates could be largely explained by the disequilibrium between the present and antecedent wave conditions (Wright and Short, 1985). These findings illustrate that in regions with coherent coastal response, a relatively simple shoreline model based on the difference between actual wave conditions and the equilibrium conditions can be successfully applied for the whole region, and support the good performance of this model at cross-shore dominated sites around the world (Splinter et al., 2014a). In Chapter 4, the use of a process based model, XBeach (Roelvink et al., 2009) demonstrated that beach antecedent state, and thus the deviation from equilibrium, was a key element in controlling beach response to extreme storms. Eroded volumes along a cross-shore dominated and energetic sandy

beach (Perranporth) were shown to be up to three times higher along an accreted beach compared to an eroded beach for the same wave conditions (Fig. 4.9).

At the individual beach scale, dune activity was shown to play a key role in beach response during storm conditions. Modelled results showed that dunes were only significantly eroded when storm conditions were synchronous with spring high tides (Fig. 4.8), in agreement with observations from Pye and Blott (2008). The results here show that sediment exchange between the dune and the beach can result in intertidal beach accretion which highlights the protective aspect of the presence of dunes. These findings were supported by Houser (2009) who observed that areas with larger foredunes and dunes along a back barrier have smaller rates of historical shoreline erosion.

In this thesis, it was shown that the type of beach response to a storm event, defined as a combination of volume change and alongshore variability, is first determined by the degree of wave exposure at a regional scale (Chapter 2). For beaches that are exposed to a similar wave climate, the disequilibrium between the present and antecedent wave conditions, along with site-specific characteristics, such as the size of the embayment or the presence of dunes, will control the magnitude of the response and recovery rate (Chapters 3 and 4).

5.2 Conclusions

This section provides the conclusions relative to the three specific objectives defined at the start of the thesis.

The first objective was to investigate the regional storm response to, and recovery from, the 2013/14 winter sequence of extreme storms along the south west coast of England.

- Beach volume time series showed that the sequence of extreme storms during the 2013/14 winter corresponded to the most erosive event over, at least, the last 10 years along the southwest coast of England.
- Based on airborne LiDAR data collected over 157 study sites, net volumetric changes of the entire intertidal beach areas during the 2013/14 winter varied between −170 m^3 m^{-1} (strong erosion) and +66 m^3 m^{-1} (mild accretion). A new parameter, LVI, which quantifies the alongshore variability in beach response, was calculated for all 157 beaches. Values close to 1 (0) imply longshore (cross-shore) sediment transport dominance, but a non-zero value for LVI can also be caused by an along-coast variation in cross-shore sediment transport. For the 157 study sites, this parameter varied between 0.2 and 1, demonstrating the high variability in beach response observed during that winter.
- A cluster analysis was used to group beach response as a function of their similarities with regard to net volumetric changes and alongshore variability. Four different beach response types were found: (1) exposed, cross-shore dominated beaches that experienced large and alongshore uniform offshore sediment losses ($dV \approx 100$ m^3 m^{-1}); (2) semi-exposed, cross-shore dominated beaches that experienced medium alongshore uniform offshore sediment

losses (dV ≈ 50 m^3 m^{-1}); (3) short beaches that experienced limited net sediment change and alongshore variability in beach response; and (4) long beaches that experienced considerable alongshore variability (i.e., horizontal rotation) and large gross sediment change, but limited net sediment change.

- The geographical distribution of the four different response types suggested regional coherence in beach behaviour, with a dominance of offshore sediment transport observed along the exposed Atlantic-facing north coast beaches, while the south coast with its prevailing oblique wave approach was more characterised by alongshore redistribution of sediment. Furthermore, regionally-coherent and synchronous behaviour over the last 10 years was observed at 10 cross-shore dominated and energetic beaches exposed to similar wave conditions.
- Three years later after the 2013/14 winter, 60% of the most impacted beaches fully or over-recovered, while the remaining 40% only showed partial or almost non-existent recovery. During this 3-year recovery period, results showed that summer conditions contribute to beach recovery but, above all, the recovery trajectory is largely and mainly forced by winter waves. Both volume changes and wave conditions during summer months represent rather small inter-annual variability compared to winter months.

The second objective was to use observed and modelled beach volume changes to determine the key factors that force and control storm response and beach recovery along the south west coast of England.

- On a regional scale, the key factors in determining the type of beach response are (1) wave exposure, essentially defined by the wave significant height and the peak wave period; and (2) the angle of storm wave approach in relation to the shoreline orientation. Large (moderate) and alongshore uniform offshore sediment losses were observed at fully (semi-exposed) beaches, respectively, while limited net sediment change was observed at sheltered beaches. For sheltered beaches, the size of the embayment was shown to be a key factor in determining the type of beach response, by controlling longshore sediment transport. Horizontal rotation was typically observed at beaches with alongshore that were longer than their cross-shore lengths. These results suggest horizontal rotation can be observed at beaches that are long enough to receive waves at an angle, while oblique waves will be refracted and become shore normal at small pocket beaches.
- Along cross-shore dominated beaches exposed to similar wave conditions, skilful hindcasts of beach volumes were obtained using an equilibrium-type model (ShoreFor). This demonstrated that the magnitude of the storm responses and recovery rates could be largely explained by the disequilibrium between the present and antecedent wave conditions. Modelling of storm response using a process based model (XBeach) demonstrated that beach antecedent state, and thus the deviation from equilibrium, was also a key element in controlling beach response to extreme storms. Modelled volumes of erosion along a cross-shore dominated beach

(Perranporth) were shown to be up to three times higher along an accreted beach compared to an eroded beach for the same wave conditions.

- When present, coastal dunes were shown to influence storm response and recovery rates if the dunes became active during high tides. Multi-annual time-series of dune volume changes at cross-shore dominated beaches showed that dunes were only significantly eroded during the 2013/14 and 2015/16 winters, which were the two most energetic winters over, at least, the last 10 years. Modelled results demonstrated that dunes were only affected by waves when a storm event was synchronous with spring high tides, and that significant dune erosion could result in *intertidal* beach accretion over one storm event. The same modelled results also showed that the magnitude of dune erosion was higher when the intertidal beach was in an eroded state compared to an accreted state for the same wave conditions.

The third objective was to examine the correlation between large scale atmospheric circulation over the North Atlantic Ocean and storm response and beach recovery along the south west coast of England.

- Time series of the West Europe Pressure Anomaly (WEPA) were used to link atmospheric variations and coastal response. Winter values of this index, that captured the 2013/14 winter sequence of storms, were shown to be positively correlated with winter-mean significant wave heights recorded along the south west coast of England. Over

the last 10 years, the inter-annual variability in winter WEPA index values were also found to be negatively correlated (R = - 0.78) with the winter-mean beach volume changes observed at cross-shore dominated beaches.

References

Aagaard, T., Orford, J., Murray, A.S., 2007. Environmental controls on coastal dune formation: Skallingen Spit, Denmark. Geomorphology 83, 29 47.

Aagaard, T., Hughes, M., Baldock, T., Greenwood, B., Kroon, A., Power, H., 2012. Sediment transport processes and morphodynamics on a reflective beach under storm and non-storm conditions. Marine Geology 326-328, 154-165.

Almeida, L.P., Vousdoukas, M.V., Ferreira, O., Rodrigues, B.A., Matias, A., 2012. Thresholds for storm impacts on an exposed sandy coastal area in southern Portugal. Geomorphology 143-144, 3–12.

Almeida, L.P., Masselink, G., Russell, P., Davidson, M., 2014. Observations of gravel beach dynamics during high energy wave conditions using a laser scanner. Geomorphology 228 (1), 15–27.

Andrews, D.G., Mcintyre, M.E., 1978. An exact theory of nonlinear waves on a Lagrangian-mean flow. Journal of Fluid Mechanics 89, 609.

Angnuureng, D.B., Almar, R., Senechal, N., Castelle, B., Addo, K.A., Marieu, V., Ranasinghe, R., 2017. Shoreline resilience to individual storms and storm clusters on a meso-macrotidal barred beach. Geomorphology 290, 265–276.

Anon, 2002. Futurecoast: Final Project Report, DEFRA.

Anthony, E.J., 2013. Storms, shoreface morphodynamics, sand supply, and the accretion and erosion of coastal dune barriers in the southern North Sea. Geomorphology 199, 8-21.

Ardhuin, F., Aksenov, Y., Benetazzo, A., Bertino, L., Brandt, P., Caubet, E., Chapron, B., Collard, F., Cravatte, S., Delouis, J.M., Dias, F., Dibarboure, G., Gaultier, L., Johnny Johannessen, J., Anton Korosov, A., Manucharyan, G., Menemenlis, D., Menendez, M., Monnie, G., Mouche, A., Nouguier, F., Nurser, G., Rampal, P., Reniers, A., Rodriguez, E., Stopa, J., Tison, C., Ubelmann, C., van Sebille, E., Xie J., 2018. Measuring currents, ice drift, and waves from space: the Sea surface KInematics Multiscale monitoring (SKIM) concept. Ocean Science 14, 337–354.

Armaroli, C., Ciavola, P., Perini, L., Calabrese, L., Lorito, S., Valentini, A., 2012. Critical storm thresholds for significant morphological changes and damage along the Emilia-Romagna coastline, Italy. Geomorphology 143–144, 34–51.

Autret, R., Dodet,G., Fichaut, B., Suanez, S., David, L., Leckler, F., Ardhuin, F., Ammann, J.,Grandjean, P., Lallemand, P., Philipot, J.F., 2016. A comprehensive hydro-geomorphic study of cliff-top storm deposits on Banneg Island during winter 2013-2014. Marine Geology 382, 37-55.

Avdeev, A.V., Goriounov, E.V., Lavrentiev, M.M., Spigler, R., 2009. A behaviour-oriented model for long-term coastal profile evolution: validation, identification, and prediction. Applied Mathematical Modelling 33 (10), 3981–3996.

Bader, J., Mesquita, M.D.S, Hodges, K.I., Keenlyside, N., Osterhus, S., Miles, M., 2011. A review on Northern Hemisphere sea-ice, storminess and the North Atlantic Oscillation: Observations and projected changes. Atmospheric Research 101, 809–834.

Baldock, T.E., Holmes, P., Bunker, S., van Weert, P., 1998. Cross-shore hydrodynamics within an unsaturated surfzone. Coastal Engineering 34, 173–196.

Barnard, P.L., Short, A.D., Harley, M.D., Splinter, K.D., Vitousek, S., Turner, I.L., Allan, J., Banno, M., Bryan, K.R., Doria, A., Hansen, J.E., Kato, S., Kuriyama, Y., Randall-Goodwin, E., Ruggiero, P., Walker, I.J., Heathfield, D.K., 2015. Coastal vulnerability across the Pacific dominated by El Nino/Southern Oscillation. Nature Geoscience 8, 801-808.

Barnard, P.L., Hoover, D., Hubbard, D.M., Snyder, A., Ludka, B.C., Allan, J., Kaminsky, G.M., Ruggiero, P., Gallien, T.W., Gabel, L., McCandless, D., Weiner, H.M., Cohn, N., Anderson, D.L., Serafin, K.A., 2017. Extreme oceanographic forcing and coastal response due to the 2015–2016 El Nino. Nature Communications 8, 14365.

Bertin, X., Prouteau, E., Letetrel, C., 2013. A significant increase in wave height in the North Atlantic Ocean over the 20th century. Global and Planetary Change 106, 77-83.

Birkemeier, W.A., 1979. The effects of the 19 December 1977 coastal storm on beaches in North Carolina and New Jersey. Shore Beach 47, 7–15.

Blaise, E., Suanez, S., Stéphan, P., Fichaut, B., David, L., Cuq, V., Autret, R., Houron, J., Rouan, M., Floc'h, F., Ardhuin, F., Cancouët, R., Davidson, R., Costa, S., Delacourt, C., 2015. Bilan des tempêtes de l'hiver 2013-2014 sur la dynamique du recul du trait de côte en Bretagne. Geomorphologie, Relief, Processus, Environment 21, 267-292.

Blekinsopp, C., Turner, I.L., Allis, M.J., Peirson, W.L., Garden, L.E., 2012. Application of LIDAR technology for measurement of time-varying free surface profiles in a laboratory wave flume. Coastal Engineering 68, 1–5.

Bolle, A., Mercelis, P., Roelvink, D., Haerens, P., Trouw, K., 2010. Application and Validation of XBeach for Three Different Field Sites. Coastal Engineering'10 Proceedings.

Boon, J., 2007. Ernesto: Anatomy of a Storm Tide. Virginia Institute of Marine Science, College of William and Mary, USA.

Bracs, M.A., Turner, I.L., Splinter K.D., Short, A.D., Mortlock, T.R., 2016. Synchronised patterns of erosion and deposition observed at two beaches. Marine Geology 380, 196-204.

Bradbury, A.P., Mason, T.E., Holt, M.W., 2004. Comparison of the performance of the Met office UK-waters wave model with a network of shallow water moored buoy data, 8th International Workshop of Wave Hindcasting and Forecasting, North Shore, Oahu, Hawaii.

Bramato, S., Ortega-Sanchez, M., Mans, C., Losada, M.A., 2012. Natural Recovery of a Mixed Sand and Gravel Beach after a Sequence of a Short Duration Storm and Moderate Sea States. Journal of Coastal Research 28 (1), 89–101.

Bray, M.J., Hooke, J.M., 1997. Prediction of soft-cliff retreat with accelerating sea level rise. Journal of Coastal Research 13, 453-467.

Brock, J.C., Wright, C.W., Sallenger, A.H., Krabill, W.B., Swift, R.N., 2002. Basis and methods of NASA Airborne Topographic Mapper lidar surveys for coastal studies. Journal of Coastal Research 18 (1), 1–13.

Bromirski, P.D., Cayan, D.R., 2015. Wave power variability and trends across the North Atlantic influenced by decadal climate patterns. Journal of Geophysical Research 120, 3419–3443.

Brooks, S.M., Spencer, T., Christie, E.K., 2017. Storm impacts and shoreline recovery: Mechanisms and controls in the southern North Sea. Geomorphology 283, 48–60.

Bruun, P., 1954. Coast erosion and the development of beach profiles. Beach erosion board technical memorandum 44, U.S. Army Engineer Waterways Experiment Station, Vicksburg, MS, USA.

Burningham, H., French, J., 2012. Is the NAO winter index a reliable proxy for wind climate and storminess in northwest Europe? International Journal of Climatology 33, 2036–2049.

Burt, S., 1993. Another new North Atlantic low pressure record. Weather 48 (4), 98–103.

Buscombe, D.D., Scott, T.M., 2008. The Coastal Geomorphology of North Cornwall: St. Ives Head to Trevose Head. Wave Hub Impact on Seabed and Shoreline Processes (WHISSP). University of Plymouth.

Callaghan, D.P., Ranasinghe, R., Roelvink, D., 2013. Probabilistic estimation of storm erosion using analytical, semi-empirical, and process based storm erosion models. Coastal Engineering 82, 64–75.

Capo, S., Lubac, B., Marieu, V., Robinet, A., Bru, D., Bonneton, P., 2014. Assessment of the decadal morphodynamic evolution of a mixed energy inlet using ocean color remote sensing. Ocean Dynamics 64 (10), 1517–1530.

Castelle, B., Turner, I.L., Ruessink, B.G., Tomlinson, R.B., 2007. Impact of storms on beach erosion: Broadbeach (Gold Coast, Australia). Journal of Coastal Research 50 (SI), 534–539.

Castelle, B., Coco, G., 2012. The morphodynamics of rip channels on embayed beaches. Continental Shelf Research 43, 10-23.

Castelle, B., Marieu, V., Bujan, S., Ferreira, S., Parisot, J.P., Capo, S., Senechal, N., Chouzenoux, T., 2014. Equilibrium shoreline modelling of a high-energy meso-macrotidal multiple-barred beach. Marine Geology 347, 85-94.

Castelle, B., Marieu, V., Bujan, S., Splinter, K.D., Robinet, A., Sénéchal, N., Ferreira, S., 2015. Impact of the winter 2013-2014 series of severe Western Europe storms on a double-barred sandy coast: beach and dune erosion and megacusp embayments. Geomorphology 238, 135-148.

Castelle, B., Bujan, S., Ferreira, S., Dodet, G., 2017a. Foredune morphological changes and beach recovery from the extreme 2013/2014 winter at a high-energy sandy coast. Marine Geology 385, 41–55.

Castelle, B., Dodet, G., Masselink, G., Scott, T., 2017b. A new climate index controlling winter wave activity along the Atlantic coast of Europe: the West Europe Pressure Anomaly. Geophysical Research Letters 44.

Castelle, B., Dodet, G., Masselink, G., Scott, T., 2018. Increased winter-mean wave height, variability and periodicity in the North-east Atlantic over 1949-2017. Geophysical Research Letters 45 (8), 3586–3596.

Choowong, M., Phantuwongraj, S., Charoentitirat, T., Chutakositkanon, V., Yumuang, S., Charusiri, P., 2009. Beach recovery after 2004 Indian Ocean tsunami from Phang-nga, Thailand. Geomorphology 104, 134–142.

Church, J.A., White, N.J., 2006. A 20th century acceleration in global sea-level rise. Geophysical Research Letters 33, L01602.

Ciavola, P., Coco, G., 2017. Coastal Storms: Processes and Impacts. Wiley, 1–22.

Clayton, K., Shamoon, N., 1998. New approach to the relief of Great Britain II. A classification of rocks based on relative resistance to denudation. Geomorphology 25, 155-171.

Coco, G., Senechal, N., Rejas, A., Bryan, K.R., Capo, S., Parisot, J.P., Brown, J.A, MacMahan, J.H.M., 2014. Beach response to a sequence of extreme storms. Geomorphology 204, 493–501.

Cooper, J.A.G., Jackson, D.W.T., Navas, F., McKenna, J., Malvarez, G., 2004. Identifying storm impacts on an embayed, high-energy coastline : examples from western Ireland. Marine Geology 210, 261-280.

Cooper, J.A.G., Pilkey, O.H., 2004b. Sea-level rise and shoreline retreat: time to abandon the Bruun Rule. Global and Planetary Change 43, 157 – 171.

Corbella, S., Stretch, D.D., 2012. Shoreline recovery from storms on the east coast of Southern Africa. Natural Hazards and Earth System Sciences 12, 11–22.

Costas, S., Alejo, I., Vila-Concejo, A., Nombela, M.A, 2005. Persistence of storm-induced morphology on a modal low-energy beach: A case study from NW-Iberian Peninsula. Marine Geology 224, 43-56.

Cowell, P.J., Stive, M.J.F., Niedoroda, A.W., Swift, D.J.P., De Vriend, H.J., Buijsman, M.C., Nicholls, R.J., Roy, P.S., Kaminsky, G.M., Clevering, A.J., Reed, C.W., De Boer, P.L., 2003. The coastal-tract (part 2): applications of aggregated modeling to lower-order coastal change. Journal of Coastal Research 19 (4), 828–848.

Daly, C., Roelvink, J.A., van Dongeren, A.R., McCall, R.T., 2010. Short wave breaking effects on law frequency waves. Proceedings 30th International Conference on Coastal Engineering, San Diego, 1–13.

Davidson, M.A., Turner, I.L., 2009. A behavioral template beach profile model for predicting seasonal to interannual shoreline evolution. J. Geol. Res. 114, F01020.

Davidson, M.A., Lewis, R.P., Turner, I.L., 2010. Forecasting seasonal to multi-year shoreline change. Coastal Engineering 57, 620–629.

Davidson, M.A., Splinter, K.D., Turner, I.L., 2013. A simple equilibrium model for predicting shoreline change. Coastal Engineering 73, 191–202.

Davidson, M.A., Turner, I.A., Splinter, K.D., Harley, M.D., 2017. Annual prediction of shoreline erosion and subsequent recovery. Coastal Engineering 130, 14–25.

Davidson-Arnott, R.G.D., Hesp, P.A., Ollerhead, J., Walker, I.J., Bauer, B.O., Delgado-Fernandez, I., Smyth, T.A.G., 2018. Sediment Budget Controls on Foredune Height: Comparing Simulation Model Results with Field Data. Earth Surface Processes and Landforms 43 (9), 1798–1810.

Dehouck, A., Dupuis, H., Sénéchal N., 2009. Pocket beach hydrodynamics: The example of four macrotidal beaches, Brittany, France. Marine Geology 266, 1–17.

Del Río, L., Plomaritis, T.A., Benavente, J., Valladares, M., Ribera, P., 2012. Establishing storm thresholds for the Spanish Gulf of Cádiz coast. Geomorphology 143-144, 13–23.

BERR: Department for Business, Enterprise and Regulatory Reform, 2008. Atlas of UK Marine Renewable Energy Resources. Technical Report. ABP Marine Environmental Research Ltd. R/3719/8 R.1432.

De Santiago, I., Morichon, D., Abadie, S., Reniers, A.J.H.M., Liria, P., 2017. A comparative study of models to predict storm impact on beaches. Natural Hazards 87, 843–865.

Dissanayake, P., Brown, J., Karunarathna, H., 2014. Modelling storm-induced beach/dune evolution: Sefton coast, Liverpool Bay, UK. Marine Geology 357, 225–242.

Dissanayake, P., Brown, J., Wisse, P., Karunarathna, H., 2015. Effects of storm clustering on beach/dune evolution. Marine Geology 370, 63-75.

Dodet, G., Bertin, X., Taborda, R., 2010. Wave climate variability in the North-East Atlantic Ocean over the last six decades. Ocean Modelling 31, 120-131.

Dolan, R., Davis, R.E., 1992. An intensity scale for Atlantic coast northeast storms. Journal of Coastal Research 8 (4), 840–853.

Dubois, R.N, 1988. Seasonal changes in beach topography and beach volume in Delaware. Marine Geology 81 (1), 79–96.

Dunstone, N., Smith, D., Scaife, A., Hermanson, L., Eade, R., Robinson, N., Andrews, M., Knight, J., 2016. Skilful predictions of the winter North Atlantic Oscillation one year ahead. Nature Geosciences 9, 809–814.

Dyer, K.R., Moffat, T., J., 1998. Fluxes of suspended matter in the East Anglian plume Southern North Sea. Continental Shelf Research 18, 1311–1331.

Elsayed, S.M., Oumeraci, H., 2017. Effect of beach slope and grain-stabilization on coastal sediment transport: An attempt to overcome the erosion overestimation by XBeach. Coastal Engineering 121, 179–196.

Emery, K.O., 1961. A simple method of measuring beach profiles. Limnology and Oceanography 6, 90–93.

Earlie, C.S., Young, A.P., Masselink, G., Russell, P.E., 2015. Coastal cliff ground motions and response to extreme storm waves. Geophysical Research Letters 42, 847–854.

Fairbanks, R.G., 1989. A 17,000-year glacio-eustatic sea level record: Influence of glacial melting rates on the Younger Dryas event and deep-ocean circulation. Nature 342, 637–642.

Feser, F., Barcikowska, M., Krueger, O., Schenk, F., Weisse, R., Xia, L., 2014. Storminess over the North Atlantic and northwestern Europe – A review. Quarterly Journal of the Royal Meteorological Society 141, 350–382.

Galappatti, R., Vreugdenhill, C.B., 1985. A depth integrated model for suspended transport. Journal for Hydraulic Research 23(4), 359–377.

Garcia-Rubio, G., Huntley D.A., Russell, P., 2014. Evaluating shoreline identification using optical satellite images. Marine Geology 359, 96–105.

Garnier, E., Ciavola, P., Spencer, T., Ferreira, O., Armaroli, C., McIvor, A., 2018. Historical analysis of storm events: Case studies in France, England, Portugal and Italy. Coastal Engineering 134, 10–23.

Ge, Z., Dai, Z., Pang, W., Li, S., Wei, W., Mei, X., Huang, H., Gu, J., 2017. LiDAR-based detection of the post-typhoon recovery of a meso-macro-tidal beach in the Beibu Gulf, China. Marine Geology 391, 127–143.

Gonçalves, J. A., Henriques, R., 2015. UAV photogrammetry for topographic monitoring of coastal areas. Journal of Photogrammetry and Remote Sensing 104, 101–111.

Goodwin, I.D., Freeman, R., Blackmore, K., 2013. An insight into headland sand bypassing and wave climate variability from shoreface bathymetric change at Byron Bay, New South Wales, Australia. Marine Geology 341, 29-45.

Gower, J.C, Ross, G.J.S, 1969. Minimum Spanning Trees and Single Linkage Cluster Analysis. Journal of the Royal Society (Applied Statistics) 18, 54-64.

Guisado-Pintado, E., Jackson, D.W.T., 2018. Multi-scale variability of storm Ophelia 2017: The importance of synchronised environmental variables in coastal impact. Science of the Total Environment 630, 287–301.

Haerens, P., Bolle, A., Trouw, K., Houthuys, R., 2012. Definition of storm thresholds for significant morphological change of the sandy beaches along the Belgian coastline. Geomorphology 143-144, 104-117.

Haigh, I.D., Wadey, M.P., Wahl, T., Ozsoy, O., Nicholls, R.J., Brown, J.M., Horsburgh, K., Gouldby, B., 2016. Spatial and temporal analysis of extreme sea level and storm surge events around the coastline of the UK. Scientific Data 3, 160107.

Hallermeier, R.J., Rhodes, P.E., 1988. Generic treatment of dune erosion for 100-year event. Coastal Engineering (Chapter 89), 1197–1211.

Harley, M., Turner, I., Short, A., Ranasinghe, R., 2011. A re-evaluation of coastal embayment rotation: the dominance of cross-shore versus alongshore sediment transport processes, Collaroy-Narrabeen Beach, SE Australia. Journal of Geophysical Research Earth Surface 116, F04033.

Harley, M.D., Turner, I.L., Short, A.D., 2015. New insights into embayed beach rotation: The importance of wave exposure and cross-shore processes. Journal of Geophysical Research Earth Surface120, 1470-1484.

Harley, M.D., Turner, I.L., Splinter, K.D., Phillips, M.S., Simmons, J.A., 2016. Beach response to Australian East Coast Lows: a comparison between the 2007 and 2015 events, Narrabeen-Collaroy Beach. Journal of Coastal Research 75 (SI), 388-392.

Harley, M.D., Turner, I.L., Kinsela, M.A., Middleton, J.H., Mumford, P.J., Splinter, K.D., Phillips, M.S., Simmons, J.A., Hanslow, D.J., Short, A.D., 2017a. Extreme coastal erosion enhanced by anomalous extratropical storm wave direction. Scientific Reports 7, 6033.

Harley, M.D., Turner, I.L., Middleton, J.H., Kinsela, M.A., Hanslow, D., Splinter, K.D., Mumford, P., 2017b. Observations of beach recovery in SE Australia following the June 2016 east coast low. Coasts & Ports 2017 Conference – Cairns, Australia.

Harris, D.L. 1963. Characteristics of the Hurricane Storm Surge. Technical paper no. 48. U.S. Weather Bureau.

Harter, C., Figlus, J., 2017. Numerical modeling of the morphodynamic response of a low-lying barrier island beach and foredune system inundated during Hurricane Ike using XBeach and CSHORE. Coastal Engineering 120, 64–74.

Hasselmann, S., Briining, C., Lionello, P., 1993. Towards a generalized Optimal Interpolation Method for the assimilation of ERS-1 SAR retrieved

wave spectra in a wave model. Second ERS-1 Symposium, Hamburg, Germany.

Hegge, B., Eliot, I., Hsu, J., 1996. Sheltered sandy beaches of Southwestern Australia. Journal of coastal research 12 (3), 748.

Herbich, J.B, 2000. Handbook of coastal engineering. McGraw-Hill Professional, New York City, USA.

Holthuijsen, L.H., Booij, N., Herbers, T.H.C., 1989. A prediction model for stationary, short-crested waves in shallow water with ambient currents. Coastal Engineering 13(1), 23–54.

Horikawa K., 1988. Nearshore dynamics and coastal processes. Univ. of Tokyo Press, Japan, pp 40-88.

Horrillo-Caraballo, J.M., Reeve, D.E., 2010. A comparison of the performance of Canonical Correlation Analysis on sand and shingle beaches. Marine Geology 274, 120–134.

Houser, C., Greenwood, B., 2005. Profile response of a lacustrine multiple barred nearshore to a sequence of storm events. Geomorphology 69, 118–137.

Houser, C., 2009. Synchronization of transport and supply in beach-dune interaction. Progress in Physical Geography: Earth and Environment 33 (6), 733–746.

Houser, C., Wernette, P., Rentschlar, E., Jones, H., Hammond, B., Trimble, S., 2015. Post-storm beach and dune recovery: Implications for barrier island resilience. Geomorphology 234, 54–63.

Huller, S., 2004. Defining the Wind: The Beaufort Scale, and How a 19th-Century Admiral Turned Science into Poetry. Crown Publishers, New York, USA.

Hulme, M., 1997. The climate in the UK from November 1994 to October 1995. Weather 52 (8), 242–257.

Hurrell, J.W., 1995. Decadal Trends in the North Atlantic Oscillation: Regional Temperatures and Precipitation. Science 269 (5224), 676–679.

Hurrell, J.W., 2001. North Atlantic Oscillation (NAO). Encyclopedia of Ocean Sciences 4, 1904–1911.

Jackson, D.W.T., Cooper, J.A.G., Del Rio, L., 2005. Geological control of beach morphodynamic state. Marine Geology 216, 297-314.

Jackson, N.L., Nordstrom, K.F., Feagin, R.A., Smith, W.K., 2013. Coastal geomorphology and restoration. Geomorphology 199, 1-7.

Janssen, T.T., Battjes, J.A., 2007. A note on wave energy dissipation over steep beaches. Coastal Engineering 54, 711–716.

Johnson, H.K., Brøker, I., Zyserman, J.A., 1994. Identification of some Relevant Processes in Coastal Morphological Modelling. Proceedings of the 24th International Conference on Coastal Engineering, ASCE, 2871-2885.

Johnson, H.K., and Zyserman, J.A, 2002. Controlling Spatial Oscillations in Bed Level Update Schemes. Coastal Engineering, 46, 109-126.

Jones, P.D., Jonsson, T., Wheeler, D.A., 1997. Extension to the North Atlantic Oscillation using early instrumental pressure observations from Gibraltar and South-West Iceland. International Journal of Climatology 17 (13), 1433–1450.

Karunarathna, H., Reeve, D.E., Spivack, M., 2009. Beach profile evolution as an inverse problem. Continental Shelf Research 29, 2234–2239.

Karunarathna, H., Pender, D., Ranasinghe, R., Short, A.D., Reeve, D.E., 2014. The effects of storm clustering on beach profile variability. Marine Geology 348, 103-112.

Karunarathna, H., Brown, J., Chatzirodou, A., Dissanayake, P., Wisse, P., 2018. Multi-timescale morphological modelling of a dune-fronted sandy beach. Coastal Engineering 136, 161–171.

Keshtpoor, M., Puelo, J.A., Gebert, J., Plant, N.G., 2013. Beach response to a fixed sand bypassing system. Coastal Engineering 73, 28-42.

Kiden, P., Denys, L., Johnston, P., 2002. Late Quaternary sea-level change and isostatic and tectonic land movements along the Belgian–Dutch North Sea coast: geological data and model results. Journal of Quaternary Science 17, (5-6), 535–546.

Kidson, C., Gilbertson, D., Haynes, J., Heywort, A., Hughes, C., Whatley, R., 2008. Interglacial marine deposits of the Somerset level, south west England. Boreas 7(4), 215–228.

Komar, P.D., 1999. Beach processes and sedimentation. Prentice-Hall, New Jersey, p. 544.

Lee, G., Nicholls, R.J., Birkemeier, W.A., 1998. Storm-driven variability of the beach-nearshore profile at Duck, North Carolina, USA, 1981-1991. Marine Geology 148, 163-177.

Lemm, A.J., Hegge, B.J., Masselink, G., 1999. Offshore wave climate, Perth (Western Australia). Marine Freshwater Research 50, 95–102.

Longuet-Higgins, M.S., Stewart, R.W, 1964. Radiation stress in water waves: a physical discussion with applications. Deep-Sea Research, 529–562.

Lopez, G., Conley, D.C., Greaves, D., 2016. Calibration, validation and analysis of an empirical algorithm for the retrieval of wave spectra from HF radar sea-echo. Journal of Atmospheric and Oceanic Technology 33, 245–261.

Loureiro, C., Ferreira, O., Cooper, J.A.G., 2012. Geologically constrained morphological variability and boundary effects on embayed beaches. Marine Geology 329-331, 1–15.

Lozano, I., Devoy, R.J.N., May, W., Andersen, U., 2004. Storminess and vulnerability along the Atlantic costalines of Europe: analysis of storm records and of a greenhouse gases induced climate scenario. Marine Geology 210, 205-225.

Luijendijk, A., Hagenaars, G., Ranasinghe, R., Baart, F., Donchyts, G., Aarninkhof, S., 2018. The State of the World's Beaches. Scientific Reports 8, 6641.

Martins, K., Blenkinsopp, C.E., Power, H.E., Bruder, B., Puleo, J.A., Bergsma, E.W.J., 2017. High-resolution monitoring of wave transformation in the surf zone using a LiDAR scanner array. Coastal Engineering 128, 37–43.

Masselink, G., Austin, M., Scott, T., Poate, T., Russell, P., 2014. Role of wave forcing, storms and NAO in outer bar dynamics on a high-energy, macro-tidal beach. Geomorphology 226, 76–93.

Masselink, G., Scott, T., Davidson, M., Russell, P., Conley, D., 2015. The extreme 2013/2014 winter storms: hydrodynamic forcing and coastal response along the southwest coast of England. Earth Surface Processes and Landforms 41, 378-391.

Masselink, G., Castelle, B., Scott, T., Dodet, G., Suanez, S., Jackson, D., Floc'h, F., 2016. Extreme wave activity during 2013/2014 winter and morphological impacts along the Atlantic coast of Europe. Geophysical Research Letter 43, 2135–2143.

May, V.J., Hansom, J.D., 2003. Coastal geomorphology of Great Britain. Geological conservation review series 28. Joint Nature Conservation Committee, Peterborough.

McCall, R.T., Van Thiel de Vries, J.S.M., Plant, N.G., Van Dongeren, A.R., Roelvink, J.A., Thompson, D.M., Reniers, A.J.H.M., 2010. Two-dimensional time dependent hurricane overwash and erosion modeling at Santa Rosa Island. Coastal Engineering 57, 668–683.

McCallum, E., 1990. The Burn's day storm, 25 January 1990. Weather 45 (5), 166–173.

McCallum, E., Grahame, N.S., 1993. The Braer storm – 10 January 1993. Weather 48 (4), 103–107.

McLean, R., Shen, J.S., 2006. From foreshore to foredune: foredune development over the last 30 years at Moruya Beach, New South Wales, Australia. Journal of Coastal Research 22, 28–36.

Meeker, L.D., Mayewski, P.A., 2002. A 1400-year high-resolution record of atmospheric circulation over the North Atlantic and Asia. The Holocene 12 (3), 257–266.

Mendoza, E.T., Jimenez, J.A., Mateo, J., 2011. A coastal storm intensity scale for the Catalan sea (NW Mediterranean). Natural Hazards Earth Systems Science 11, 2453–2462.

Merrill, R. T., 1993. Tropical Cyclone Structure - Chapter 2, Global Guide to Tropical Cyclone Forecasting, WMO/TC-No. 560, Report No. TCP-31. World Meteorological Organization, Geneva, Switzerland.

Miller, J.K., Dean, R.G., 2004. A simple new shoreline model. Coastal Engineering 51, 531–556.

Moon, I.J., Ginis, I., Hara, T., Tolman, H.L., Wright, C.W., Walsh, E.J., 2003. Numerical simulation of sea surface directional wave spectra under hurricane wind forcing. Journal of Physical Oceanography 33, 1680-1705.

Mortlock, T.R., Goodwin, I.D., 2016. Impacts of enhanced central Pacific ENSO on wave climate and headland-bay beach morphology. Continental Shelf Research 120, 14-25.

Morton, R.A., Paine, J.G., Gibeaut, J.C., 1994. Stages and Durations of post-Storm Beach Recovery, Southeastern Texas Coast, U.S.A. Journal of Coastal Research 10 (4), 884–908.

Nahon, A., Idier, D., Fenies, H., Mugica, J., Senechal, N., Mallet, C., 2015. Role of North Atlantic Climate Variability On Barrier-Spit Oscillations: The Cap Ferret. Coastal Sediments'15 Proceedings.

Nairn, R.B., Roelvink, J.A., Southgate, H.N., 1990. Transition zone width and implications for modeling surfzone hydrodynamics. Proceedings 22th International Conference on Coastal Engineering, 68–81.

Nerem, R. S., Beckley, B.D., Fasulloc, J.T., Hamlington, B.D., Masters, D., Mitchum, G.T., 2018. Climate-change–driven accelerated sea-level rise detected in the altimeter era. Proceedings of the National Academy of Sciences of the United States of America, 1717312115.

Niemann, S.L., Jensen, J.H., Zyserman, J.A., Brøker, I., Baek, S., 2006. Morphological Modelling of a Danish Tidal Inlet. Proceedings of ICCE 2006, San Diego.

Ojeda, E., Guillen, J., 2008. Shoreline dynamics and beach rotation of artificial embayed beaches. Marine Geology 253, 51-62.

Pender, D., Karunarathna, H., 2013. A statistical-process based approach for modelling beach profile variability. Coastal Engineering 81, 19–29.

Petit, J.R., Jouzel, J., Raynaud, D., Barkov, N.I., Barnola, J.M., Basile, I., Bender M., Chappellaz, J., Davisk, M., Delaygue, G., Delmotte, M., Kotlyakov, V. M., Legrand, M. , Lipenkov, V. Y., Lorius, C., Pe´pin, L., Ritz, C., Saltzmank E.,

Stievenard, M., 1999. Climate and atmospheric history of the past 420,000 years from the Vostok ice core, Antarctica. Nature 399, 429–436.

Pierson, W.J., Moskowitz, L., 1964. A proposed spectral form for fully developed wind seas based on the similarity theory of S.A. Kitaigorodskii. Journal of Geophysical Research 69 (24), 5181–5190.

Phillips, O.M., 1977. The dynamics of the upper ocean. Cambridge University Press 366.

Phillips, M.S., Harley, M.D., Turner, I.L., Splinter, K.D., Cox, R.J., 2017. Shoreline recovery on wave-dominated sandy coastlines: the role of sandbar morphodynamics and nearshore wave parameters. Marine Geology 385, 146–159.

Plant, N.G., Holman, R.A., Freilich, M.H., Birkemeier, W.A., 1999. A simple model for interannual sandbar behavior. Journal of Geophysical Research 104 (C7), 15,755–15,776.

Plomaritis, T.A., Benavente, J., Laiz, I., Del Rio, L., 2015. Variability in storm climate along the Gulf of Cadiz: The role of large scale atmospheric forcing and implications to coastal hazards. Climate Dynamics, 445 (9), 2499–2514.

Poate, T., 2011. Morphological response of high-energy macrotidal beaches. PhD thesis, University of Plymouth.

Poate, T., Masselink, G., Russell, P., Austin, M., 2014. Morphodynamic variability of high-energy macrotidal beaches, Cornwall, UK. Marine Geology 350, 97–111.

Poate, T., Masselink, G., McCall, R., Russell, P., Davidson, M., 2015. UK storms 2014: gravel beach response. Proceedings Coastal Sediments, ASCE, San Diego, USA.

Poelhekke, L., Jäger, W.S., van Dongeren, A., Plomaritis, T.A., McCall, R., Ferreira, O., 2016. Predicting coastal hazards for sandy coasts with a Bayesian Network. Coastal Engineering 118, 21–34.

Prodger, S., Russell, P., Davidson, M., Miles, J., Scott, T., 2016. Understanding and predicting the temporal variability in sediment grain size characteristics on high energy beaches. Marine Geology 376, 109-117.

Pye, K., Blott, S.J., 2008. Decadal-scale variation in dune erosion and accretion rates: An investigation of the significance of changing storm tide frequency and magnitude on the Sefton coast, UK. Geomorphology 102, 652–666.

Pye, K., Blott, S.J., 2016. Assessment of beach and dune erosion and accretion using LiDAR: Impact of the stormy 2013–14 winter and longer term trends on the Sefton Coast, UK. Geomorphology 266, 146-167.

Qi, H., Cai, F., Lei, G., Cao, H., Shi, F., 2010. The response of three main beach types to tropical storms in South China. Marine Geology 275, 244–254.

Reniers, A.J.H.M., Roelvink, J.A., Thornton, E.B., 2004. Morphodynamic modeling of an embayed beach under wave group forcing. Journal of Geophysical Research 109, 1–22.

Roberts, T.M., Wang, P., Puleo, J.A., 2013. Storm-driven cyclic beach morphodynamics of a mixed sand and gravel beach along the Mid-Atlantic Coast, USA. Marine Geology 346, 403–421.

Robinet, A., Castelle, B., Idier, I., Le Cozannet, G., Deque, M., Charles, E., 2016. Statistical modelling of interannual shoreline change driven by North Atlantic climate variability spanning 2000–2014 in the Bay of Biscay. Geo-Marine Letters 36, 479–490.

Roelvink, J.A., 1993. Dissipation in random wave group incident on a beach. Coastal Engineering 19, 127–150.

Roelvink, D., Reniers, A., van Dongeren, A., van Thiel de Vries, J., McCall, R., Jamie Lescinski, J., 2009. Modelling storm impacts on beaches, dunes and barrier islands. Coastal Engineering 56, 1133–1152.

Roelvink, D., van Dongeren, A., McCall, R., Hoonhout, B., van Rooijen, A., van Geer, P., de Vet, L., Nederhoff, K., Quataert, E., 2015. XBeach Technical Reference: Kingsday Release. Deltares, UNESCO-IHE Institute of Water Education and Delft University of Technology

Różyński, G., 2003. Data-driven modelling of multiple longshore bar evolution and interactions. Coastal Engineering 48 (3), 151–170.

Ruessink, B.G., Miles, J.R., Feddersen, F., Guza, R.T., Elgar, S., 2001. Modeling the alongshore current on barred beaches. Journal of Geophysical Research 106 (22), 451–463.

Ruggiero, P., Kaminsky, G.M., Gelfenbaum, G., Voigt, B., 2005. Seasonal to Interannual Morphodynamics along a High-Energy Dissipative Littoral Cell. Journal of Coastal Research 21 (3), 553–578.

Ruiz de Alegria-Arzaburu, A., Masselink, G., 2010. Storm response and beach rotation on a gravel beach, Slapton Sands, U.K. Marine Geology 278, 77–99.

Sallenger, A.H., 2000. Strom Impact Scale for Barrier Islands. Journal of Coastal Research 16 (3), 890–895.

Sallenger, A.H.J., Krabill, W., Swift, R., Brock, J., 2001. Quantifying Hurricane-Induced Coastal Changes Using Topographic Lidar. Coastal Dynamics '01 proceedings. American Society of Civil Engineers, Reston, Virginia, USA, 1007-1016.

Sánchez-Arcilla, A. and Lemos, C.M., 1990. Surf-zone Hydrodynamics. Centro Internacional de Métodos Numéricos de Ingeniería, 310 p.

Santos V.M., Haigh, I.D., Wahl, T., 2017. Spatial and Temporal Clustering Analysis of Extreme Wave Events around the UK Coastline. Journal of Marine Science and Engineering 5 (28), 1–19.

Saulter, A., 2017. North West European Shelf Production Centre NORTHWESTSHELF_ANALYSIS_FORECAST_WAV_004_012 Quality Information Document. Copernicus Marine Environment Monitoring service.

Saye, S.E., van der Wal, D., Pye, K., Blott, S.J., 2005. Beach-dune morphological relationships and erosion/accretion: An investigation at five sites in England and Wales using LiDAR data. Geomorphology 72, 128-155.

Schambach, L., Grilli, A.R., Grilli, S.T., Hashemi, M.R., King, J.W., 2018. Assessing the impact of extreme storms on barrier beaches along the Atlantic coastline: Application to the southern Rhode Island coast. Coastal Engineering 133, 26–42.

Scott, T. M., 2009. Beach morphodynamics and associated hazards in the UK. PhD thesis, University of Plymouth.

Scott, T., Masselink G., Russell P., 2011. Morphodynamic characteristics and classification of beaches in England and Wales. Marine Geology 286, 1–20.

Scott, T., Masselink, G., O'Hare, T., Saulter, A., Poate, T., Russell, P., Davidson, M., Conley, D., 2016. The extreme 2013/2014 winter storms: Beach recovery along the southwest coast of England. Marine Geology 382, 224-241.

Senechal, N., Gouriou, T., Castelle, B., Parisot, J.-P., Capo, S., Bujan, S., Howa, H., 2009. Morphodynamic response of a meso- to macro-tidal intermediate beach based on a long-term data set. Geomorphology 107, 263–274.

Senechal, N., Coco, G., Castelle, B., Marieu, V., 2015. Storm impact on the seasonal shoreline dynamics of a meso- to macrotidal open sandy beach (Biscarosse, France). Geomorphology 228, 448-461.

Serreze, M.C., Carse, F., Barry, R.G., Rogers J.C., 1997. Icelandic Low Cyclone Activity: Climatological Features, Linkages with the NAO, and Relationships with Recent Changes in the Northern Hemisphere Circulation. Journal of Climate 10, 453–464.

Sherman, D.J., Hales, B.U., Potts, M.K., Ellis, J.T., Liu, H., Houser, C., 2013. Impacts of Hurricane Ike on the beaches of the Bolivar Peninsula, TX, USA. Geomorphology 199, 62-81.

Short, A.D., 1999. Handbook of Beach and Shoreface Morphodynamics. John Wiley & Sons, Chichester, UK.

Short, A.D., 2010. Role of geological inheritance in Australian beach morphodynamics. Coastal Engineering 57, 92–97.

Short, A.D., Bracs, M.A., Turner, I.A., 2014. Beach oscillation and rotation: local and regional response at three beaches in southeast Australia. Journal of Coastal Research 66, 712-717.

Simmons, J.A., Harley, M.D., Turner, I.L., Splinter, K.D., 2017. Quantifying calibration data requirements for coastal erosion models: how many storms is enough? Coasts & Ports 2017 Conference – Cairns, Australia.

Slingo, J., Belcher, S., Scaife, A., McCarthy, M., Saulter, A., McBeath, K., Jenkins, A., Huntingford, C., Marsh, T., Hannaford, J., Parry, S., 2014. The Recent Storms and Floods in the UK. Met Office and Centre for Ecology and Hydrology Report.

Smagorinsky, J., 1963. General circulation experiments with the primitive equations I. The basic experiment. Monthly Weather Review 91, 99–164. Soulsby, R.L., 1997. Dynamics of Marine Sands. London: Thomas Telford Publications.

Splinter, K.D., Strauss, D.R., Tomlinson, R.B., 2011. Assessment of post-storm recovery of beaches using video imaging techniques: a case study at Gold

Coast, Australia. IEEE Transactions on Geoscience Remote Sensing 49 (12), 4704–4716.

Splinter, K.D., Palmsten, M.L., 2012. Modeling dune response to an East Coast Low. Marine Geology 329–331, 46-57.

Splinter, K.D., Turner, I.L., Davidson, M.A., 2013. How much data is enough? The importance of morphological sampling interval and duration for calibration of empirical shoreline models. Coastal Engineering 77, 14–27.

Splinter, K.D., Turner, I.L., Davidson, M.A., Barnard, P., Castelle, B., Oltman-Shay, J., 2014a. A generalized equilibrium model for predicting daily to interannual shoreline response. Journal of Geophysical Research Earth Surface 119 (9), 1936-1958.

Splinter, K.D., Carley, J.T., Golshani, A., Tomlinson, R., 2014b. A relationship to describe the cumulative impact of storm clusters on beach erosion. Coastal Engineering 83, 49–55.

Splinter, K.D., Kearney, E.T., Turner, I.L., 2018. Drivers of alongshore variable dune erosion during a storm event: Observations and modelling. Coastal Engineering 131, 31–41.

Steers, J., 1960. The Coast of England and Wales in Pictures. Cambridge University Press, London.

Stephenson, D.B., Pavan, V., Collins, M., Junge, M.M., Quadrelli, R., participating CMIP2 modelling groups, 2006. North Atlantic Oscillation response to transient greenhouse gas forcing and the impact on European winter climate: a CMIP2 multi-model assessment. Clim. Dyn. 27, 401–420.

Stive, M.J.F., de Vriend, H.J., 1994. Shear stresses and mean flow in shoaling and breaking waves. Proceedings 24th International Conference on Coastal Engineering, 594–608.

Stive, M.J.F., Aarninkhof, S.G.J., Hamm, L., Hanson, H., Larson, M.,Wijnberg, K.M., Nicholls, R.J., Capobianco, M., 2002. Variability of shore and shoreline evolution. Coastal Engineering 47, 211–235.

Stockdon, H.F., Holman, R.A., Howd, P.A., Sallenger, A.H., 2006. Empirical parameterization of setup, swash, and runup. Coastal Engineering 53, 573–588.

Stocker, T.F., Qin, D., Plattner, G.K., Tignor, M., Allen, S.K., Boschung, J., Nauels, A., Xia, Y., Bex, V., Midgley, P.M, 2013. IPCC, 2013: The Physical Science Basis. Contribution of Working Group I to the Fifth Assessment Report of the Intergovernmental Panel on Climate Change Cambridge University Press, Cambridge, United Kingdom and New York, NY, USA, 1535 pp.

Suanez, S., Cariolet, J.M., Cancouët, R., Ardhuin, F., Delacourt, C., 2012. Dune recovery after storm erosion on a high-energy beach: Vougot Beach, Brittany (France). Geomorphology 139-140, 16–33.

Sutherland, J., Peet, A.H., Soulsby, R.L., 2004. Evaluating the performance of morphological models. Coastal Engineering 51, 917– 939.

Svendsen, I.A., 1984. Mass flux and undertow in a surf zone. Coastal Engineering 8, 347–365.

Thom, B.H., Hall, W., 1991. Behaviour of beach profiles during accretion and erosion dominated period. Earth Surface Processes and Landforms 16, 113–127.

Thomas, T., Phillips, M.R., Lock, G., 2015. An analysis of subaerial beach rotation and influences of environmental forcing adjacent to the proposed Swansea Bay Tidal Lagoon. Applied Geography 62, 276-293.

Travers, A., 2007. Low-energy beach morphology with respect to physical setting: a case study from Cockburn Sound, Southwestern Australia. Journal of Coastal Research 23 (2), 429-444.

Trenberth, K.E., Hoar, T.J., 1997. El Niño and climate change. Geophysical Research Letters 24 (23), 3057–3060.

Trouet V., Scourse, J.D., Raible, C.C., 2012. North Atlantic storminess and Atlantic Meridional Overturning Circulation during the last Millennium: Reconciling contradictory proxy records of NAO variability. Global and Planetary Change 84-85, 48–55.

Turki, I., Medina, R., Coco, G., Gonzalez, M., 2013. An equilibrium model to predict shoreline rotation of pocket beaches. Marine Geology 346, 220-232.

Turner, I.L., Harley, M.D., Short, A.D., Simmons, J.A., Bracs, M.A., Phillips, M.S., Splinter, K.D., 2016. A multi-decade dataset of monthly beach profile surveys and inshore wave forcing at Narrabeen, Australia. Scientific Data 3, 160024.

Valiente, N.G., Masselink, G., Scott, T., Conley, D., McCarroll, R.J., submitted. Depth of closure: a multi-criteria approach for a macrotidal, embayed and exposed coast. Journal of Geophysical Research.

Van Rijn, L.C., 1985. Sediment transport, part III: bed forms and alluvial roughness. Journal of Hydraulic Engineering 110 (12), 1733–1754.

Van Rijn, L.C., 2007. Unified View of Sediment Transport by Currents and Waves: part I and II. Journal of Hydraulic Engineering 133 (6), 649–667.

Van Thiel de Vries, J.S.M., 2009. Dune erosion during storm surges. PhD thesis, Delft Unversity of Technology, Delft.

Vieira da Silva, G., Toldo Jr, E.E., da F. Klein, A.H., Short, A.D., Woodroffe, C.D., 2016. Headland sand bypassing - Quantification of net sediment transport in embayed beaches, Santa Catarina Island North Shore, Southern Brazil. Marine Geology 379, 13-27.

Vousdoukas, M.I., Almeida, L.P.M., Ferreira, Ó., 2012a. Beach erosion and recovery during consecutive storms at a steep-sloping, meso-tidal beach. Earth Surface Processes and Landforms 37 (6), 583–593.

Vousdoukas, M.I., Ferreira, Ó., Almeida, L.P., Pacheco, A., 2012b. Toward reliable storm-hazard forecasts: XBeach calibration and its potential application in an operational early-warning system. Ocean Dynamics 62, 1001–1015.

Vousdoukas, M.I., Mentaschi, L., Voukouvalas, E., Verlaan, M., Feyen, L., 2017. Extreme sea levels on the rise along Europe's coasts. Earth's future 5 (3), 304–323.

Walstra, D.J.R., Roelvink, J.A., Groeneweg, J., 2000. Calculation of wave-driven currents in a 3D mean flow model. Proceedings 27th International Conference on Coastal Engineering, 1050–1063.

Wang, X.L., Swail, V.R., 2002. Trends of Atlantic wave extremes as simulated in a 40-yr wave hindcast using kinematically reanalysed wind fields. Journal of Climate 15, 1020-1035.

Wang, P., Kirby, J.H., Haber, J.D., Horwitz, M.H., Knorr, P.O., Krock, J.R., 2006. Morphological and sedimentological impacts of hurricane Ivan and immediate post-storm beach recovery along the Northwestern Florida barrier-island coasts. Journal of Coastal Research 6, 1382–1402.

Wheaton, J.M., Brasington, J., Darby, S.E., Sear, D.A., 2010. Accounting for uncertainty in DEMs from repeat topographic surveys: improved sediment budgets. Earth Surface Processes and Landforms 35, 136-156.

White, S.A., Wang, Y., 2003. Utilizing DEMs derived from LiDAR data to analyze morphologic change in the North Carolina coastline. Remote Sensing of Environment 85, 39-47.

Wiggins, M., Scott, T., Masselink, G., Russell, P., Stokes, C., Garcia Valiente, N., 2018. Embayment Dynamics Using Multi-Method Surveys: An Assessment of Seasonal to Decadal Barrier Response to a Variable Bi-Modal Wave Climate. AGU Ocean Sciences'18 Proceedings.

Wright, L.D., Thom, B.G., 1977. Coastal depositional landforms: a morphodynamic approach. Progress in Physical Geography: Earth and Environment 1 (3), 412–459.

Wright, L.D., Short, A.D., 1984. Morphodynamic variability of surf zones and beaches: a synthesis. Marine Geology 56, 93–118.

Wright, L.D., Short, A.D., Green, M.O., 1985. Short-term changes in the morphodynamic states of beaches and surf zones; an empirical predictive model. Marine Geology 62, 339–364.

Wyatt, L.R., 1995. The effect of fetch on the directional spectrum of Celtic Sea storm waves. Journal of Physical Oceanography 25, 1550–1559.

Yates, M.L., Guza, R.T., O'Reilly, W.C., 2009. Equilibrium shoreline response: observations and modelling. Journal of Geophysical Research 114, C09014.

Young, I.R., Sieger, S., Babanin A.V., 2011. Global trends in wind speed and wave height. Science 332, 451-455.

Yu, F., Switzer, A.D., Lau, A.Y.A, Yeung, H.Y.E, Chik, S.W., Chiu, H.C., Huang, Z., Pile, J., 2013. A comparison of the post-storm recovery of two sandy beaches on Hong Kong Island, southern China. Quaternary International 304, 163–175.

Zhang, K., Douglas, B.C., Leatherman, S.P., 2000. Twentieth-century storm activity along the US east coast. Journal of Climate 13, 1748–1761.

Zhang, K., Douglas, B., Leatherman, S., 2002. Do Storms Cause Long-Term Beach Erosion along the U.S. East Barrier Coast? J. Geol. 110 (4), 493–502.